# The thermodynamic controls on sulfide saturation in silicate melts with application to Ocean Floor Basalts.

Hugh St.C. O'Neill

Research School of Earth Sciences, Australian National University, Canberra, ACT 2601, Australia.

Email: (hugh.oneill@anu.edu.au)

IN PRESS CITATION:

O'Neill, H. St.C. (in press). The thermodynamic controls on sulfide saturation in silicate melts with application to Ocean Floor Basalts. AGU Geophysical Monograph, Redox variables and mechanisms in magmatism and volcanism. Editors R. Moretti and D. R. Neuville, John Wiley and Sons.

## Abstract

A thermodynamic model to calculate the "Sulfide Content at Sulfide Saturation" or SCSS of basaltic and intermediate composition silicate melts has been built from four independently measurable thermodynamic entities, namely the standard state Gibbs free energy of the saturation reaction, the "sulfide capacity", and the activities of FeO in the silicate melt and of FeS in the coexisting sulfide:

$\ln [S^{2-}]_{SCSS} = \Delta G^{o}_{FeO-FeS}/RT + \ln C_{S^{2-}} - \ln a_{FeO}^{sil\ melt} + \ln a_{FeS}^{sulf}$

The model was calibrated for silicate melts of basic and intermediate composition from published experimental results as a function of temperature, silicate melt composition, and sulfide matte composition in the system Fe-Ni-Cu-S-O at 1 bar. The likely effects of pressure and $H_2O$ content on SCSS were included in an exploratory way. The model was tuned against the large dataset of S

contents in OFB glasses of Jenner and O'Neill (2012), giving it a precision comparable to that of the S analyses themselves, which is ~ 5%. All but 3% the OFB glasses were found to be sulfide saturated within uncertainty; these 3% have lost S by devolatization, revealed by their low S/Se. Applying the model to other OFB datasets suggests sulfide saturation is ubiquitous, including olivine-hosted melt inclusions proposed previously to be sulfide undersaturated. The sulfur fugacity ($fS_2$) of undegassed Ocean Floor Basalts varies proportionally to $fO_2$, with $\log_{10}fS_2$ typically within the range -0.6 to +0.4.

## 1. Introduction

In the Earth sciences, quantifying the thermochemistry of sulfur dissolved in magmatic silicate melts is needed for understanding the behaviour of chalcophile elements during partial melting and magmatic differentiation, sulfur degassing from volcanic eruptions, core formation in the early solar system, and for modelling the petrogenesis of many kinds of magmatic ore deposits. Meanwhile, in the technologically directed applied sciences, the thermochemical description of sulfur dissolved in the oxide-silicate melts found as slags or fluxes is needed wherever this element is present, one important application being the desulfurization of steel (e.g., Schrama et al. 2017). Accordingly, the thermochemistry of S in silicate melts has received considerable technological attention. While the fundamental principles are obviously of mutual interest, there are aspects to the understanding of S in silicate melts in the geological context that are irrelevant to technological applications, and vice versa. In the technological sector, the compositional space encompassing silicate melts of practical interest is vast, as well shown by the list assembled by Kang and Pelton (2009) of silicate (and aluminate) melts whose "sulfide capacity" (defined below) has been determined experimentally. Yet this dataset includes hardly any realistic magmatic silicate melt compositions. These tend to be richer in $SiO_2$ (> 40 wt%), with a limited range of alumina contents, and atomic Si/Al between 2.5 and 4.5. Metallurgical slags are often either almost free of alumina, or alternatively have high Al/Si beyond the range found in nature. Natural magmas have modest but non-negligible alkali contents,

53 with most plotting on the standard total alkali-silica diagram used for rock classification
54 ($Na_2O+K_2O$ vs. $SiO_2$) between 2 and 10 wt% ($Na_2O+K_2O$), whereas metallurgical slags either have
55 negligible alkalis (e.g., most steel-making slags), or, elsewhere, $Na_2O$ as the main or even sole
56 basic-oxide constituent (e.g., Chan and Fruehan 1986, 1988). In terms of melt structure, most
57 magmatic melt compositions have NBO/T, the ratio of non-bridging oxygens to tetrahedrally
58 coordinated cations, between 0 and 1.5, whereas few of the compositions listed by Kang and Pelton
59 (2009) have NBO/T < 2. "Water" (H as $H_2O$) is a major component in many magmas, but is almost
60 absent in slags, because the dissolution of more than trace amounts of $H_2O$ in silicate melts requires
61 geological pressures. And of course such pressures are not relevant to metallurgical processes,
62 which generally occur not far from atmospheric pressure.
63 There is a further difference. The technologist needs to predict S solubility in a slag perhaps to a
64 factor of two or so, but over the vast range of slag compositions mentioned above. For example,
65 they may need to know how much lime should be added to a slag to reduce S in the steel by a factor
66 of, say, five. To the petrologist, the precision with which sulfide solubilities need to be known is far
67 greater, albeit only within a relatively narrow range of melt compositions. For example, among
68 Ocean Floor Basalts, almost the entire range of recovered glass samples analysed for S fall within a
69 factor of three (Jenner and O'Neill 2012), so predicting S solubilities to a factor of two would be
70 useless. From the perspective of basalt petrology, the aspirational target is to predict the "Sulfide
71 Content at Sulfide Saturation", or SCSS, which is how much S dissolved as $S^{2-}$ there is in a silicate
72 melt in equilibrium with a sulfide phase, to somewhere approaching the analytical accuracy to
73 which S contents can be measured. In basaltic glasses, this appears to be at about ± 5%. Formidable
74 though this challenge may seem, the theme of this review is that it can now be met, thanks to the
75 efforts of many experimental petrologists over the last few decades.
76 The equilibrium that describes SCSS is:

77 $$\underset{\text{silicate melt}}{FeO} + 1/2\ S_2 = \underset{\text{sulfide melt}}{FeS} + 1/2\ O_2 \qquad (1)$$
78

As emphasised by O'Neill and Mavrogenes (2002), this equilibrium can be deconstructed into four thermodynamic entities: 1) the standard-state free energy of the reaction, which is a function of temperature and pressure alone; 2) the "sulfide capacity" of the melt; 3) the activity of FeO in the silicate melt; and 4) the activity of FeS in the coexisting sulfide (often molten, when it is appropriately called a matte). Entities 2), 3) and 4) are dependent on composition as well as temperature and pressure. In principle, each one of these entities can be measured experimentally, and independently of each other. In practice there are experimental limitations, but at least at atmospheric pressure all four items have indeed been measured independently of each other. The standard state free energy and activities of FeO in silicate melts and FeS in sulfide mattes are familiar thermodynamic quantities, but the "sulfide capacity" of a silicate melt is not, which has caused some confusion as to its nature, leading to uncertainty as to how it may depend on melt composition. Its relationship with other potentially useful thermodynamic properties of silicate melts, for example their "carbonate capacity" has also been underappreciated.

**Sulfide Capacity**

One area in which the technological sciences provided guidance was in establishing the notion of the "sulfide capacity", denoted $C_{S^{2-}}$ (Fincham and Richardson 1954). These authors studied the solubility of S in some simple-system silicate melts (and one aluminate melt) in equilibrium with $SO_2$-$H_2$-$CO_2$-$N_2$ gas mixtures, which were used to control the fugacities of sulfur and oxygen ($fS_2$ and $fO_2$). While they mention steelmaking as an application of their work, they emphasized that their goal was a broader understanding of silicate melt thermochemistry. They noted that "Previous attempts to elucidate the chemistry of sulphur in molten silicates (e.g., Grant and Chipman 1946) have been based on the measurements of the equilibrium distribution of sulphur between complex slags and molten iron. Although a considerable amount of quantitative information has been amassed, the results are too complicated to permit the development of a clear picture from them." If this is a reasonable view from within the restricted context of steelmaking, how much more so is it

for geological processes? Their call for some judicious reductionism has much influenced the approach of this present review.

Fincham and Richardson (1954) found that, while keeping other compositional parameters and temperature constant, the sulfur concentration in the melt changed proportionally to $(fS_2)^{1/2}$, when $fO_2$ was low as well as constant. Likewise, when keeping $fS_2$ constant, they found that S concentrations changed proportionally to $(fO_2)^{-1/2}$. These observations implied that S was dissolving only as the sulfide species, $S^{2-}$, and did so by replacing $O^{2-}$. This has sometimes been summarized by writing the reaction:

$$\underset{\text{sil melt}}{O^{2-}} + \tfrac{1}{2}\, S_2 = \underset{\text{sil melt}}{S^{2-}} + \tfrac{1}{2}\, O_2 \qquad (2)$$

There is no implication that $O^{2-}$ is an abundant species in the silicate melt, which it is not in the compositional space of natural magmas (Mysen and Richet 2005). Rather, $O^{2-}$ should be viewed as a "structural element", by analogy with vacancies or interstitials in the point-defect thermodynamics of crystals (e.g., Schmalzried 1995). In this formalism, the "structural elements" are treated like thermodynamic components, with chemical potentials that vary monotonically with the logarithms of their concentrations. Whether structural elements can actually have definable chemical potentials is a moot point, but this is the hypothesis. It follows from this hypothesis that a quantity resembling an equilibrium constant may be written for reaction (2), namely $[S^{2-}]/[O^{2-}](fO_2/fS_2)^{1/2}$, where the square brackets denote concentration. It is then assumed that $[O^{2-}]$ is unaffected by $[S^{2-}]$, at least for small amounts of $S^{2-}$ to the melt, which motivates the definition of the sulfide capacity of the melt ($C_{S^{2-}}$) as the constant of proportionality between $[S^{2-}]$ and $(fO_2/fS_2)^{1/2}$:

$$C_{S^{2-}} = [S^{2-}](fO_2/fS_2)^{1/2} \qquad (3)$$

where $[S^{2-}]$ is the sulfur content of the melt in any convenient units, like parts per million by weight.

O'Neill and Mavrogenes (2002) pointed out that an analogous reaction could be written using orthosilicate and framework structural units of the type actually found in silicate melts:

$$\underset{\text{sil melt}}{\tfrac{1}{2}\, SiO_4^{4-}} + \tfrac{1}{2}\, S_2 = \underset{\text{sil melt}}{S^{2-}} + \underset{\text{sil melt}}{\tfrac{1}{2}\, SiO_2} + \tfrac{1}{2}\, O_2 \qquad (4)$$

This reaction has the same dependence on $(fO_2/fS_2)^{1/2}$, also has two "structural elements" ($S^{2-}$ and $SiO_4^{4-}$), and in addition one definable thermodynamic component ($SiO_2$). In principle, reactions that conform even more closely to silicate melt structure could be formulated. According to Mysen (1983) "three-dimensional network units are the most common in natural magmatic liquids. These units will also contain most of the aluminum. Consequently, the anionic structure of anhydrous magmatic liquids at or near 1 atm pressure may be described as a combination of nearly pure $Si_2O_6^{4-}$ (NBO/Si = 2) and $Si_2O_5^{2-}$ (NBO/Si = 1) units, together with three-dimensional units in which the aluminum is located". This insight suggests the reaction:

$$\underset{\text{sil melt}}{Si_2O_6^{4-}} + \tfrac{1}{2}\, S_2 = \underset{\text{sil melt}}{S^{2-}} + \underset{\text{sil melt}}{Si_2O_5^{2-}} + \tfrac{1}{2}\, O_2 \qquad (5)$$

All these ways of representing the relationship between $fS_2$, $fO_2$ and the $S^{2-}$ concentration of the silicate melt, denoted here as $[S^{2-}]$, come to the same thing, namely $[S^{2-}]$ is proportional to $(fS_2/fO_2)^{1/2}$, provided that $[S^{2-}]$ is sufficiently low that it does not noticeably perturb the concentrations of the other structural elements in the reactions (i.e., $O^{2-}$, $SiO_4^{2-}$, etcetera). In the case of reaction (4) this implies that $[S^{2-}]$ is too low to affect the ratio $[Si_2O_5^{2-}]/[Si_2O_6^{4-}]$. The proportionality between $[S^{2-}]$ and $(fS_2/fO_2)^{1/2}$ is critical; the concept of a sulfide capacity would not be of much use if this proportionality did not hold.

Fincham and Richardson (1954) went on to show that at high oxygen fugacity (obtained with $SO_2$-$O_2$ gas mixes) the proportionality changed, from which they inferred that S was dissolving as sulfate ($SO_4^{2-}$), hence the definition of the sulfate capacity $C_{SO_4^{2-}}$:

$$C_{SO_4^{2-}} = [SO_4^{2-}](fS_2)^{-1/2}(fO_2)^{-3/2} \qquad (6)$$

At intermediate $fO_2$ the levels of S dissolving in the silicate melts dropped below detection limits, implying that S in oxidation states between 2- (in $S^{2-}$) and 6+ (in $SO_4^{2-}$) in the melt are unimportant. This precludes a significant role for S dissolving as $S^{4+}$, or sulfite ($SO_3^{2-}$) in silicate melts at atmospheric pressure. Whether $S^{4+}$ may play a role at higher pressure, where it is physicaly possible for $pSO_2$ to reach values very much greater than 1 bar, remains a grey area – see Métrich et al. (2009) and the discussion on S X-ray spectroscopy below. The fact that their S solubility data

could be fitted to the two relationships (1) and (2) only also meant that experimentally detectable roles could be precluded for S dissolved in silicate melts as elemental S, other molecular S species (e.g., $S_2$), polysulfide species (e.g., $S_3^-$), or thiosulfite, thiosulfate, and so on.

The range of melt compositions investigated by Fincham and Richardson (1954) was limited, and they were unable to obtain reproducible results on their Fe-containing composition. They also only looked at a limited range of temperatures. The task of exploring the extent of the compositional space, T and $fO_2$ over which the Fincham-Richardson sulfide and sulfate solubility laws hold was left for subsequent experimental investigation.

The first attempt to test the Fincham-Richardson relationship on a geologically relevant composition (a komatiite) was by Shima and Naldrett (1975), using $fS_2$ from $10^{-4}$ to $10^{-1.4}$ bars and just two different $fO_2$s at 1450ºC. They confirmed that $[S] \propto (fS_2)^{1/2}$ at both $fO_2$s, but the proportionality between the two $fO_2$s was only to the power of 0.4, so the relationship looked to fail that part of the test. An even more emphatic lack of agreement was reported later (Buchanan et al. 1983). O'Neill and Mavrogenes (2002) then tested twelve Fe-free compositions in the system CaO-MgO-$Al_2O_3$-$SiO_2$ over as wide a range of both $fO_2$ and $fS_2$ as their experimental method allowed, but only at one temperature, 1400ºC. The low $fO_2$ and high $fS_2$ limits were set by the $CO_2$-CO-$SO_2$ gas mixes that they used, and the requirement that the partial pressures of all three gases sum to 1 bar. (This combination of input gases does not go to as low $fO_2$ as the $CO_2$-$H_2$-$SO_2$ mixes of Fincham and Richardson 1954, but has the experimental advantage that achieving the equilibrium gas-phase speciation from the input gas is faster, and there is less susceptibility to thermal segregation in the temperature gradients of conventional gas-mixing muffle furnaces). The high $fO_2$ and low $fS_2$ limits were set by the dissolved S falling below the limit of quantification feasible with the electron microprobe. Contrary to the earlier studies, it was found that the Fincham-Richardson relationship was followed within experimental uncertainty. O'Neill and Mavrogenes (2002) also tested six Fe-containing compositions, and here again the results showed agreement with the Fincham-Richardson hypothesis within experimental uncertainty. The $fO_2$-$fS_2$ range that could be

185 accessed experimentally while keeping melt composition constant was not as great as for the Fe-
186 free compositions, because the melt compositions lost some of their FeO towards lower $fO_2$ and/or
187 higher $fS_2$, due to exsolution of FeS-rich sulfide melt. Provided the Fincham-Richardson relation
188 can be assumed to hold, this is not disadvantageous, because it throws valuable experimental light
189 on the relationship between $C_{S^{2-}}$ and melt composition (see next section).
190 All the compositions examined by O'Neill and Mavrogenes (2002) to test the Fincham-
191 Richardson relationship were broadly similar in terms of melt descriptors like optical basicity or
192 NBO/T (Non-Bridging Oxygens to Tetrahedral cations) to natural basalts, *sensu latissimo*, with
193 NBO/T from just above 0 to less than 2. Quantifying solubilities of S as $S^{2-}$ in "acidic" melts with
194 NBO/T ~ 0 was not possible because the solubilities of S in such melts are so low under the
195 experimentally accessible conditions of $fO_2$ and $fS_2$ in gas-mixing experiments at atmospheric
196 pressure that adequately precise results cannot be obtained with the electron microprobe. At present
197 there are no unambiguous tests of the Fincham-Richardson relationship for such melts, but this
198 would feasible with the much better limits of detection afforded by SIMS (< 1 ppm S according to
199 Hauri et al. 2002).
200 There are currently few published experiments against which to test the Fincham-Richardson
201 relationship for sulfate solubilities (Eqn. 2). An exception is the study of Holmquist (1966), who
202 verified that the relationship of Eqn. (5) generally held well in $Na_2O$-$SiO_2$ melts at 1150 – 1250ºC,
203 except at very high concentrations, above several weight percent S. Results mentioned in abstract
204 (O'Neill and Mavrogenes 2019) confirm the relationship for a wide variety of more magmatically
205 relevant silicate melt compositions.
206
207 *The experimental sulfur solubility minimum*
208 One of the main ways that Fincham and Richardson (1954) chose to present their experimental
209 results has subsequently proved unfortunate. The problem that Fincham and Richardson faced was
210 how to display the way that the total amount of S dissolved in a silicate melt changes with $fO_2$ in

going from the sulfide-dominated to the sulfate-dominated regions of $fO_2$. Clearly connecting the two variables of dissolved S and $fO_2$ cannot be addressed without taking into account what a third variable, most lucidly $fS_2$, is doing (Eqns. 2 and 5). Illustrating their results under the specification that $fS_2$ be kept constant was not a practical option for Fincham and Richardson, because to obtain measurable S as $S^{2-}$ in the sulfide field they needed $fS_2$ to be in the region of $10^{-4}$ bars, whereas to get measurable S as $SO_4^{2-}$ in the sulfate field, $fS_2$ needed to be $< 10^{-10}$ bars (depending on temperature). This low $fS_2$ stems from the requirement for high $fO_2$. So the quantity that they kept constant for their plots of [∑S] versus log $fO_2$ was the concentration of $SO_2$ in their input gas mix, which was either 1% or 2%. Note, this is in the input gas mix, and is not the $SO_2$ concentration in the gas at equilibrium in the experiments. The resulting plots showed a V-shaped dependence of dissolved S on log $fO_2$. This same representation was subsequently used by Katsura and Nagashima (1974). Such a variable has no meaning outside the laboratory: for example, nature is not known to meter vapour composed of unequilibrated gas species into magma chambers. Nor is the input gas composition relevant to experiments that do not use gas mixing, such as those under pressure. But somehow the idea that there is a minimum in the solubility of sulfur in silicate melts as a function of oxygen fugacity crept into popular culture. This myth has no substance. Unless a third variable is specified, such as $fS_2$ (or $fSO_2$), or the presence and composition of a saturating phase (like a sulfide matte), nothing can be said about the relationship between the two variables of S content and $fO_2$. In nature, silicate melts with redox speciations towards the reduced end of the terrestrial spectrum, like Ocean Floor basalts, have FeS-rich sulfide matte as their saturating phase, whereas the relevant saturating phase under oxidizing conditions, as for some convergent margin magmatism, might be anhydrite (e.g., Luhr 2008). There is no continuity in the chemical potentials of sulfur-containing components between the two phases (that is, sulfide matte and anhydrite), hence S contents at phase saturation cannot be conceived as a continuous function of $fO_2$ between such conditions.

**The thermodynamic meaning of the sulfide capacity**

One way of interpreting the capacities $C_{S^{2-}}$ and $C_{SO_4^{2-}}$ is as the phenomenological constants of proportionality in the relationships of (2) and (5), as established by experiment. The experiments also show that the capacities vary with the major-element composition of the silicate melt, and temperature. To get a better understanding of these dependences, particularly the functional form of the dependence on melt composition, it is necessary to look beyond the phenomenology, into the thermodynamic foundations. The principle should be the same for both $C_{S^{2-}}$ and $C_{SO_4^{2-}}$ (and indeed for other similar possible "capacities", see Wagner 1975); here they will be addressed for $C_{S^{2-}}$.

Haughton et al. (1974) suggested that the sulfide capacities measured in their experiments at 1200ºC and atmospheric pressure using CO-$CO_2$-$SO_2$ gas mixtures could be fitted to an equation with the form:

$$\ln C_{S^{2-}} = A_0^{S^{2-}} + \sum X_M A_M^{S^{2-}} \quad (7)$$

The justification for this for was supplied later by O'Neill and Mavrogenes (2002) from the theory of reciprocal solutions. The thermodynamics of such solutions with mixing on two (or more) sublattices is a well-trod path in physical chemistry (e.g., Flood et al. 1954), and has long been the common choice in the thermochemical modelling of slags (e.g., Hillert 1998, 2001). Indeed, it forms the basis of most currently used models for calculating $C_{S^{2-}}$ in metallurgical contexts (e.g., Reddy and Blander 1987; Pelton et al. 1993; Kang and Pelton 2009).

In these multicomponent ionic solutions, cations mix on one sublattice, anions on the other. Consider the simplest case, the solution $(A^{x+}, B^{x+})(X^{x-}, Y^{x-})$. There exist four end-member compositions, AX, BX, AY and BY, which together define the limits of the free-energy surface in compositional space, to which all the other contributions to the free energy of the solution are additional, including that from the configurational entropy. The existence of such a free energy surface is not dependent on details of melt structure; it is more fundamental, depending only on the uncontested assumption of charge balance between electropositive elements forming cations (A and B) and electronegative elements forming anions (X and Y). With this assumption, individual ions

($A^{x+}$ etc.) and $A^{x+}B^{x+}$ or $X^{x-}Y^{x-}$ are disregarded as thermodynamic components, because they cannot be independently varied.

The total free energy of the solution may be visualized as being built up from this surface in multicomponent hyperspace by adding the other types of free energies, of which that contributed by the configurational entropy of mixing on each sublattice is fundamental. The free energy of the solution must consist of these two contributions at least; others may or may not be important. These others, collated here under the term "the excess free energy of mixing" include heats of mixing and deviations in the entropies of mixing from whatever model is used for the configurational entropy. The total free energy is therefore given by $G_{melt} = G^{o}_{end-members} + G_{config} + G_{excess}$.

Assuming that a silicate melt consists of cation and anion sublattices, the three contributions are evaluated as follows:

1) $G^{o}_{end-members}$ is the sum of the free energies of the pure end-member components, weighted according to the mole fractions of these components. When normalized to the single-anion basis, these components have the general formula $M_{x/z}X$, where M is a cation of valence z, and X are anions of valence x. The fundamental assumption of the reciprocal solution theory is that all possible components that fulfill the criterion of charge balance are present, such that:

$$G^{o}_{end-members} = \sum_{M,X} X_M^{cat} X_X^{an} \mu^{o}_{M_{x/z}X} \quad (8)$$

Here $X_M^{cat}$ is the mole fraction of $M^{z+}$ cations on the cation sublattice, and likewise $X_X^{an}$ is the mole fraction of $X^{x-}$ anions on the anion sublattice. Note that $\sum_M X_M^{cat} = \sum_X X_X^{an} = \sum_{M,X} X_M^{cat} X_X^{an} = 1$. The notation for chemical potential (μ) is used rather than Gibbs free energies for convenience, including avoiding the need to define a reference state, but may be understood to be equivalent in practice (the reference state always cancel out across a balanced chemical reaction). The important point is that the standard state free energy, $\mu^{o}_{M_{x/z}X}$, of every possible stoichiometric component $M^{z/2}X$ enters into the model. To take an example relevant to the present discussion, the chemical potential of FeS in a

multicomponent silicate melt ($\mu_{FeS}$) ineluctably implies something about the value of, say, $\mu^o_{Na_2S}$, unless there is no Na in the melt. The standard-state chemical potential of each possible end-member, $\mu^o_{M_{x/z}X}$, contributes to $G^o_{end-members}$ proportionally to its statistical weight, $X_M^{cat} X_X^{an}$. The logic of this is best understood by noting that the chemical potential of each and every charge-balanced component $M_{x/z}X$ can be in principle evaluated ($\mu_{M_{x/z}X} \equiv \partial G_{melt}/\partial n_{M_{x/z}X}$), and by definition $\mu_{M_{x/z}X} = \mu^o_{M_{x/z}X} + RT \ln a_{M_{x/z}X}$, therefore the free energy of the solution contains information on $\mu^o_{M_{x/z}X}$ for each and every $M_{x/z}X$, so long as some M and some X are present.

2) $G_{config}$ is the ideal configurational entropy that accrues from mixing of cations and anions separately on each sublattice. The usual model is:

$$G_{config} = -RT[\sum_M nX_M^{cat} \ln (X_M^{cat}) + \sum_X X_X^{an} \ln (X_X^{an})] \quad (9)$$

here $n_{cat}$ and $n_{an}$ are the fraction of sites available for mixing of the cations and anions respectively.

3) $G_{excess}$ is the excess free energies of mixing, which accounts for heats of mixing, deviations from the ideal configurational free energy of mixing, and the free energy from any non-configurational entropy of mixing. $G_{excess}$ is conventionally expressed using activity coefficients for cations and anions separately on each sublattice ($\gamma_M^{cat}$ and $\gamma_X^{an}$), by analogy with the configurational free energy:

$$G_{ex} = -RT[\sum_M X_M^{cat} \ln (\gamma_M^{cat}) + \sum_X X_X^{an} \ln (\gamma_X^{an})] \quad (10)$$

O'Neill and Mavrogenes (2002) presented the next stage of the argument using oxide and sulfide components $M_{z/2}O$ and $M_{z/2}S$, but, as they pointed out, a similar argument could be developed using silicate anion structural elements, such as, for example, orthosilicate unites $SiO_4^{2-}$ and polymerized $SiO_2$ units, as for reactions (4) and (5) above. Given our present understanding of the structure of silicate melts (e.g., Mysen and Richet 2005), choosing such structural units might only yield a tractable model between the orthosilicate-equivalent composition at NBO/T = 4, and a fully polymerized melt at NBO/T ~ 0. In actuality, most of the experimental studies of $S^{2-}$ solubility

in the geological literature are on melt compositions with NBO/T between 0.05 and 2, and, as noted above, there are few if any precise measurements of $C_{S^{2-}}$ on compositions with NBO/T at or about 0 because the low levels of $S^{2-}$ in such melts are near to the analytical limits of quantification by EMPA under experimentally accessible conditions.

With orthosilicate and silica components, the relationship between $[S^{2-}]$ in the silicate melt and $fO_2$ and $fS_2$ is given by:

$$\underset{\text{sil melt}}{\tfrac{1}{2}\,Mg_2SiO_4} + \tfrac{1}{2}\,S_2 = \underset{\text{sil melt}}{MgS} + \underset{\text{sil melt}}{\tfrac{1}{2}\,SiO_2} + 1/2\,O_2 \qquad (11)$$

The selection of $Mg^{2+}$ as the cation used to describe the equilibrium is arbitrary; for example, $Fe^{2+}$ or Ca would do as well. It is essential to acknowledge this point: the reciprocal theory of mixing on sublattices is not merely an hypothesis, but is mandated by the requirement of internal consistency. This internal consistency means that writing Eqn (11) using Ca or $Fe^{2+}$ (etc.) rather than Mg should end up giving exactly the same result, which reciprocal solution theory ensures that it does. Other attempts that try to define the activity of FeS in silicate melts without invoking reciprocal solution theory do not meet the requirement of internal consistency and are accordingly wrong. There may be some misconception in petrological thermodynamics, carried over from pioneering days, that an astute choice of components in a multicomponent phase can circumvent having to know the thermodynamic properties of other components in the phase. This has much truth in simple crystalline solutions where there is mixing on only one crystallographic site, but in more complex solutions with mixing on multiple sites, it is a fallacy. Because of the reciprocal solution effect, one cannot choose to define, for example, the activity of FeS in a silicate melt, without implying information about the activity of, say, MgS; this in turn means implying information about the standard state properties of MgS. Hence it is inescapable that the standard state properties of MgS and all other charge-balanced end members must be contained within the model.

All the components in Eqn. (11) are valid thermodynamic components, because they can be independently varied. In formal terms, $(\partial G_{melt}/\partial n_i)_{T,P,n_j}$ ($n_j \neq n_i$) is definable, and, moreover,

experimentally measurable. This is not the case for charged species, or "structural elements" in the jargon of point-defect theory (Schmalzried 1995), like $O^{2-}$ and $S^{2-}$, because $(\partial G_{melt}/\partial n_{O^{2-}})_{T,P,n_j}$ is not independently variable due to the charge-balance constraint, and is not definable in conventional chemical thermodynamics where only temperature, pressure and composition are the variables. There is no implication in Eqn. (11) that a gas phase need be present, as $S_2$ and $O_2$ refer to the components of the system, which may be defined without specifying the phases in the system.

At equilibrium:

$$\mu_{MgS} - \tfrac{1}{2}\,\mu_{Mg_2SiO_4} = \tfrac{1}{2}\,RT\ln(fS_2/fO_2) - \tfrac{1}{2}\,\mu_{SiO_2} \qquad (12)$$

The evaluation of $\mu_{MgS}$ and $\mu_{Mg_2SiO_4}$ from Eqns. (7) to (9) gives:

$$\mu_{MgS} = \mu^o_{MgS} + \sum_{N\neq Mg}(-X_N^{cat} X_{SiO_4}^{an}\,\Delta\mu^o_{rec}[S-SiO_4]) + RT\ln(X_{Mg}^{cat}) + RT\ln(X_S^{an})$$
$$+ RT\ln(\gamma_{Mg}) + RT\ln(\gamma_S) \qquad (13)$$

This equation contains a term in $X_S^{an}$, which is the concentration of $S^{2-}$ in the melt expressed as a mole fraction. The term $\Delta\mu^o_{rec}[S-SiO_4]$ is the change in free energy of the homogeneous equilibrium in the melt; such equilibria are often known as reciprocal reactions:

$$\tfrac{1}{2}\,Mg_2SiO_4 + N_{2/z}S = MgS + \tfrac{1}{2}\,N_{4/z}SiO_4 \qquad (14)$$

$$\Delta\mu^o_{rec}[S-SiO_4] = (\mu^o_{MgS} - 1/2\,\mu^o_{Mg_2SiO_4}) - (\mu^o_{N_{2/z}S} - 1/2\mu^o_{N_{4/z}SiO_4}) \qquad (15)$$

Likewise for $\mu_{Mg_2SiO_4}$:

$$\mu_{Mg_2SiO_4} = \mu^o_{Mg_2SiO_4} + \sum_{N\neq Mg}(X_N^{cat} X_S^{an}\,\Delta\mu^o_{rec}[S-SiO_4]) + 2\,RT\ln(X_{Mg}^{cat}) + RT\ln(X_{SiO_4}^{an})$$
$$+ 2RT\ln(\gamma_{Mg}) + RT\ln(\gamma_{SiO4}) \qquad (16)$$

Substituting (12) to (15) into (11), putting $X_{SiO_4}^{an} = 1$ (that is, $X_S^{an}$ is small, and the $SiO_2$ units do not mix with the charged species $S^{2-}$ and $SiO_4^{2-}$ on the anion sublattice) and rearranging gives:

$$\ln X_S^{an} = \sum_M X_M^{cat}\,(\tfrac{1}{2}\,\mu^o_{M_{4/z}SiO_4} - \mu^o_{M_{2/x}S})/RT - \tfrac{1}{2}\ln a_{SiO_2}$$
$$- \ln\gamma_S + \tfrac{1}{2}\ln\gamma_{SiO4} + \tfrac{1}{2}\ln(fS_2/fO_2) \qquad (17)$$

This shows that the S content of the melt depends proportionally on $(fS_2/fO_2)^{1/2}$, as in the definition of the sulfide capacity, $C_{S^{2-}}$, in Eqn. (2). Eliminating the term in $(fS_2/fO_2)^{1/2}$ between (17) and (3) gives:

$$\ln C_{S^{2-}} = B_0^{S^{2-}} + c \ln a_{SiO_2} + \sum X_M B_M^{S^{2-}} \quad (18)$$

where the term $B_0^{S^{2-}}$ also accounts for the conversion from mole fractions on the anion sublattice to weight fractions (conveniently parts per million by weight, while $B_M^{S^{2-}} = k(\frac{1}{2}\mu^o_{M_{4/z}SiO_4} - \mu^o_{M_{2/x}S})/RT$, where $k$ is a constant, the same for all M. The activity coefficients, $\gamma_S$ and $\gamma_{SiO4}$, will for simplicity be assumed to vary only with the $M^{x+}$ cation fractions in the melt composition, but this is likely only within a limited range of melt compositions, say with NBO/T between 0.2 and 2, which covers most silicate melt compositions apart from the granite/rhyolite extreme. The average values of $\gamma_S$ and $\gamma_{SiO4}$ within this range are implicitly incorporated in the $B_0^{S^{2-}}$ term.

Equation (18) also contains a term in the activity of silica, $a_{SiO_2}$, which may be expected to be a function of the cation mole fractions in the melt. Assume that over a reasonably limited range of silicate melt compositions, it has the functional form $\ln (a_{SiO_2})^n = C_0 + X_M C_M$. This permits simplification, to Eqn. (6): $\ln C_{S^{2-}} = A_0^{S^{2-}} + \sum X_M A_M^{S^{2-}}$, where $A_0^{S^{2-}} = B_0^{S^{2-}} + C_0$, and $A_M^{S^{2-}} = B_M^{S^{2-}} + C_M$. In order to achieve a good fit to the data, the cations M include the usual ones that form the basic oxide components important in natural-composition silicate melts ($Na^{1+}$, $Mg^{2+}$, $K^{1+}$, $Ca^{2+}$, $Mn^{2+}$, and $Fe^{2+}$), but also $Al^{3+}$ and $Ti^{4+}$, whose structural positions in the melts are thought to be different, and in different ways (Mysen and Richet 2005). Si is not included in the sum of these M cations explicitly, because it is implicitly included from the closure condition, $\sum X_M = 1$. The mole fractions are defined on the single-cation basis ($NaO_{0.05}$, MgO, $AlO_{1.5}$, $SiO_2$, etc.), despite Eqns. (10) to (16) being developed with mole fractions on the single-anion basis; for some reason, this way gives a noticeably better fit.

The importance of this derivation of $C_{S^{2-}}$ from solution thermodynamics is that it establishes that the logarithm of the sulfide capacity $C_{S^{2-}}$ should vary linearly with the mole fractions. This

theoretical relationship was subjected to detailed experimental scrutiny by O'Neill and Mavrogenes (2002), who investigated nearly 200 different melt compositions covering various proportions of the above cations, with NBO/T ranging from 0 to 2 (the mean NBO/T of the compositions they measured is 0.85, with a standard deviation of 0.3), at 1400ºC. Such a high experimental temperature was necessary to access a wide range of melt compositions, and was not meant to mimic magmatic temperatures. The tests included experiments adding progressive amounts of one component to a base composition, the particularly important case being the addition of FeO to a $CaO$-$MgO$-$Al_2O_3$-$SiO_2$ composition, with results shown in Fig. 13 of O'Neill and Mavrogenes (2012). The reason that this example is so important is that it refutes the notion that there are thermodynamically relevant $Fe^{2+}$ - $S^{2-}$ "complexes" in the silicate melts. Rather, the simple log-linear Eqn. (7) performs well, except at very high FeO contents where FeO loses some of its potency for dissolving $S^{2-}$ (the opposite trend to that which would come from complex formation). This interesting phenomenon will be addressed further below.

The model may be tested from a different perspective, namely the magnitudes of the different $A_M^{S^{2-}}$ terms compared to those expected from standard thermodynamic data. An enabling assumption is that the $C_M$ terms used to parameterize $a_{SiO_2}$ are relatively small, such that neglecting them for the present exposition allows the approximation $A_M^{S^{2-}} \propto (\frac{1}{2}\mu^o_{M_{4/z}SiO_4} - \mu^o_{M_{2/x}S})/RT$, where the latter is the difference between the free energies of the orthosilicates and the sulfides. This is an important insight, because if this relationship is valid, it would enable estimates of the effects of melt composition on other "capacities" – sulfate, carbonate, phosphate, etcetera, providing a thermodynamically based alternative to other concepts like NBO/T or "optical basicity" that have been invoked to predict melt thermodynamic properties. The relationship is tested in Fig. 1, using the values of $A_M^{S^{2-}}$ from O'Neill and Mavrogenes (2002) plus that for $A_{Mn}^{S^{2-}}$ from Evans et al. (2008). For the free energies of formation of the orthosilicate and sulfide components, the data for the solid phases at 1400 K were used as a proxy for what is actually required, which is the free energies of the components in the liquid phase in silicate melts extrapolated to infinite dilution at the

415 temperature of interest (here 1673 K). At least this proxy has the merits of consistency for all
416 components. These data are from the JANAF tables (Chase et al. 1998) or Robie and Hemingway
417 (1995).

418 The reason for not trying to build a model from reaction (5), which may be a more realistic
419 approximation to the structure of most silicate melts of geological interest, is that the analogous
420 thermodynamic data for crystalline substances proxying for the $M^{2/x}Si_2O_5$ units are mostly not
421 available, and for the $Si_2O_6^{4-}$ dimer units in the melt (NBO/Si = 2), the equivalent crystalline
422 stoichiometry corresponds to that of the chain silicates (e.g., pyroxenes), which seems dubiously
423 appropriate as structural proxies. The orthosilicate stoichiometry has the same $SiO_4^{4-}$ structural units
424 in crystals as in melts.

425 There is a fair positive correlation (R = 0.80) between $A_M^{S^{2-}}$ and $(\frac{1}{2}\mu^o_{M_{4/z}SiO_4} - \mu^o_{M_{2/x}S})/1400R$.
426 O'Neill and Mavrogenes (2002) pointed out that there was no such correlation between the values
427 of $A_M^{S^{2-}}$ and the analogous terms $(\mu^o_{M_{2/z}O} - \mu^o_{M_{2/x}S})/RT$, indicating that the ability of a basic oxide
428 component $M_{x/2}O$ to contribute to the sulfide capacity of a silicate melt is lessened by the strength
429 of the chemical bonding of the $M^{x+}$ cation to the silicate units in the melt. Thus $Ca^{2+}$ is less effective
430 at enhancing $C_{S^{2-}}$ than $Fe^{2+}$ because $Ca^{2+}$ - $SiO_4^{4-}$ interactions are far stronger than $Fe^{2+}$ - $SiO_4^{4-}$
431 interactions in silicate melts, well known from the thermodynamics of the simple binaries CaO-
432 $SiO_2$ and FeO-$SiO_2$ (e.g., Mysen and Richet 2005).

433 This correlation also shows that the large magnitude of $A_{Fe}^{S^{2-}}$ relative to the other $A_M^{S^{2-}}$, except
434 $A_{Mn}^{S^{2-}}$, is not an anomaly, but is that expected from the reciprocal solution theory, given the relative
435 magnitudes of the free energies of formation of $Fe_2SiO_4$ and FeS. There is no reason to postulate
436 complexes between $Fe^{2+}$ and $S^{2-}$ in the silicate melts. The correlation predicts that the effects of $Ni^{2+}$
437 and $Cu^{1+}$ on $C_{S^{2-}}$ should be even larger than those of $Fe^{2+}$ and $Mn^{2+}$. Evans et al. (2008) found that
438 $A_{Ni}^{S^{2-}}$ and $A_{Cu}^{S^{2-}}$ could not be measured experimentally with available methods, because at the $fS_2$-
439 $fO_2$ conditions needed to achieve measurable $S^{2-}$ in the silicate melt, the Ni and Cu were stripped
440 out into immiscible sulfide melts. It is the same strength of the $Ni^{2+}$-$S^{2-}$ and $Cu^{1+}$-$S^{2-}$ chemical

441 bonding in the silicate melts compared to the rather feeble $Ni^{2+}$-$SiO_4^{4-}$ and $Cu^{1+}$-$SiO_4^{4-}$ bonding,
442 causing the large values of $A_{Ni}^{S^{2-}}$ and $A_{Cu}^{S^{2-}}$, that also causes the immiscible sulfide melts to form;
443 two sides of the same coin. The correlation in Fig. 1 suggests $A_{Ni}^{S^{2-}} \approx 30$ and $A_{Cu}^{S^{2-}} \approx 60$; to estimate
444 the latter the free energy of formation of the non-existent orthosilicate $Cu_4SiO_4$ from the oxides was
445 taken to be zero.

446 This information on the likely values of $A_{Ni}^{S^{2-}}$ and $A_{Cu}^{S^{2-}}$ is somewhat nugatory, as the stripping
447 out of Ni and Cu into a sulfide melt keeps Ni and Cu concentrations in the silicate melt to the $10^2$
448 ppm level, at which they have no discernible effect on $C_{S^{2-}}$ (Evans et al. 2008). Put another way,
449 the atomic ratios of Ni and Cu to Fe in terrestrial basalts are both about $10^{-3}$, therefore given these
450 values of $A_{Ni}^{S^{2-}}$ and $A_{Cu}^{S^{2-}}$, neglecting Ni and Cu has an equivalent effect to decreasing the
451 concentration of FeO in the silicate melt by 0.1 and 0.2 % relative, well below the best analytical
452 precision. The effect of Ni and Cu on SCSS is entirely through their obvious influence on the
453 activity of FeS in the sulfide melt. If NiO in the silicate melt has negligible effect on $S^{2-}$ solubility,
454 then the corollary is that $S^{2-}$ has negligible effect on the activity of NiO in the silicate melt, for
455 example, in the context of the partitioning of Ni between olivine and silicate melt. This point is
456 addressed in Tuff and O'Neill (2010).
457
458 *The $Fe^{3+}$ problem*

459 Given that the direct measurement of sulfide capacities requires knowing both $fO_2$ and $fS_2$, it
460 can be done most easily and also precisely at atmospheric pressure in gas-mixing experiments,
461 where the sum of the partial pressures of all gas species are limited to 1 bar. Unfortunately,
462 increasing $fO_2$ to where $Fe^{3+}/(Fe^{3+}+Fe^{2+})$ in the silicate melt is more than a couple of percent enters
463 the regime of the experimental S solubility minimum, where S solubilities fall below the limit of
464 quantification of the electron microprobe. Thus only the effect of $Fe^{2+}$ on $C_{S^{2-}}$ is known, and the
465 influence of $Fe^{3+}$ is currently completely mysterious. The correlation used to guestimate $A_{Ni}^{S^{2-}}$ and
466 $A_{Cu}^{S^{2-}}$ (Fig. 1) is useless, because thermodynamic data for the non-existent sulfide $Fe^{3+}S^{2-}_{1.5}$ are not

available, unsurprisingly. A couple of thoughts arise. One possibility is that the electron configurations of $Fe^{3+}$ is the same as that of $Mn^{2+}$ ($Ar3d^5$), and size differences between cations are less important in the environment of silicate melts where cation-anion interatomic distances are not influenced by crystal symmetries, suggesting that $A_{Fe^{3+}} \sim A_{Mn}$. As the latter is similar to $A_{Fe^{2+}}$ (Evans et al. 2008), changing $Fe^{3+}/(Fe^{3+}+Fe^{2+})$ would have no effect on $C_{S^{2-}}$. Alternatively, on the grounds that $Fe^{3+}$ may play a similar structural role to $Ti^{4+}$ in silicate melts, $A_{Fe^{3+}}$ may be similar to $A_{Ti}$, and increasing $Fe^{3+}/(Fe^{3+}+Fe^{2+})$ would decrease $C_{S^{2-}}$ accordingly. That changing the oxidation state of a key cationic component of a silicate melt may have a huge effect on $C_{S^{2-}}$ has been claimed for vanadium. Allertz et al. (2016) showed that increasing $fO_2$ by six orders of magnitude at 1600ºC increased $C_{S^{2-}}$ by over two orders of magnitude in CMAS-based melts with 3.6 to 9.5 wt% V; the increase is presumably due to the V changing from predominantly 2+ to predominantly 3+. Is V a trustworthy analogue for Fe?

*Sulfate capacities, $C_{SO_4^{2-}}$*

Following the same logic, the equilibrium between orthosilicate and framework structural units that defines the sulfate capacity, $C_{SO_4^{2-}}$, would be:

$$\underset{\text{sil melt}}{\tfrac{1}{2}\,SiO_4^{4-}} + \tfrac{1}{2}\,S_2 + 3/2\,O_2 = \underset{\text{sil melt}}{SO_4^{2-}} + \underset{\text{sil melt}}{\tfrac{1}{2}\,SiO_2} \qquad (19)$$

This suggests that the dependence of $C_{SO_4^{2-}}$ on silicate melt composition should take the same form as that for $C_{S^{2-}}$, namely:

$$\ln C_{SO_4^{2-}} = A_0^{SO_4^{2-}} + \sum X_M A_M^{SO_4^{2-}} + \qquad (20)$$

where $A_0^{SO_4^{2-}} = B_0^{SO_4^{2-}} + C_0$, $A_M^{SO_4^{2-}} = B_M^{SO_4^{2-}} + C_M$, with $B_M^{SO_4^{2-}} = k(\frac{1}{2}\mu^o_{M_{4/z}SiO_4} - \mu^o_{M_{2/x}SO_4})/RT$.

The difference between the coefficients for of each M cation for $C_{SO_4^{2-}}$ and $C_{S^{2-}}$ is therefore:

$$A_M^{SO_4^{2-}} - A_M^{S^{2-}} = k(\mu^o_{M_{2/x}S} - \mu^o_{M_{2/x}SO_4})/RT \qquad (21)$$

In taking the difference, most of the approximations used in deriving the individual values of $A_M^{S^{2-}}$ and $A_M^{SO_4^{2-}}$ would cancel out, like the effect of the activity of silica. This then further suggests that the dependence of $C_{SO_4^{2-}}$ on silicate melt composition could be predicted from the experimental measurements on $C_{S^{2-}}$, together with the readily available standard-state thermodynamic data on sulfates and sulfides.

The ratio of sulfide to sulfate dissolved in a silicate melt follows from the definitions of $C_{S^{2-}}$ and $C_{SO_4^{2-}}$ :

$$[SO_4^{2-}]/[S^{2-}] = C_{SO_4^{2-}}/C_{S^{2-}}\ (fO_2)^2 \qquad (22)$$

The $fO_2$ at which $[SO_4^{2-}]/[S^{2-}]$ is 1, denoted here as $(fO_2)_{S6+/S2-}$, is therefore $(C_{S^{2-}}/C_{SO_4^{2-}})^{1/2}$. For present purposes, the anion complex $SO_4^{2-}$ may be taken as equivalent to $S^{6+}$. Substituting Eqns. (7) and (20) into (22) gives:

$$\ln([SO_4^{2-}]/[S^{2-}]) = +2 \ln fO_2 + (A_0^{SO_4^{2-}} - A_0^{S^{2-}}) + \sum X_M (A_M^{SO_4^{2-}} - A_M^{S^{2-}}) \qquad (23)$$

where the effect of silicate melt composition is contained in the last term on the right-hand side, whose thermochemical significance is given by Eqn. (21).

From this, it may be predicted that, at a given T, P and $fO_2$, increasing FeO in the melt would increase $(fO_2)_{S6+/S2-}$, while increasing CaO and $Na_2O$ would decrease $(fO_2)_{S6+/S2-}$.

The value of $(fO_2)_{S6+/S2-}$ is not well constrained for anhydrous basaltic melts. The inescapable experimental problem is that it falls in the region of the ambient-pressure experimental S solubility minimum. It has been approximately located at about the $fO_2$ of the quartz-fayalite-magnetite equilibrium (QFM) by Fincham and Richardson (1954) and Katsura and Nagashima (1974) from extrapolation of solubilities measured at higher and lower $fO_2$. (Oxygen fugacities are conveniently discussed relative to some isobarically invariant "buffer" such as QFM because condensed-phase redox equilibria all tend, to a first approximation, to have similar slopes in 1/T-log $fO_2$ space. For reference, QFM is given by $\log_{10} fO_{2(QFM)} = 8.58\text{-}25050/T$ at 1 bar (O'Neill 1987), and $\Delta QFM = \log_{10}(fO_2/fO_{2(QFM)})$).

516 Recently this approach has been expanded upon by Nash et al. (2019), who exploited the lower
517 limits of detection afforded by SIMS to investigate the solubilities of S in the region of the
518 solubility minimum. Their experiments were at 1300ºC, and used CO-$CO_2$-$SO_2$ gas mixes. They
519 assumed that total S solubilities at higher $fO_2$ in excess of those predicted for $S^{2-}$ from the Fincham-
520 Richardson relation at low $fO_2$, were due to additional $S^{6+}$. This they corroborated by S K-edge
521 XANES spectroscopy. They found that values of $(fO_2)_{S6+/S2-}$ for six melt compositions lay in the
522 range ΔQFM 0 to +0.6, concordant with the earlier studies. Increasing $(fO_2)_{S6+/S2-}$ correlated
523 qualitatively with increasing FeO in the melt, although the effect was smaller than expected from
524 the sensitivity of $C_{S^{2-}}$ to FeO (O'Neill and Mavrogenes 2002).

525 Other information on where $(fO_2)_{S6+/S2-}$ lies in silicate melts comes from X-ray spectroscopic
526 characterization of $S^{6+}/S^{2-}$ in quenched glasses prepared under pressure, and necessarily containing
527 $H_2O$ in order to control $fO_2$. These measurements have been problematic because of beam-damage
528 issues, see Wilke et al. (2008, 2011), Métrich et al. (2009) and Jugo et al. (2010). The majority view
529 is that $S^{4+}$ (that is, sulfite, $SO_3^{2-}$) found spectroscopically by XANES is caused by beam damage, at
530 least in glasses of low-pressure provenance (both natural and synthetic). The probability is that most
531 X-ray fluorescence measurements of S oxidation state obtained with the electron microprobe are
532 badly affected by beam damage (Wilke et al. 2008), but because this technique only gives the
533 average oxidation state of S, $S^{4+}$ is not itself distinguished (unlike with XANES), making it difficult
534 to judge exactly what is going on. Because of this knowledge gap, the test for beam damage is
535 whether the measured $S^{6+}/S^{2-}$ follows the theoretical dependence on $(fO_2)$, which is that $[S^{6+}]/[S^{2-}]$
536 $\propto (fO_2)^2$ (Eqn. 22), provided that the assumption of negligible $S^{4+}$ is accepted. At present, among
537 studies that cover a sufficiently meaningful range of $fO_2$, the only experiments to pass this test to
538 date are those of Jugo et al. (2010) and Botcharnikov et al. (2011), who used XANES to quantify
539 $S^{6+}/\sum S$ in a series of glasses quenched from hydrated basaltic and andesitic melts with about 5 wt%
540 $H_2O$ at 1050ºC and 0.2 GPa, and those of Nash et al. (2019), described above. Jugo et al. (2010)

fitted their results to an equation with the stoichiometry of the speciation constrained at the theoretical value:

$$S^{6+}/\sum S = 1/(1 + 10^{(2.1-2\ \Delta QFM)}) \quad (24)$$

Hence $(fO_2)_{S6+/S2-}$ is at ΔQFM+1.05. Botcharnikov et al. (2011) then found that this equation described their results on their andesitic composition within uncertainty.

For comparison, the change in oxidation state of the main redox-variable element in basalts, Fe, given by Berry et al. (2018) is:

$$Fe^{3+}/\sum Fe = 1/(1 + 10^{(1.0575-0.25\ \Delta QFM)}) \quad (25)$$

The relationship between $S^{6+}/\sum S$ and $Fe^{3+}/\sum Fe$ from combining these two equations to eliminate ΔQFM is shown in Fig. 2. On the face of it, the range of $Fe^{3+}/\sum Fe$ measured in MORB glasses coincides with $S^{6+}/\sum S$ going from zero to as much as 30%, but this depends on the rather dubious equivalence between hydrated basalts at 1050ºC and the natural MORB glasses, which are quenched from ~ 1200ºC and contain little $H_2O$ (see below).

A different view emerges from the recent study of Nash et al. (2019), who calculated $Fe^{3+}/Fe^{2+}$ for the experiments at 1300ºC in which they had estimated $S^{6+}/S^{2-}$ (as described above), and also for those of Jugo et al. (2010) and Botcharnikov et al. (2011) at 1050ºC. They then fitted these data to an expression also constrained to the theoretical stoichiometry, which included a dependence on temperature. To constrain this latter variable better (given that the available data are from only two temperatures and those at 1050ºC are hydrous melts) they invoked thermochemical data for crystalline-phase analogues of the melt components. As regards the effect of melt composition, their data were too scattered to resolve any (see their Fig. 6). The relationship between $S^{6+}/\sum S$ and $Fe^{3+}/\sum Fe$ from their equation, calculated at 1190º (the average for anhydrous MORB glasses in equilibrium with olivine according to the magmathermometer of Putirka 2008), is also shown in Fig. 2. With their formulation, even the more oxidized MORB glasses would contain only a few percent $S^{6+}/\sum S$. As will be shown below, the evidence from the SCSS of MORB glasses is more concordant with this view.

567 The temperature-dependence of S speciation relative to QFM in silicate melts remains
568 somewhat contentious. Nash et al. (2019) inferred that decreasing temperature shifts $(fO_2)_{S6+/S2-}$ to
569 higher ΔQFM (i.e., decreasing temperature stabilizes $S^{2-}$ relative to $S^{6+}$ at a given ΔQFM), which is
570 in the opposite direction to that anticipated by Métrich et al. (2009). That $S^{6+}$ forms an anionic
571 complex, $SO_4^{2-}$, may seem at first sight to endow this speciation with low configurational entropy,
572 but as the effects of entropy are always relative, the entropies of the alternative arrangements need
573 to be considered. Assuming the same orthosilicate and framework species as for modeling of $C_{S^{2-}}$,
574 the two alternatives for redox speciation in a melt containing both Fe and S could be described by
575 the homogeneous equilibrium:

576 $$S^{2-} + 8\ Fe^{3+} + 2\ SiO_4^{4-} = SO_4^{2-} + 8\ Fe^{2+} + 2\ SiO_2 \quad (26)$$

577 From the point of view of configurational entropy, both sides of this reaction contain the same
578 number of species, but two of the 11 species on the right-hand side (RHS) are polymerized $SiO_2$
579 units in the melt, which might be expected to have lower entropy, implying that the speciation
580 might proceed towards the RHS with decreasing temperature.

581 The experiments of Luhr (1990) on sulfur solubilities in hydrous melts as a function of
582 temperature and $fO_2$ (at 0.2 and 0.4 GPa) show that at 900ºC and above, total S in the oxidized
583 experiments was higher than experiments at QFM (see Fig. 10 of Luhr 1990), whereas at 800 and
584 850ºC it was the same in the oxidized experiments as in the pyrrhotite-saturated experiments at
585 QFM. This is suggestive that, contrary to the entropy argument, increasing temperature favours the
586 RHS of reaction (26), but it is not definitive as the oxidized experiments did not contain pyrrhotite.

587 The isochemical redistribution of species according to reaction (26) involves only electron
588 hopping between atoms with coordination changes on the scale of interatomic distances, and is
589 therefore likely very fast, arguably so fast as to be unquenchable from liquidus temperatures (cf.
590 Berry et al. 2003). If the right-hand side of (26) were favoured on cooling (the opposite to the
591 inference from the experiments of Luhr 1990), it might explain the small amounts of sulfate

identified by XANES spectroscopy in some natural basaltic glasses (Métrich et al. 2009; Jugo et al. 2010).

The only available indication of the effect of pressure on the $S^{2-}/SO_4^{2-}$ transition is the study of Matjuschkin et al (2016), which indicates that increasing pressure may move $(fO_2)_{6+/2}$ to higher $\Delta$QFM. Measurements of $S^{6+}/\sum S$ and $Fe^{3+}/\sum Fe$ on the same melt compositions over a range of $fO_2$ (probably from QFM-1 to QFM+2) as a function of temperature and pressure are much needed. But this is a formidable experimental challenge.

*Other capacities for anions and anion complexes in silicate melts*

The "capacity" idea could be extended to other anionic substitutions in silicate melts, for example, $CO_2$ dissolving as carbonate, $CO_3^{2-}$:

$$\underset{\text{sil melt}}{\tfrac{1}{2}\ SiO_4^{4-}} + CO_2 = \underset{\text{sil melt}}{CO_3^{2-}} + \underset{\text{sil melt}}{\tfrac{1}{2}\ SiO_2} \quad (27)$$

for which the carbonate capacity would be given by:

$$C_{CO_3^{2-}} = [CO_3^{2-}]fCO_2 \quad (28)$$

with $A_0^{CO_3{}^{2-}} - A_M^{S^{2-}} = k(\mu^o_{M_{2/x}S} - \mu^o_{M_{2/x}CO_3})/RT$. Likewise, to predict the effect of composition on chlorine in silicate melts, which is difficult to measure experimentally because $Cl_2$ gas volatilizes most of the oxide components in one-atmosphere experiments, the chloride capacity would be defined as:

$$\underset{\text{sil melt}}{1/4\ SiO_4^{4-}} + \tfrac{1}{2}\ Cl_2 = \underset{\text{sil melt}}{Cl^-} + \underset{\text{sil melt}}{1/4\ SiO_2} + \tfrac{1}{4}\ O_2 \quad (29)$$

$$C_{Cl^-} = [Cl^-](fCl_2)^{1/2}(fO_2)^{1/4} \quad (30)$$

and $A_0^{Cl^-} - A_M^{S^{2-}} = k(1/2\mu^o_{M_{2/x}S} - \mu^o_{M_{1/x}Cl})/RT$.

A suggestion to relate the various "capacities" of silicate melts to one another was made by Carl Wagner in one of his last contributions (Wagner 1975). Wagner, who has been called the "Father of Solid-state Chemistry" (Martin 2001), defined a "basicity" for a silicate melt of a specified composition using carbonate capacities:

$$B_{carb} = C_{CO_3^{2-}}/C^*_{CO_3^{2-}} \quad (31)$$

where $C^*_{CO_3^{2-}{}_C}$ is the carbonate capacity of a reference melt (he suggested one with composition 0.4 CaO, 0.4 $SiO_2$ and 0.2 $Al_2O_3$). Wagner (1975) also discusses how such a definition of "basicity" for a silicate melt provides a more rational measure than the "activity" of $O^{2-}$, which, despite its appearance as a "structural element" in definitions of capacities like Eqn (2), is not, as Wagner pointed out, a usefully definable quantity, thermodynamically.

Wagner (1975) then proposed that the capacities of other anionic species $Z^{n-}$ (e.g., $S^{2-}$, $SO_4^{2-}$, $Cl^-$ among many others) could be related to this basicity by:

$$C_{Z^{\nu-}} = C^*_{Z^{\nu-}} (B_{carb})^{2/\nu} \quad (32)$$

One of the benefits of deriving the thermochemical meaning of these "capacities" from reciprocal solution theory with mixing on sublattices is that it goes straight to the heart of the problem with Wagner's suggestion (which he alluded to himself): it implicitly assumes that the quantities $(\frac{1}{2}\mu^o_{M_{4/z}SiO_4} - \mu^o_{M_{\nu/x}Z})$ are the same for all anionic species Z, and for all relevant elements M. A few minutes perusing a thermochemical database would reveal that this is obviously not the case. The escape clause is that in a majority of basic slag compositions these M cations are dominated by only two, namely Mg and Ca, and it is possible to get away with taking the difference $[(\mu^o_{Ca_{\nu/x}Z} - \mu^o_{Mg_{\nu/x}Z})$ as being constant within limited horizons. Looking a bit further, it is the great stability of the FeS component in silicate melts compared to MgS or CaS (cf. $FeCO_3$ compared to $CaCO_3$ or $MgCO_3$), with the consequence for sulfide capacities, that provides the exception disproving this rule handsomely – although MnS would do as well as FeS.

**A new parameterization of sulfide capacity for basaltic melts**

From the point of view of reproducing the experimental data, there are nevertheless a few ad-hoc "improvements" that can be made to the simple relationship of Eqn. (7), albeit at the cost of divorcing the parameters $A_M^{S^{2-}}$ from their thermochemical roots. O'Neill and Mavrogenes (2002)

644 showed that adding a cross term in $X_{Fe}X_{Ti}$ is needed to account for $Fe^{2+}$ - Ti interactions in the melt
645 (see Fig. 14 of O'Neill and Mavrogenes 2002). Smythe et al. (2017) suggested a similar cross-term
646 in $X_{Fe}X_{Si}$, and in the fitting to be described below, it was confirmed that this term was very
647 effective at improving the fit of the experimental data.
648 A well known but hitherto unaddressed problem is that the linear relationship between ln $C_{S^{2-}}$
649 and the cation mole fractions $X_M$ breaks down is at high FeO contents, between 15 and 20 wt% FeO
650 according to O'Neill and Mavrogenes (2002). This phenomenon has been confirmed by several
651 studies on SCSS (see section below). The deviation is in the direction of lower $S^{2-}$ in the silicate
652 melt than the linear relationship established at < 15 wt% FeO would predict, the opposite to that
653 expected from formation of $Fe^{2+}$ - $S^{2-}$ complexes. The deviation becomes noticeable at $S^{2-}$
654 concentrations that are relatively low compared to those of $Fe^{2+}$, for example at ~ 3500 ppm S in
655 melt at 20 wt% FeO, which in molar proportions of S to FeO is still only less than 1 to 10 (see
656 Table 13 of O'Neill and Mavrogenes 2002). Other experiments on Fe-free compositions with high
657 CaO exceed this $S^{2-}$ content with no such deviations apparent (e.g., nearly 6000 ppm dissolve in the
658 AD+Wo composition run 17/2/97 in Table 2 of O'Neill and Mavrogenes 2002), indicating,
659 importantly, that the Fe problem is not due to the assumption of constant "activities" of "structural
660 elements" like $O^{2-}$ breaking down in the derivation of Eqn. 3. Another curious feature is that the
661 change of $C_{S^{2-}}$ with $X_{Fe}$ is linear within experimental uncertainty up to ~ 15 wt% FeO, but then
662 breaks sharply to a different linear trend of ln $C_{S^{2-}}$ vs $X_{Fe}$ (see Fig. 15 of O'Neill and Mavrogenes
663 2002).
664 This is a peculiar phenomenon, for which there is no explanation at present, and more
665 experimental information would be useful. There seem to be no experiments that have tested the
666 Fincham-Richardson relationship in high FeO melts; for example, it would be interesting to
667 measure $C_{S^{2-}}$ at various $fO_2$ and $fS_2$, on a composition with, say, 30 wt% FeO in the melt. The
668 propensity for high FeO, high $S^{2-}$ melts to exsolve FeS-rich sulfide microblobs on quenching
669 despite using the standard rapid-quenching techniques (Métrich et al., 2009; Wykes et al. 2015), has

so far prevented obtaining samples suitable for spectroscopy (Métrich et al, 2009). The departure from the simple theory at high FeO has hindered applying sulfide solubility models to many extraterrestrial basalts, which often have FeO > 15 wt%. In view of the lack of theoretical insight but the need for something to be done, it seems expedient to forgo a thermodynamically based model, and find a parameterization of $C_{S^{2-}}$ as a function of melt composition that includes FeO-rich basaltic melts. The shape of the departure from linearity suggests the arctangent function or the error function; the latter was used here. With these three additions to the simple Eqn. (7), all the data from O'Neill and Mavrogenes (2002), including the high FeO compositions, plus those at 1400ºC from Tuff and O'Neill (2010), were fitted by weighted least squares regression. The function minimized was $[(\ln (C_{S^{2-}})_{obs} - \ln (C_{S^{2-}})_{calc})/s(\ln C_{S^{2-}})]^2$, where the weight $s(\ln C_{S^{2-}})$ was obtained by propagating the uncertainty in measured S, $s([S]_{obs})$ as observed, or 3%, whichever was larger, plus uncertainties in log $fO_2$ and log $fS_2$ of 0.05 each. Typically $s(\ln C_{S^{2-}})$ is about 0.1 (that is, 10%), except for experiments with very low S contents (< 500 ppm), which may have substantially larger uncertainties, and the 12 CMAS and one CMAS+Ti compositions from Table 1 of O'Neill and Mavrogenes (2002), in which the multiple measurements produce a lower uncertainty of 0.03 to 0.05. The regression gave:

$$\ln C_{S^{2-}}(1673K, 1\ bar) = -5.330 + 6.7\,(X_{Na}+X_K) + 1.8\,X_{Al} + 4.9\,X_{Mg} + 8.1\,X_{Ca} + 5.0\,X_{Ti} + 8.9\,X_{Fe^*} - 22.2\,X_{Fe^*}X_{Ti} + 7.2\,X_{Fe^*}X_{Si} - 2.06\,\mathrm{erf}(-7.2\,X_{Fe^*}) \quad (33)$$

where $X_{Fe^*}$ is $(X_{Fe} + X_{Mn})$, and mole fractions are defined on the single cation basis ($NaO_{0.05}$, MgO, $AlO_{1.5}$, $SiO_2$, etcetera). The agreement between the parameterization and the input data (n = 228) is shown in Fig. 3a. The reduced chi-squared ($\chi^2_\nu$) is 1.2, indicating a good fit to the data, apart from two CMAS compositions. One is the CMAS7E composition from Table 1 of O'Neill and Mavrogenes (2002). It is a challenge to model the compositional dependence of $C_{S^{2-}}$ for the twelve CMAS compositions from that Table, because of the small uncertainty in $C_{S^{2-}}$ that comes from the multiple experiments (10 or 12 on each composition). Whilst this challenge is mostly met, the misfit to CMAS7E is a notable failure. The parameterization also fails to fit an anomalous datum from

696 Tuff and O'Neill (2010), N81B1, which was discussed in that paper. Due to the large number of
697 data, these two outliers have negligible effect, but they were removed from the fitting procedure
698 anyway.
699
700 *Temperature dependence of* $C_{S^{2-}}$
701 Because the compositional terms come from reciprocal reactions, they are likely to be
702 dominated by enthalpy changes, hence the form of the parameterization for other temperatures is
703 proposed to be:
704 $$\ln C_{S^{2-}}(T, 1\ \text{bar}) = A^H/T + A^S + (1673/T)\,[6.7\,(X_{Na}+X_K) + 1.8\,X_{Al} + 4.9\,X_{Mg} + 8.1\,X_{Ca}$$
705 $$+ 5.0\,X_{Ti} + 8.9\,X_{Fe^*} - 22.2\,X_{Fe^*}X_{Ti} + 7.2\,X_{Fe^*}X_{Si}] - 2.06\,\text{erf}(-7.2\,X_{Fe^*}) \qquad (34)$$
706 where $A_0 = A^H/T + A^S$. With $(A^H/1673 + A^S)$ constrained to -5.330 to meld with the 1400ºC fit,
707 these parameters were evaluated to be $A_H = -23590$ and $A_S = 8.77$, obtained as follows.
708 The experimental study of Haughton et al. (1974), being ambitious in scope, has had much
709 influence on previous petrologically focused reviews of the behavior of $S^{2-}$ in silicate melts
710 (Poulson and Ohmoto 1990; Wallace and Carmichael 1992; Ariskin et al. 2013). The study
711 consisted of 100 experiments at 1200ºC, divided into two groups: Series I experiments (n = 37)
712 investigated a single base composition at different $fO_2$ and $fS_2$, with the composition varied in its
713 FeO from addition of $Fe_2O_3$ and/or separation of immiscible sulfide. Their Series II experiments (n
714 = 63) investigated different starting compositions at the same $fO_2$ and $fS_2$, with all compositions
715 designed to be saturated FeS-rich melt. As pointed out in O'Neill and Mavrogenes (2002), their
716 results show a lot of scatter. For example, replicate experiments agree poorly, and the results of the
717 Series I experiments are incommensurate with those of Series II. Two causes are likely,
718 equilibration problems and difficulties analyzing S at relatively low levels by electron microprobe.
719 The silicate melts were held in alumina crucibles, which results in continuous reaction with the
720 crucible during the experiment, because the original melt compositions are not saturated in alumina.
721 This effect also biases the melt compositions studied to high $Al_2O_3$. In addition, some precipitation

722 of FeS during the quenching might be anticipated, given the relatively slow quenching rates
723 possible with the alumina crucibles. The S content in one experiment in Series I, 4F1, which was
724 run at a higher $fO_2$ than any other experiment in the study, was reported at 270 ppm, which,
725 although low, is far higher than any value that would reasonably be expected for any extrapolation
726 (< 50 ppm), attesting to analytical difficulties. The scatter of the data has meant that attempts to
727 parameterize the results of Haughton et al. (1974) have led to complicated scenarios involving
728 hypothetical Fe-S species or complexes in the silicate melt (Poulson and Ohmoto 1990; Ariskin et
729 al. 2013), or to the idea that SCSS varies with $fO_2$ and $fS_2$ at constant melt composition (Wallace
730 and Carmichael 1992), which it does not, apart from second order effects like changing $Fe^{3+}/Fe^{2+}$
731 (Mavrogenes and O'Neill 1999). These points are discussed further below. Here, the results of
732 Haughton et al. (1974) were used only to obtain an estimate of $A_0$ at 1200ºC. To do this, both series
733 were fitted to Eqn. (34), with the result shown in Fig. 3b. Together with some additional
734 information from the author's own preliminary results at 1300ºC and 1500ºC, these results were
735 used to estimate $A_H$ = -23590 and $A_S$ = 8.77.
736 More data over a wider range of temperatures are needed to decrease the considerable
737 uncertainty on these values. The effects of pressure and volatile contents (with $H_2O$ of particular
738 interest) on $C_{S^{2-}}$ cannot at present be measured to useful accuracy by existing experimental
739 methods directly, but their contributions to SCSS is accessible experimentally and will be reviewed
740 below.
741
742 **Sulfide content at sulfide saturation (SCSS)**
743 The term "sulfur content at sulfide saturation", meaning the amount of sulfur dissolved in a
744 silicate melt in equilibrium with a sulfide phase (usually but not necessarily a FeS-rich sulfide
745 melt), and acronymed as SCSS, was introduced by Shima and Naldrett (1975). Because some non-
746 negligible proportion of the sulfur dissolved in silicate melts in equilibrium with some sulfides will
747 be $SO_4^{2-}$ towards the high end of the range of oxygen fugacities of natural magmas, and there are

possibly other S species present at high pressure or hydrous melts (for example $HS^-$), the quantity is less ambiguously labelled "sulfide content at sulfide saturation". This is the meaning of SCSS that will be used here.

The equilibrium between a silicate melt and a sulfide matte (Eqn. 1) gives the relationship:

$$-\Delta G^{o}_{FeO-FeS}/RT = -\ln a^{sil\ melt}_{FeO} + \ln a^{sulf}_{FeS} + \ln (fO_2/fS_2)^{1/2} \quad (35)$$

Substituting Eqn. (3), the definition of $C_{S^{2-}}$, into (35) to eliminate $(fO_2/fS_2)$ gives:

$$\ln [S]_{SCSS} = \Delta G^{o}_{FeO-FeS}/RT + \ln C_{S^{2-}} - \ln a^{sil\ melt}_{FeO} + \ln a^{sulf}_{FeS} \quad (36)$$

Therefore, SCSS depends on four quantities:

1) the standard state free energy of the reaction (1), $\Delta G^{o}_{FeO-FeS}$, which is the difference between the two free energies of formation from the elements:

$$\underset{\text{solid}}{Fe} + \tfrac{1}{2}\, O_2 = \underset{\text{sil melt}}{FeO} \quad (37)$$

$$\underset{\text{solid}}{Fe} + \tfrac{1}{2}\, S_2 = \underset{\text{sulf melt}}{FeS} \quad (38)$$

The free energy of reaction (37), $\Delta G^{o,sil\ melt}_{FeO}$, is taken from Holzheid et al. (1997), who combined the data for crystalline but non-stoichiometric "FeO" in equilibrium with Fe metal from O'Neill and Pownceby (1994) with those for the melting of FeO from Barin (1989), which gave:

$$\Delta G^{o,sil\ melt}_{FeO}\ (J\ mol^{-1}) = -244118 + 115.559\ T - 8.474\ T \ln(T) \quad (39)$$

The data for $\Delta G^{o,sulf\ melt}_{FeS}$ are less accurately known, with different assessments or tabulations of thermodynamic data differing by up to 10 kJ $mol^{-1}$ at relevant temperatures, reflecting different measurements reported in the literature, see Waldner and Pelton (2005) for a review. Here it was assumed that $\Delta G^{o,sulf\ melt}_{FeS} = \Delta H^{o}_{FeS} - T\ \Delta S^{o}_{FeS}$, with the values of $\Delta H^{o}_{FeS}$ and $\Delta S^{o}_{FeS}$ to be optimized in the fitting. Whether these optimized values fall within the range of experimentally measured values provides a critical test of the modelling. The effect of pressure on $\Delta G^{o,sulf\ melt}_{FeS}$ could in principle be evaluated from the partial molar volumes of FeO in silicate melts (Lange and Carmichael 1990) and of FeS in sulfide melts (e.g., Kress et al. 2008). However, for the purpose of calculating SCSS this information is insufficient because the effects of pressure on the other quantities in Eqn. (36) are not

775 known. Henceforward the effects of pressure will be regarded as having to be parameterized
776 empirically from the SCSS data.
777 2) The sulfide capacity $C_{S^{2-}}$ has been evaluated above as a function of composition and
778 temperature, however, its pressure dependence, and the compositional effects of $H_2O$ and other
779 volatile species, remain unknown. An hypothesis to explain the currently available experimental
780 data on the effect of $H_2O$ on SCSS will be proposed later, but first only supposedly anhydrous
781 experiments will be considered.
782 3) The activity of FeO in silicate melts is related to its mole fraction by $a_{FeO}^{sil\ melt} = X_{FeO}^{sil\ melt}$
783 $\gamma_{FeO}^{sil\ melt}$. The activity coefficients, $\gamma_{FeO}^{sil\ melt}$, have been measured by equilibration with Fe metal
784 according to reaction (37) at atmospheric pressure, using gas-mixing methods, from 1150 to
785 1500ºC. The upper temperature limit is an experimental one, set by the melting point of Fe metal
786 (1538ºC). Achieving good accuracy is relatively easy in such measurements compared to most
787 matters in the world of experimental petrology, and studies on silicate melts with compositions of
788 geological relevance are available from Roeder (1974), Doyle and Naldrett (1986), Doyle (1988,
789 1989), O'Neill and Eggins (2002), Borisov et al. (2004, 2006) and Borisov (2007). In addition,
790 Holzheid et al. (1997) obtained measurements in equilibrium with Fe-Ni-Co alloys. These studies
791 provide over 600 experimental observations, dominated by the Doyle datasets (512 data, all at
792 1327ºC), but the coverage of melt composition is not even. Although the Doyle opus is of great
793 value, it does show a marked predilection for melts high in K, also in Ti, an aversion to Na, and
794 almost a dismissal of Mg; in fact, high MgO compositions are generally lacking in all the studies,
795 and high $SiO_2$ compositions, such as relevant to rhyolites (say, $X_{SiO2} > 0.65$), are not represented at
796 all. On the plus side, there is good agreement among all these studies, as noted by O'Neill and
797 Eggins (2002), and by Borisov (2007). When referenced to the standard state of Eqn. (37), the
798 experimental data show that $\gamma_{FeO}^{sil\ melt}$ varies between 0.7 and 2 for most compositions (e.g., Fig. 4).
799 Although this is a relatively small variation compared to activity coefficients of other oxide
800 components in silicate melts (O'Neill and Eggins 2002; Wood and Wade 2013), this factor of three

maps on to a factor of three for $[S]_{scss}$ (Eqn. 36). It therefore needs to be taken into account, by parameterizing $\gamma_{FeO}^{sil\,melt}$ as a function of melt composition and temperature. The experimental observations show that $\gamma_{FeO}^{sil\,melt}$ increases with alkali content (Na and K), and decreases with Ti, with a minimum in plots against $X_{SiO2}$ near 0.55 (O'Neill and Berry 2006; Borisov 2007). As well as reproducing these features, a parameterization needs to ensure that $\gamma_{FeO}^{sil\,melt} \rightarrow 1$ as $X_{FeO} \rightarrow 1$. To take these factors into account, the experimental data were fitted to the equation:

$$RT \ln \gamma_{FeO}^{sil\,melt} = (1\text{-}X_{FeO})^2 [W_0 + W_{Mg}X_{MgO} + W_{Ca}X_{CaO} + W_{Na}X_{NaO1.5} + W_{K}X_{KO1.5} + W_{Ti}X_{TiO2}] + (1\text{-}X_{FeO}) [U_1X_{SiO2} + U_2(X_{SiO2})^2] \quad (40)$$

(the W terms are not Margules coefficients, just ad-hoc parameters). All the experimental data were recalculated to the same standard state using Eqn. (37), with all compositions converted to mole fractions on the single-cation basis. An initial best fit was obtained, but to aid internal consistency a further refinement was done in conjunction with the fitting of the SCSS data, see below.

4) The activity of FeS in sulfide melts presents a somewhat different problem to that of FeO in silicate melts, simply because FeS will be the dominant component in the envisaged applications of Eqn. (36). For example, in Ocean Floor Basalts, $X_{FeO}$ is only about 0.1, whereas $a_{FeS}^{sulf}$ varies from about 0.7 to 0.9 (see below). The contributing factors are dilution by O substituting for S, and, in part of the experimental database but ubiquitously in natural systems, dilution by other chalcophile elements, of which Ni and Cu are predominant in nature. There is continuous miscibility between liquid FeS and liquid Fe above the melting point of the latter (e.g., Waldner and Pelton 2005), such that with decreasing $fO_2$, and/or decreasing $fS_2$, Fe-S melts become increasingly metal-rich (Fe/S > 1). However, below Fe/S = 1, the contours of $fS_2$ vs. mole fraction of FeS on the join Fe-FeS are quite flat (Waldner and Pelton, their Fig. 5), indicating, incidentally, that liquid immiscibility would develop at lower temperatures, were it possible to undercool Fe-S melts. Hence $a_{FeS}^{sulf}$ is rather insensitive to changes to composition in this range. For example, Mavrogenes and O'Neill (1999) calculated that $a_{FeS}^{sulf}$ was ~ 0.5 in sulfide melts in their experiments in the limiting case of equilibrium with solid Fe metal (see also Ballhaus et al. 2017). Sulfide melts with large metal

827 excesses (Fe/S >> 1) were not included in the experimental database considered here, so this aspect
828 of the $a_{FeS}^{sulf}$ problem was ignored.

829 The amount of oxygen dissolved in liquid sulfide mattes is a function of $fO_2$, $fS_2$, and both Ni
830 and Cu contents, and temperature (Fonseca et al. 2008), indicating considerable complexity.
831 However, switching from system variables ($fO_2$, $fS_2$) to focus on the composition of a coexisting
832 silicate melt suggests that the equilibrium between silicate and sulfide melts may be:

833 $$\underset{\text{sil melt}}{FeO} = \underset{\text{sulf melt}}{FeO} \quad (41)$$
834

835 Hence the amount of the FeO component in the sulfide matte should vary with $a_{FeO}^{sil\ melt}$. Kiseeva
836 and Wood (2013) showed that on a mole fraction basis, $X_{FeO}^{sulf} \simeq X_{FeO}^{sil\ melt}$, which is confirmed
837 here, more-or-less, from the data used in the SCSS fitting that reported oxygen contents of the
838 sulfide melt, although there is considerable scatter (Fig. 5). Measuring the oxygen content of sulfide
839 melts is difficult, because of the complex textures produced on quenching (Kress 1997; Fonseca et
840 al. 2008), and the task is made harder when silicate melt is present, because this phase provides a
841 refuge for oxygen fleeing the sulfide melt during its crystallization on quenching.

842 For Ni and Cu, it has been proposed from available partitioning data that these elements may be
843 treated as inert diluents (Smythe et al. 2017). By this hypothesis, $a_{FeS}^{sulf}$ may be approximated in
844 sulfide mattes that are not metal-rich (that is, their atomic M/(S+O) do not differ greatly from unity)
845 in equilibrium with silicate melts by:

846 $$a_{FeS}^{sulf} = \left(1 - k_{Ox} X_{FeO}^{sil\ melt}\right)\left[\frac{Fe}{Fe+Ni+Cu+\cdots}\right]_{sulf} \quad (42)$$

847 Here $k_{Ox}$ is an equilibrium constant for reaction (41), and $\left[\frac{Fe}{Fe+Ni+Cu+\cdots}\right]_{sulf}$ is the atomic ratio of
848 Fe to other cationic diluents in the matte. In natural terrestrial basalts, only Ni and Cu are
849 significant, but other chalcophile elements are present in the sulfide of a few of the experimental
850 studies used as input to the model (Table 1), and all were treated similarly. Trials showed that using
851 the simpler $X_{FeO}^{sil\ melt}$ rather than the more logical $a_{FeO}^{sil\ melt}$ in the above expression returned a
852 slightly better result. A linear least-squares best fit found $k_{Ox}$ = 1.20 ± 0.04 (Fig. 5), but given the

scatter in the data, $k_{Ox}$ was put at 1 following the suggestion of Kiseeva and Wood (2013), which made no perceptible difference to the SCSS fitting.

By splitting the SCSS problem up in this four-fold way, a better understanding is achieved of how SCSS responds to the different variables (T, P, silicate and sulfide melt compositions). This will enable a quantitative sensitivity analysis. The four-fold way is also useful in divining where model inadequacies may lie, and what further work would be most beneficial.

*Fitting the experimental data on SCSS on anhydrous compositions*

The experimental studies from which the data used to model SCSS were taken are listed in Table 1. These experiments are all at relatively low $fO_2$, where $SO_4^{2-}$ should be negligible. Only nominally anhydrous experiments were considered; the effect of $H_2O$ will be addressed briefly below. Experiments at > 5 GPa were also not considered, due to the large changes in silicate melt structure expected at higher pressures and high liquidus temperatures introducing extra experimental uncertainty. Given the lack of experimental information on $\gamma_{FeO}^{sil\ melt}$ at high $SiO_2$, so were compositions with $X_{SiO2} > 0.62$. The limited information available hints at a large increase in $\gamma_{FeO}^{sil\ melt}$ with $X_{SiO2}$ at higher $SiO_2$ (O'Neill and Berry 2006; Borisov 2007). Data on compositions with < 1 wt% FeO were also excluded for reasons described later. To account for the effect of pressure in Eqn. (36), two terms were added, the usual one in P/T but modified by a second term in erf(P)/T, to allow for coordination changes in the silicate melt. This extra term will be discussed in detail below. The model to which the data were fitted was:

$$\ln [S]_{SCSS} = [\Delta G_{FeO}^{o,sil\ melt} - \Delta H_{FeS}^{o} + T\Delta S_{FeS}^{o}]/RT + \ln C_{S^{2-}} - \ln X_{FeO}^{sil\ melt} - \ln \gamma_{FeO}^{sil\ melt} + \left(1 - X_{FeO}^{sil\ melt}\right)\left[\frac{Fe}{Fe+Ni+Cu+\cdots}\right]_{sulf} + (C_1 P + C_2\, \mathrm{erf}(C_3 P))/T \quad (43)$$

where the parameters to be determined are $\Delta H_{FeS}^{o}$, $\Delta S_{FeS}^{o}$, $C_1$, $C_2$ and $C_3$ from the SCSS experiments, plus the coefficients in Eqn. (40) for $\gamma_{FeO}^{sil\ melt}$ from the entirely separate $a_{FeO}^{sil\ melt}$ vs. $X_{Fe}$ experiments.

The fitting was by weighted least squares, minimizing the objective function $((\ln [S]_{SCSS(obs)} - \ln[S]_{SCSS(calc)})/s(\ln[S]_{SCSS}))^2$, subject to the constraint that a second objective function for the optimization of $\gamma_{FeO}^{sil\ melt}$, namely $(((RTln\gamma_{FeO}^{sil\ melt})_{obs} - (RTln\gamma_{FeO}^{sil\ melt})_{calc})/s(RTln\gamma_{FeO}^{sil\ melt}))^2$, did not increase by more than 2.5% above its best fit value obtained independently of the SCSS data. The 2.5% limit corresponds to less than a percent change in the level of significance. This procedure ensures internal consistency between the different parts of the model. It also has the beneficial effect of bringing more of the relevant compositional space for silicate melts into the parameterization of $\gamma_{FeO}^{sil\ melt}$, and the fact that this can be done within the 2.5% limit chosen shows that, despite the 600 experimental observations, more data are needed on a wider compositional range (particularly towards high MgO, and as pointed out above, high $SiO_2$). For the weighting, $s\left(RTln\gamma_{FeO}^{sil\ melt}\right)$ was taken as 800 J mol$^{-1}$ for every datum. This value corresponds approximately to s(log $fO_2$) = 0.03 and 5% relative uncertainty in $X_{FeO}^{sil\ melt}$. The value of s($[S]_{SCSS}$) was taken as reported, or 5%, whichever was larger. This uncertainty dominates the other uncertainties in the SCSS measurements, namely temperature, pressure, major-element composition, and the minor amounts of $H_2O$ expected to contaminate most high-pressure experiments but which are usually not measured. The exception is at very low $X_{FeO}^{sil\ melt}$, where $s(X_{FeO}^{sil\ melt})$ becomes dominant as $[S]_{SCSS}$ rises sharply (Wykes et al. 2015). For this reason, and because the composition of the sulfide liquid in equilibrium with such compositions is somewhat uncertain (possibilities include M/S>>1 and the presence of what are normally lithophile components in the sulfide matte), the data with < 1wt% FeO were not used.

A major problem with combining experimental datasets from different experimental studies performed in different laboratories and addressing different volumes of T-P-compositional space is the way that systematic error can translate into misleading effects. For example, consider a study that reports S contents that are systematically too high, perhaps due to instrument calibration. If that study provided most of the data at, say, high pressure, then this systematic error in S analysis would translate into the modeling as an erroneously enhanced effect of pressure. For analytical aspects, the

effects of this type of problem can be ameliorated by reporting analyses of widely available standards. Many of the input studies listed in Table 1 have done this using the natural glass VG2 (USNM 111240/52; Jarosewich 1980) with c. 1400 ppm S, which provides a valuable point of comparison (Table 2). The inter-laboratory differences are considerable in some cases. The homogeneity of VG2 is unknown, and the amount of S, although typical of Ocean Floor Basalt glasses, is well below that found in some reduced glasses let alone in oxidized ones with S as $SO_4^{2-}$. It would be helpful to have inter-laboratory comparisons available for other standard glasses, perhaps synthetic, with tested homogeneity and higher sulfur contents, one with S as $S^{2-}$ and another with S as $SO_4^{2-}$.

Of all the initially included studies, only the data of Holzheid and Grove (2002) could not be well fitted, consistently returning calculated values of $[S]_{SCSS}$ higher than observed. This may be due to failure to account for $\gamma_{FeO}^{sil\ melt}$ adequately in these high MgO compositions, alternatively the effect of pressure on depressing $[S]_{SCSS}$ appears higher in these experiments than in others. Although there is no independent reason to do so, the data of Holzheid and Grove (2002) were removed from the fitting, except for their four experiments with high Ni in the sulfide.

The numerical value of $C_3$ was found to be insignificantly different from 1 (units in $GPa^{-1}$), so it was fixed at this value, which then gave $C_1$ = -291 K $GPa^{-1}$ and $C_2$ = 351 K. For reaction (38), the optimization produced:

$$\Delta G_{FeS}^{o,sulf\ melt}\ (\text{J mol}^{-1}) = -106340 + 23.893\ T \qquad (44)$$

This gives –70.5 kJ $mol^{-1}$ at 1500 K, in between the values tabulated by Barin (1989) and Robie and Hemingway (1995), namely - 70.0 and -73.4 kJ $mol^{-1}$, respectively. This agreement is a notable affirmation of the model, because the determination of $G_{FeS}^{o,sulf\ melt}$ is independent of anything to do with silicate melts. The free energy for reaction (35) is therefore:

$$\Delta G_{FeO-FeS}^{o}\ (\text{J mol}^{-1}) = 137778 - 91.666\ T + 8.474\ T \ln(T) \qquad (45)$$

The reduced chi-squared for the regression, $\chi_\upsilon^2$, was 3.7 (n = 407, four refined parameters). Including the term for pressure in erf(P)/T decreased $\chi_\upsilon^2$ from 4.8, a significant improvement since a

930 third of the experiments are at ambient pressure. The rather high value of $\chi_\upsilon^2$ is explicable at least in
931 part by inter-laboratory differences in determining S (cf. Table 2), pressure, temperature, oxidation
932 state, unanalyzed $H_2O$ in high pressure experiments, and other factors that may differ between
933 studies, and which were not included in the uncertainties used for weighting.

934 The parameterization of $\gamma_{FeO}^{sil\,melt}$ gave:

935 $$\text{RT ln } \gamma_{FeO}^{sil\,melt} = (1\text{-}X_{FeO}^{sil\,melt})^2\,[28870 - 14710\,X_{MgO}^{sil\,melt} + 1960\,X_{CaO}^{sil\,melt}$$

936 $$+ 43300\,X_{NaO_{0.5}}^{sil\,melt} + 95380\,X_{KO_{0.5}}^{sil\,melt} - 76880\,X_{TiO_2}^{sil\,melt}]$$

937 $$+ (1 - X_{FeO}^{sil\,melt})\,[-62190\,X_{SiO_2}^{sil\,melt} + 31520\,(X_{SiO_2}^{sil\,melt})^2] \quad (46)$$

938 with $\chi_\upsilon^2 = 2.9$. Note the large effect that the alkalis, Na and even more so K, have on increasing
939 $\gamma_{FeO}^{sil\,melt}$. The comparison between the measured values of $\gamma_{FeO}^{sil\,melt}$ and those calculated from this
940 parameterization is shown in Fig. 4.

941 $Fe^{3+}/\sum Fe$ in the silicate melts in the experiments that measured $\gamma_{FeO}^{sil\,melt}$ would be insignificantly
942 different from zero, because all these experiments were in equilibrium with metallic Fe. No
943 provision for $Fe^{3+}$ was made in the fitting of the SCSS experiments, either. Because of the
944 constraints on how experiments are done, $Fe^{3+}/\sum Fe$ in the silicate melts of the SCSS database are <
945 0.02 for atmospheric-pressure experiments (see Tuff and O'Neill 2010, their Table 5), but likely a
946 little more in many of the higher-pressure experiments, which, because of the prevalence of
947 graphite in the pressure assemblies if not the sample capsules, usually return redox conditions about
948 a log unit in log $fO_2$ below the graphite-$CO_2$ buffer, hence two log units below the quartz-fayalite-
949 magnetite equilibrium (Frost and Wood 1997), corresponding to approximately 0.03 in $Fe^{3+}/\sum Fe$ at
950 atmospheric pressure.

951

952 *The effect of pressure on SCSS*

953 Experimental studies have established that SCSS decreases substantially with increasing
954 pressure at high pressures (Wendlandt 1982; Mavrogenes and O'Neill 1999; Holzheid and Grove
955 2002; Smythe et al. 2017), as shown in Fig. 6. The important consequence is that "primary"

magmas should erupt undersaturated in sulfide, if the temperature decrease during their ascent is no more than adiabatic (Mavrogenes and O'Neill 1999). However, Liu et al. (2007) found no difference in SCSS between 0.5 and 1 GPa in two pairs of experiments, although the uncertainty was large (see their Fig. 2). The present fitting exercise showed that this view has merit. If only the data in the interval from 0 to 1.5 GPa were considered, there would appear to be little or no effect of pressure. The possibility exists that the effect of pressure changes with pressure. This is not surprising; previously, it has been assumed in fitting experimental data that the relevant $\int VdP$ terms in the four quantities in Eqn (36) could be approximated by a constant: that is, ln $[S]_{SCSS}$ varied linearly with P/T (Mavrogenes and O'Neill 1999). This simplification has long been accepted as a viable first-order approximation in solid-state reactions, where, in essence, it assumes that the effects of the thermal expansivities and bulk moduli of the individual crystalline phases in the reaction cancels out across the reaction. But silicate melts have different P-V characteristics from crystalline phases. With increasing pressure, the main aluminosilicate structural units change, while the average coordinating number of the nearest-neighbour anions forming the coordination polyhedra around the $M^{x+}$ cations tends to increase. Possibly the coordination environment of the $S^{2-}$ anions also change with pressure. Such changes are more akin to order-disorder phenomena or even phase transitions than to the effects of compressibility on the $\int VdP$ terms in crystals, so carrying over an approximation from experience with crystals may not be such a good idea. Trials fitting the data with polynomials, such that ln $[S]_{SCSS}$ varied with terms in $C_n P^n/T$, produced a marked hump in $[S]_{SCSS}$ vs. P in the range 0 to 1 GPa, where there are almost no data to constrain reality. As a hump seems implausible, compared to no change in $[S]_{SCSS}$ vs. P in this range , the relationship was described using an error function in Eqn. (43), despite reservations about employing this function twice in one paper. The form of the suggested pressure-dependence is compared to the conventional views in Fig. 6. Above ~ 1 GPa, there is little difference from the conventional assumption.

With increasing pressure above ~ 5 GPa, SCSS becomes very low (e.g., Li and Agee 2001), confirming the trend in Fig. 6, but precise experimental measurements are difficult because of the high silicate liquidus temperatures, and the fact that the melts do not quench to glasses, making it difficult to know if the tiny sulfide globules commonly encountered are exsolved on quenching or not.

Experimental studies to date have not been designed to cope with the possibility that the pressure dependence of SCSS may be non-linear. For example the classic study of Wendlandt (1982) investigated pressures only between 1.25 and 3 GPa, completely missing the hypothetical low-pressure inflection shown in Fig. 6. A more detailed look at the pressure-dependence of SCSS between 0 and 1 GPa is needed.

*The dependence of SCCS on FeO*

SCSS depends on the FeO content in the silicate melt mainly in two ways (Eqn. 36). The $C_{S^{2-}}$ term causes a linear increase of SCSS with increasing $X_{FeO}^{sil\ melt}$, except, as reviewed above, at high FeO (> 15 wt%), whereas the $a_{FeO}^{sil\ melt}$ term causes a logarithmic decrease of SCSS with increasing $X_{FeO}^{sil\ melt}$ (modulated somewhat by changes in $\gamma_{FeO}^{sil\ melt}$ with $X_{FeO}$). These competing effects may conveniently be studied by measuring SCSS on a compositional pseudo-binary between a FeO-free "matrix" composition and FeO, with temperature and pressure kept constant. Such a series eventuates anyway in 1-atmosphere experiments conducted over a range of $fO_2$ and $fS_2$, when FeO is removed from an initial composition by exsolution of an FeS-rich matte in response to decreasing $fO_2$ and/or increasing $fS_2$ (Haughton et al. 1974; O'Neill and Mavrogenes 2002). The result is that graphs of SCSS vs. FeO (wt%) for these pseudo-binaries should have an asymmetric U shape. Demonstrating this with 1-atmosphere experiments has been unconvincing, because sufficiently high $fS_2$ cannot be imposed to access much of the left-hand side of the "U" (Haughton et al. 1974; O'Neill and Mavrogenes 2002). To get around this, Wykes et al. (2015) performed a series of experiments at 1400ºC and 1.5 GPa. The results are compared to the present model in Fig. 7. The

1007 fix of parameterizing $C_{S^{2-}}$ at high FeO with an error-function term (Eqns. 33 and 34) works well in
1008 describing the data to the highest FeO measured (30 wt%). For a comparison of these data against
1009 previous models, see Wykes et al. (2015), their Fig. 9. The model also works well for the data at < 1
1010 wt% FeO, which were not used in the SCSS fitting. Also plotted on this diagram are some
1011 previously unpublished data (Table 3), using the same starting composition and Re capsules as
1012 described in Wykes et al. (2015), but with water added. The Re capsules did not hold the $H_2O$
1013 quantitatively, but some $H_2O$ was found in the recovered glasses, as determined by FTIR. The
1014 concentration of $H_2O$ actually increased from the added amount in one run (G76). The major
1015 elements and S analyses were obtained by EMPA, as described in O'Neill and Mavrogenes (2002),
1016 but as the major elements were only determined by Energy Dispersive Spectrometry (EDS), they
1017 have been recalculated to 100% taking into account the analysed S and $H_2O$ contents. The latter
1018 were measured as described in Liu et al. (2005).
1019
1020 *The effect of $H_2O$*
1021 Naldrett and Richardson (1967) showed that $H_2O$ had no perceptible effect on the melting point
1022 of pyrrhotite-magnetite assemblages at 0.2 GPa, implying that this component has negligibly small
1023 solubility in Fe-S-O melts at these conditions. This is supported by the experiments of Moune et al.
1024 (2009), who report pyrrhotite, not sulfide melt, at 1045ºC, ~ 0.3 GPa. Thus the effect of $H_2O$ can be
1025 isolated to what happens in the silicate melt. In the context of the four-fold way, two variables, $C_{S^{2-}}$
1026 and $a_{FeO}^{sil\ melt}$, will be affected by adding $H_2O$, but the presence of H in the system could perhaps
1027 also result in S dissolving as anionic species in addition to the species that predominate in dry
1028 systems ($S^{2-}$ and $SO_4^{2-}$), for example $HS^-$, or perhaps, by analogy with $OH^-/H_2O$ speciation, as
1029 molecular $H_2S$ in high-$SiO_2$ melts (Clemente et al. 2004). At present there is no compelling
1030 evidence for $HS^-$ in FeO-containing hydrous basic or intermediate melts (Wilke et al. 2011; Wykes
1031 et al. 2015), and the following discussion will assume that only $S^{2-}$ is present in the relevant $fO_2$
1032 range.

Adding $H_2O$ to silicate melts is thought to break up framework silicate units, which decreases the activity of $SiO_2$. From reaction (10), this should increase $S^{2-}$ in the silicate melt. However, potential additional anion units like $OH^-$ or $SiO_3OH^{3-}$ (the hydroxylated orthosilicate unit), add complexity to the anion sublattice, with input into the reciprocal solution formalism that cannot be predicted at present. But there is a simpler effect that first needs to be addressed. It is dilution. Adding $H_2O$ to a silicate melt adds oxygen anions to the anion sublattice, and when converted into mole fractions, petrologically reasonable amounts can be seen to be large: for typical basaltic compositions, 5 wt% $H_2O$ correspond to about 0.25 in $X_{HO_{0.5}}^{sil\ melt}$ (mole fraction on the single-cation basis). The mole fractions of all the other oxide components $X_{MO_{x/2}}^{sil\ melt}$ are lowered, by a factor of (1-$X_{HO_{0.5}}^{sil\ melt}$). By itself, this dilution effect should influence SCSS in two ways: 1) by lowering $a_{FeO}^{sil\ melt}$; 2) by lowering all the $X_{MO_{x/2}}^{sil\ melt}$ (M≠H) in the model for $C_{S^{2-}}$ (Eqn. 34).

Potentially, $H_2O$ could change $\gamma_{FeO}^{sil\ melt}$. Not much is known about how $H_2O$ affects individual activity coefficients in silicate melts, but a qualitative judgment can be made from the observation that $H_2O$ has only a minimal influence on the partitioning of $Fe^{2+}$ and Mg between olivine and silicate melt (Toplis 2005). This indicates that any effect of $H_2O$ cancels out in the ratio $\gamma_{FeO}^{sil\ melt}$ / $\gamma_{MgO}^{sil\ melt}$, which would be unlikely if the effect of $H_2O$ on either activity coefficient were huge. Therefore, it is assumed that $\gamma_{FeO}^{sil\ melt}$ may be evaluated as per Eqn. (46), with no additional terms.

This "dilution" hypothesis was tested against the available experimental database for SCSS in $H_2O$-containing silicate melts, as follows. Only experiments at sufficiently low $fO_2$ that $S^{6+}/S^{2-}$ should be near zero were considered: Moune et al. (2009); Fortin et al. (2015); D'Souza and Canil (2018); and Table 3. The sulfide capacities of hydrous melts may conceptually be divided into two parts, that due to the anhydrous oxide components, taking account of their dilution by the factor of (1-$X_{HO_{0.5}}^{sil\ melt}$), called here $C_{S^{2-}}^{dil}$, and that due to terms in $X_{HO_{0.5}}^{sil\ melt}$, called here $C_{S^{2-}}^{H}$, such that $C_{S^{2-}}$= $C_{S^{2-}}^{dil}\,C_{S^{2-}}^{H}$. The calculated SCSS due only to dilution is then:

$$\ln [S]_{SCSS}(dil) = \Delta G^{o}_{FeO-FeS}/RT + \ln a_{FeS}^{sulf} + \ln C_{S^{2-}}^{dil} - \ln X_{FeO}^{sil\ melt} - \ln \gamma_{FeO}^{sil\ melt} \quad (47)$$

and the difference between the measured S and this calculated $[S]_{SCSS}(dil)$ is given by:

$$\ln C_{S^{2-}}^{H} = \ln [S]_{obs} - \ln [S]_{SCSS}(dil) \quad (48)$$

The calculated values of $\ln C_{S^{2-}}^{H}$ from the input experiments are plotted against $X_{HO_{0.5}}^{sil\ melt}$ in Fig. 8a, which shows that they scatter around a fairly well defined curve of somewhat parabolic shape. Some scatter would be expected from the effect of $H_2O$ on the activity of $SiO_2$. D'Souza and Canil (2018) also proposed a strong effect of Na and K, from the difference between the two compositions studied by them. With these considerations, the experimental data were fitted by non-linear least-squares regression assuming uncertainties in both S and $H_2O$ contents, with s([S]) taken as 5% or as reported, whichever is larger, and s($H_2O$) as 0.1 wt% + 0.05[$H_2O$], to parameterize $C_{S^{2-}}^{H}$ as:

$$\ln C_{S^{2-}}^{H} = X_{HO_{0.5}}^{sil\ melt} (6.4 + 12.4\ X_{HO_{0.5}}^{sil\ melt} - 20.3\ X_{SiO_2}^{sil\ melt} + 73\ (X_{NaO_{0.5}}^{sil\ melt} + X_{KO_{0.5}}^{sil\ melt})) \quad (49)$$

The uncertainties in the reported $H_2O$ contents have almost as much influence on the regression as those on the S contents, and cannot be neglected; they must also be propagated through the entire model, because of their effect on calculating the mole fractions of the other components. The reduced chi-squared for the fit was 5.0, indicating that the model is too simplistic, if the weighting of the data is reasonable; but as the four experimental studies address different compositions at different temperatures and pressure, to use more variables could be misleading. The experiments of Moune et al. (2009), all at 1045ºC, ~ 0.3 GPa, were saturated with pyrrhotite, not FeS-rich matte, requiring calculation of the activity of FeS relative to the standard state of liquid FeS. This was done using the enthalpy of melting and the melting temperature of pure FeS of 32.34 kJ $mol^{-1}$ at 1468 K from Robie and Hemingway (1995), to give $a_{FeS}^{sulf} = 1.35$, with $X_{FeO}^{sulf}$ taken to be zero (no dissolved O in pyrrhotite). No correction was attempted for the stoichiometry of the pyrrhotite (i.e., deviations from atomic Fe/S = 1), as this was not reported. Pyrrhotite in comparable experiments is only a little metal-deficient, with Fe/S ~ 0.96 (Luhr 1990). The concentrations of S calculated from the model (Eqns. 47 to 49) are compared to the observed values in Fig. 8b. Most of the data are reproduced to within ± 10%.

The net effect of adding $H_2O$ to a silicate melt is a tradeoff between the dilution effect (where obviously $C_{S^{2-}} > C_{S^{2-}}^{dil}$) and the increase in $C_{S^{2-}}$ due to the addition of the $C_{S^{2-}}^{H}$ term. The dilution effect depends to a large extent on the FeO content of the melt, hence there should be a substantial difference in the net effect of adding $H_2O$ between high and low FeO compositions. For low FeO compositions, adding $H_2O$ should increase $C_{S^{2-}}$, and vice versa. Presumably, for the effect of $H_2O$ on the sulfate capacity, $C_{SO_4^{2-}}$, the same principle would apply ($C_{SO_4^{2-}} = C_{SO_4^{2-}}^{dil} - C_{SO_4^{2-}}^{H}$).

At present, nothing seems to be known about the effects on the solubilities of either $S^{2-}$ or $SO_4^{2-}$ of $CO_2$, whose own solubility in silicate melts becomes considerable above ~ 2 GPa, nor of other volatile species.

**Application to mid-ocean ridge and similar basalts**

The geochemistry of ocean floor basaltic (OFB) magmatism has been intensively studied from the perspective of the glassy rinds on erupted pillows. These glasses typically contain ~$10^3$ ppm total sulfur (Mathez 1976; Czamanske and Moore 1977), which is in the range quantifiable by electron microprobe to about 5% precision with a bit of care. Métrich et al. (2009) used XANES spectroscopy to show that the oxidation state of nearly all the S in three representative glasses was $S^{2-}$, with 4 to 8% as $SO_4^{2-}$, which they proposed was produced on cooling. Many of the glasses contain globules of quenched sulfide mattes, often nearly spherical in shape, with diameters mostly in the range 10 to 100 μm, with an average of 27 μm according to Patten et al. (2012), although some up to 600 μm have been reported elsewhere (e.g., Czamanske and Moore 2007). The textures of the phase assemblages in the globules vary, at least in part due to differences in cooling rates (e.g., Patten et al. 2012). Bulk compositions of the globules are more reliably estimated for those with finer-grained textures, and are fairly rich in Ni and Cu. For example, the average Ni and Cu contents of 14 fine-grained globules from Patten et al. (2012) are 6.1 ± 2.9 and 8.5 ± 4.0 wt% respectively, with atomic Fe/(Fe+Ni+Cu) being 0.78 ± 0.05.

1109 The existence of these globules has been attributed to the erupted basalts being at sulfide
1110 saturation (Mathez 1976; Czamanske and Moore 1977), hence the S contents of their host basalt
1111 glasses should correspond to their SCSS at their eruption temperature and pressure. Several
1112 attempts have been made to compare their measured S contents against models for the SCSS, but
1113 this requires knowing the temperature of the basalt at the time the sulfide matte separated from the
1114 silicate liquid, plus correction for its Ni and Cu contents. Only the recent work of Smythe et al.
1115 (2017) has addressed this issue quantitatively, although Ariskin et al. (2013) did consider Ni.
1116 Another issue is that the $Fe^{3+}/\sum Fe$ in OFB glasses is typically about 10% (Berry et al. 2018), which
1117 must lower $a_{FeO}^{sil\ melt}$ by about this amount compared to calculations that assume all Fe in the silicate
1118 melt to be $Fe^{2+}$.
1119 The model for SCSS derived from experimental data in this contribution may be tested against
1120 the global dataset of Ocean Floor Basaltic glasses of Jenner and O'Neill (2012), for which S
1121 concentrations in 329 samples were determined by EMPA. The advantages of this dataset for
1122 present purposes is that it is eclectic in geographical locations and tectonic nuances, and that the
1123 determination of S concentrations was standardized against the OFB glass VG2 (Table 2). The S
1124 concentrations are the means of at least five individual analyses on each sample, with standard
1125 deviations giving an indication of sample homogeneity. In order to apply the SCSS model, some
1126 enabling assumptions need to be made, as follows.
1127 1) Sample temperatures were estimated using the magmathermometer of Putirka (2008), his
1128 Eqn. (15), with $H_2O$ put to zero. This thermometer assumes the presence of olivine, hence
1129 is inappropriate for the most evolved OFB glasses, but with the necessary caveat it will be
1130 used here in extrapolation for all OFB glasses with > 4 wt% MgO. The equilibrium
1131 pressure was taken to be the pressure from which the samples were recovered, or 0.03
1132 GPa if this was not known, but the effects of pressure are trivial with the present model.
1133 2) The $H_2O$ content of OFB glasses is generally < 0.5 wt% (e.g., Michael 1995; Le Voyer et
1134 al. 2015; Shimizu et al. 2016), and in view of the absence of experimental data on the

effect of $H_2O$ at the relevant pressures and temperature, the low sensitivity of SCSS to $H_2O$ in this range (Fig. 8), and the lack of direct determination of $H_2O$ in the dataset of Jenner and O'Neill (2012), $H_2O$ has initially been assumed to be zero. This assumption will be examined subsequently (see below).

3) The approximation used in modelling the experimental data, that $Fe^{3+}$ in the silicate melts is low enough to be neglected, is not valid for OFB glasses. During OFB petrogenesis $Fe^{3+}$ behaves as a Lightly InCompatible trace Element (LICE), whose concentration as the oxide component in wt% is given by $\ln[Fe_2O_3] = 1.46 - 0.177\,[MgO]$ (Berry et al. 2018; O'Neill et al. 2018). Because $Fe^{3+}/Fe^{2+}$ has been measured in only a subset of the samples analysed for S by Jenner and O'Neill (2012), it was estimated from the above relationship against MgO. Potentially, $Fe^{2+}$-$Fe^{3+}$ interactions in the melt could also affect $\gamma_{FeO}^{sil\ melt}$, so an extra term, $W_{Fe^{3+}} X_{Fe^{3+}O_{1.5}}^{sil\ melt}$, was added to Eqn. 46, with $W_{Fe^{3+}}$ to be determined by fitting to the natural data, as described below. As discussed previously, there is no information at all on how $Fe^{3+}$ affects $C_{S^{2-}}$, so for the calculation of this quantity, $Fe^{2+}O$ was put equal to total FeO.

4) Although the composition of the sulfide is not known, it should be specified by the composition of the silicate melt, assuming equilibrium. As diluents of FeS, only Ni, Cu and O are present in sufficient amounts to affect $a_{FeS}^{sulf}$. For Ni, the equilibrium between sulfide and silicate melts is:

$$FeO + NiS = FeS + NiO \qquad (50)$$

sil melt sulf sulf sil melt

Hence the atomic ratio Ni/Fe in the sulfide is given by:

$$\text{Ni/Fe (atomic)} = K_{Ni/Fe}^{*}\,[Ni]/[Fe^{2+}O] \qquad (51)$$

The concentrations of Ni and $Fe^{2+}O$ in the silicate melt are input in ppm and wt% respectively, where $[Fe^{2+}O] = [FeO_{tot}] - 0.8998\,[Fe_2O_3]$. The equilibrium constant $K_{Ni/Fe}^{*}$ includes implicitly the ratio of the activity coefficients of NiO and $Fe^{2+}O$ in the silicate melt ($\gamma_{NiO}^{sil\ melt}/\gamma_{Fe^{2+}O}^{sil\ melt}$). The

change of $\gamma_{NiO}^{sil\ melt}$ with silicate melt composition parallels that of $\gamma_{Fe^{2+}O}^{sil\ melt}$ (O'Neill and Eggins 2002), so that this ratio is relatively insensitive to composition and may be approximated as a constant. The stoichiometry of the equivalent Cu-$Fe^{2+}$ exchange reaction is not so convenient, because the oxidation state of Cu is 1+ in the silicate melt and potentially a mixture of $CuS_{0.5}$ and CuS components in the sulfide matte, depending on $fS_2$ (e.g., Ripley et al. 2002), but to keep things simple, it is proposed that Cu/Fe (atomic) may be approximated in the same way over the limited range of conditions appropriate to OFB. Hence:

$$a_{FeS}^{sulf} = \left(1 - X_{Fe^{2+}O}^{sil\ melt}\right)(1/(1+K_{Ni/Fe}^{*}\ [\mathrm{Ni}]/[\mathrm{Fe^{2+}O}] + K_{Cu/Fe}^{*}\ [\mathrm{Cu}]/[\mathrm{Fe^{2+}O}]) \quad (52)$$

These enabling assumptions require three unknown parameters, $W_{Fe^{3+}}$, $K_{Ni/Fe}^{*}$ and $K_{Cu/Fe}^{*}$, the values of which were estimated by "tuning" the model to fit the data of Jenner and O'Neill (2012) by least squares, minimizing $(([S]_{obs} - [S]_{SCSS,\ calc})/s[S]_{obs})^2$, where $[S]_{obs}$ was taken as 5% or as given by Jenner and O'Neill (2012), whichever is larger. Because Ni and Cu decrease, and $Fe^{3+}$ increases monotonically with MgO in OFB glasses, these three parameters are highly correlated with each other.

Of the 329 OFB glasses, 11 were identified as possibly having lost S or being sulfide-undersaturated, and removed from consideration. These samples will be revisited below. Of the remaining 318 glasses, Jenner and O'Neill (2002) identified 17 in which the standard deviation of the S analyses was far above analytical precision, and this heterogeneity was confirmed by replicating the analyses in another session. Although these samples cannot be at equilibrium, their large standard deviations give them little weight in the regression, and they were retained. Initial fitting gave $W_{Fe^{3+}}$ within uncertainty of zero, so it was fixed at this value, giving $K_{Ni/Fe}^{*}$ = 0.013, and $K_{Cu/Fe}^{*}$ = 0.025, with a reduced chi-squared, $\chi_{\nu}^{2}$, of 1.45.

The agreement between the measured S content, $[S]_{obs}$, and the calculated SCSS, is shown in Fig. 9a. Generally, OFB glasses not occurring as melt inclusions have degassed some $CO_2$, with their remaining $CO_2$ often postulated to correspond to the $CO_2$ solubility at the water depth at which they erupted (e.g., Dixon and Stolper 1995). On the present evidence, this degassing does not

1187 usually cause perceptible S loss. Exceptions are 11 data with low $[S]_{obs}$, which are independently
1188 distinguishable by their low S/Se ratio (Fig. 9b), implying that they have lost S by volatilization,
1189 since Se is less volatile than S (Jenner et al. 2010). None of these S-deficient samples (VG numbers
1190 1672, 1673, 1674, 1677, 4750, 4751, 4754, 4755, 6822, 8550, 8555), were erupted at particularly
1191 shallow depths. Elsewhere, Nilsson and Peach (1993) demonstrated a correlation between S loss
1192 and $Fe^{3+}/\sum Fe$ determined by wet chemistry in back-arc basin glasses from the Lau Basin; see also
1193 Jenner et al. (2010). Here the only glass for which $Fe^{3+}/Fe^{2+}$ has been measured is VG6822 (Berry
1194 et al. 2018), whose oxidation state is unexceptional (Fig. 10), so in this particular case its S loss by
1195 degassing was not promoted by an unusually high oxidation state compared to other OFB glasses.
1196 Two of the samples (VG8550 and VG8555, from the Tuzo Wilson seamounts) have significantly
1197 lower S/Se than that expected from just S loss (Fig. 9b), which is intriguing. One possibility is if the
1198 devolatilizing magma contained abundant sulfide globules, which were resorbed back into the
1199 silicate melt during S loss.

1200 The calculated compositions of the sulfide mattes that are assumed to be in equilibrium with
1201 each glass provide another test of the model. Observed compositions of bulk sulfide globules from
1202 OFB are available from Czamanske and Moore (1977) and Patten et al. (2012). As the former study
1203 does not give the compositions of the host basalts, only their $TiO_2$ contents, this variable was used
1204 in Fig. 11 to compare Ni/Fe and Cu/Fe measured in the real sulfide globules with the calculated
1205 ratios in the hypothetical sulfide in equilibrium with each of the glasses from Jenner and O'Neill
1206 (2012). For both Ni/Fe and Cu/Fe, the calculated values fall within the range of those observed,
1207 indicating that the values of $K^*_{Ni/Fe}$ and $K^*_{Cu/Fe}$ from the model are reasonable. The large scatter in
1208 the Ni/Fe and Cu/Fe ratios in the natural sulfide globules evident in these figures reflects a lack of
1209 equilibrium between glass and sulfide and/or the difficulties of analyzing the bulk globules on
1210 account of their crystallization to polyphase assemblages.

1211 The good agreement between $[S]_{obs}$ and $[S]_{SCSS}$ shown in Fig. 9a indicates that $S^{6+}$ is no more
1212 than a few percent of total S in these glasses, a possible exception being VG 614, which has the

highest $[S]_{obs}$ of any glass in the dataset, and the lowest MgO (4.85 wt%). This finding is compatible with the model of Nash et al. (2019) for $S^{6+}/\sum S$ as a function of $Fe^{3+}/\sum Fe$ (Fig. 2). It is reinforced by comparing the values of $Fe^{3+}/\sum Fe$ that were measured by XANES spectroscopy by Berry et al. (2108) in a subset of 35 of the OFB glasses of Jenner and O'Neill (2012) with the difference between $[S]_{obs}$ and the calculated SCSS (Fig. 10). There is almost no correlation ($R^2$ = 0.16), which also implies that the $fO_2$ of OFB glasses lies below the threshold at which $S^{6+}/\sum S$ becomes more than a few percent (see Fig. 2). That the model fits the data with the tuning parameter $W_{Fe^{3+}} \sim 0$ is circumstantial evidence that the effect of changing $Fe^{3+}/Fe^{2+}$ on $C_{S^{2-}}$ may be small. The way that $Fe^{3+}/\sum Fe$ influences SCSS seems to be entirely through its lowering of $X_{FeO}^{sil\ melt}$ from that which would be calculated assuming $Fe^{3+}/\sum Fe = 0$.

An Excel spreadsheet called "SCSS_Calculator.xlsx" for calculating SCSS according to the routine described above is included in Supporting Information.

*Sensitivity analysis*

For each variable X, the sensitivity may be defined as $\partial[S]_{SCSS}/\partial n_X$, where $n_X$ is a convenient unit of the variable. The values of $\partial[S]_{SCSS}/\partial n_X$ were calculated for representative glass with a typical composition (VG 390), and are given in Table 4.

These sensitivities may be used to calculate a representative non-systematic uncertainty (i.e., precision) in $[S]_{SCSS}$, under the approximation of the equation for the propagation of small errors:

$$s([S]_{SCSS}) = [\sum(s(X)/n_X)^2(\partial[S]_{SCSS}/\partial n_X)^2]^{1/2} \quad (53)$$

Taking $s(MO_{x/2})$ = 0.1 wt% (M = Na, Mg, Al, Ca, and Fe as $FeO_t$), s(MnO) and $s(TiO_2)$ = 0.03 wt%, $s(SiO_2)$ = 0.2 wt%, s(T) = 20 K, s(Ni) and s(Cu) = 10 ppm, and $s(Fe^{3+}/\sum Fe)$ = 0.03, propagates to $s([S]_{SCSS})$ = 64 ppm, or about 5.5% of the average S content of the undegassed OFB glasses of Jenner and O'Neill (2012), which is 1150 ppm. The largest contribution to the uncertainty comes from temperature, followed by $Fe^{3+}/\sum Fe$, then $FeO_t$, but reasonably accurate knowledge of the Ni and Cu contents of the silicate glass are also needed. Easy to overlook would

1239 be the effect of MnO, which contributes to $C_{S^{2-}}$ as much as does FeO on a proportional basis, but
1240 does not contribute to $a_{FeO}^{sil\ melt}$. Consequently, ignoring the ~ 0.2 wt% MnO typical of OFB would
1241 alone cause an error in SCSS of 3%. The sensitivity of the model to the effect of pressure is
1242 speculative only, given the present lack of constraints on the effects of pressure at less than 1 GPa
1243 (Fig. 6), and was therefore not included.
1244
1245 *Is neglecting $H_2O$ in OFB glasses justified?*
1246 Although $H_2O$ has not been directly measured in the OFB glasses analysed by Jenner and
1247 O'Neill (2012), their $H_2O$ contents may be estimated approximately, using the observation that
1248 $H_2O$/Ce in OFB glasses is reasonably constant (e.g., Michael 1995). Assuming $H_2O$/Ce = 200, the
1249 "tuning" procedure was repeated for the 318 undegassed glasses of Jenner and O'Neill (2012), with
1250 all mole fractions lowered by the factor (1-$X_{HO_{0.5}}^{sil\ melt}$) to calculate $C_{S^{2-}}^{dil}$ , the addition of the term in
1251 $C_{S^{2-}}^{H}$, the calculated temperature lowered by 12.83 K per wt% $H_2O$ as specified by the
1252 magmathermometer of Putirka (2015), his Eqn. 15, and $W_{Fe^{3+}}$, $K_{Ni/Fe}^{*}$ and $K_{Cu/Fe}^{*}$ taken as tuning
1253 parameters. With this model, it is possible to achieve a statistically better fit ($\chi_\nu^2$ = 1.16), but at the
1254 expense of a very large negative $W_{Fe^{3+}}$, which seems physically unreasonable (although it could be
1255 compensating for an effect of $Fe^{3+}/Fe^{2+}$ on $C_{S^{2-}}$), and a larger $K_{Cu/Fe}^{*}$, which translates into higher
1256 Cu/Fe ratio in the coexisting sulfide, contrary to the inference from the analysed sulfides (cf. Fig.
1257 11b). On the other hand, constraining $W_{Fe^{3+}}$ = 0 gives $\chi_\nu^2$ = 1.80, only a little less good than the
1258 model assuming zero $H_2O$, but with lower $K_{Ni/Fe}^{*}$ and $K_{Cu/Fe}^{*}$, which give Ni/Fe and Cu/Fe in good
1259 agreement with the available sulfide analyses.
1260 The conclusions is that while the effects of small amounts of $H_2O$ in OFB glasses on SCSS may
1261 not be negligible, they cannot be quantified at present. However, the zero-$H_2O$ assumption looks to
1262 be a good approximation, and will be used for the following discussions, even where $H_2O$ is known,
1263 to ensure unbiased comparisons.
1264

*Comparison with previous models*

With the exception of the recent study of Smythe et al. (2017), previous modeling of SCSS in silicate liquids of geological interest has concentrated on reproducing the available experimental data in systems without Ni and Cu (Moretti and Ottonello 2005; Moretti and Baker 2008), and are therefore not directly applicable natural systems containing Fe-Ni-Cu-S-O sulfides.

The model of Smythe et al. (2017) and that of this work are compared in Fig. 12a by applying both to the dataset of Jenner and O'Neill (2012), with liquidus temperatures calculated the same way, that is, with the magmathermometer of Putirka (2008). There is excellent agreement over most of the range of $[S]_{obs}$, from 800 to 1500 ppm, but above 1500 ppm S, the model of Smythe et al. returns higher values of SCSS, which would correspond to such samples being sulfide-undersaturated. Figure 12b shows that the difference between the two models is largely due to the different ways that the effects of $FeO_t$ are handled. The model of Smythe et al. does not include the ad-hoc adjustment made in this work for the non-linear decrease of ln $C_{S^{2-}}$ vs. $X_{FeO}^{sil\,melt}$ (Eqns. 33 and 34), and does not parameterize $\gamma_{FeO}^{sil\,melt}$ as a function of composition. On the other hand, Smythe et al. (2017) use a more sophisticated treatment of $a_{FeS}^{sulf}$. Despite this, the calculated values of Ni/Fe in the sulfide from the model of this work appear more realistic when compared to actual sulfide globule analyses (Fig. 11a). The calculated Cu/Fe ratios are similar over the range of $TiO_2$ contents of the glass for which there are actual sulfide globule analyses (Fig. 11b).

*Application to other OFB glass datasets.*

Some recent studies have reported sulfur contents in OFB glasses determined by SIMS together with the necessary compositional data including Ni and Cu (Le Voyer et al. 2015, 2017; Shimizu 2016). The latter study presents new analyses of a number of glasses from Macquarie Island previously analysed for all relevant elements by Kamenetsky et al. (2000) and Kamenetsky and Eggins (2012), including S by EMPA. This replication is a valuable resource for ground-truthing analytical precision (not just for S), and also provides a test of accuracy, of the "necessary but not

1291 sufficient" kind. The average agreement between the S analyses by the two methods is very good
1292 (Fig. 13a). Non-linear regression of the data assuming that the relative uncertainties are the same in
1293 both methods, gives $[S]_{SIMS} = 1.01\ [S]_{EMPA}$, and setting the reduced chi-squared to unity gives the
1294 most probable value of this uncertainty as 5.8%. If the SIMS analyses were more precise then the
1295 EMPA would be less precise, and vice versa, but 5.8% for EMPA seems reasonable based on the
1296 VG2 analyses (Table 2). Kendrick et al. (2014) also report replicate measurements of S by both
1297 SIMS and EMPA for some Ocean Island basaltic glasses, with fewer samples (n = 18) but over a
1298 wider range of S contents, because of variable S loss by degassing. There is less good agreement,
1299 with $[S]_{SIMS} = 1.07\ [S]_{EMPA}$ (Fig. 13a), largely due to the samples with higher S contents, above the
1300 ~ 1400 ppm of the VG2 standard. The most probable uncertainty assuming equal uncertainties is
1301 similar, at 5.0%.
1302 In addition to their replication of the S analyses, Shimizu et al. (2016) also report analyses of the
1303 major- and trace elements in the Macquarie Island glasses that replicate those of Kamenetsky and
1304 co-workers, giving some information on the accuracy of calculated SCSS. The values of SCSS
1305 calculated from the dataset of Shimizu et al. (2016) are displaced to higher SCSS (Fig. 13b).
1306 Because of the way the model is assembled, it is easy to find the culprits: they are the Ni and Cu
1307 analyses, which are on average 7% and 14% lower respectively in the dataset of Shimizu et al.
1308 (2016). This 51ulphur51es just how important it is to know the Ni and Cu contents of a basalt liquid
1309 to judge whether it was sulfide-saturated or not. The comparison of $[S]_{obs}$ with the SCSS model is
1310 shown for both datasets in Fig. 14. The analyses of Kamenetsky et al. (2000) and Kamenetsky and
1311 Eggins (2012) scatter around the model SCSS, although a few are offset to considerably higher
1312 SCSS than $[S]_{obs}$, indicating that they may be sulfide-undersaturated. The dataset of Shimizu et al.
1313 (2016) is displaced to higher SCSS, as expected from Fig. 13b.
1314 Shimizu et al. (2016) report S and all the necessary data for the SCSS model for basaltic glasses
1315 from two other geotectonic localities, Northern East Pacific Rise (NEPR) off-axis seamounts, and
1316 the Quebrada-Discovery-GoFar (QDG) transform fault system. The comparison between $[S]_{obs}$ and

SCSS is shown in Fig. 15. There is a systematic offset of 9% for both datasets, with $[S]_{obs}$ being higher than the calculated SCSS. The SCSS models of Smythe et al. (2017) give the same result, almost exactly. Given the complexity of the SCSS models, the only reasonable explanation for why the offset is so systematic is that the calibration of the SIMS for S differs from what has been typically used for EMPA, on which the model is based. Evidence supporting this proposition is: 1) the reported value for VG2 by SIMS (Le Voyer et al. 2017) is higher than most EMPA values by ~ 5% (Table 2); and 2) the 7% offset of SIMS compared to EPMA analyses from Kendrick et al. (2014) shown in Fig. 13a. There is, however, the problem that the Macquarie Island glasses do not show the same offset (Fig. 13a). The offset is opposite to that expected of undersaturation in sulfide, and towards extra S as $SO_4^{2-}$. This seems unlikely, because if there was significant $SO_4^{2-}$, small but plausible variations $fO_2$ (as monitored by $Fe^{3+}/\sum Fe$) should cause more scatter in $[S]_{obs}$ (cf. Fig. 2). A small subset from the NEPR seamounts do seem to contain excess S beyond likely uncertainty (Fig. 15), implying non-negligible $SO_4^{2-}$ and inviting further investigation by XANES.

For olivine-hosted melt inclusion glasses from OFB, there is fair agreement between analysed S and calculated SCSS for those samples in which the necessary Ni and Cu contents have been measured (Le Voyer et al. 2017), shown in Fig. 16a, but only if the original analyses, uncorrected for presumed post-entrapment crystallization, are used. The correction used by Le Voyer et al. (2017) hardly changes the Fe, Ni, Cu or S contents of the trapped melt from their measured values, but mainly affects MgO, hence the calculated temperature from the magmathermometer of Putirka (2008). The result is, the larger the *calculated* degree of post-entrapment crystallization, the greater the difference between $[S]_{obs}$ and the *calculated* SCSS (Fig. 16b). This emphasizes the sensitivity of SCSS to temperature. Intriguingly, here is also a correlation between the calculated percentage of post-entrapment crystallization and the uncorrected SCSS (Fig. 16b), which can be interpreted as showing that the degree of disequilibrium between the melt inclusion and its olivine host is correlated with undercooling as monitored by the difference between $[S]_{obs}$ and calculated SCSS. Olivine phenocrysts in OFB are often (perhaps mostly) not in Mg-Fe equilibrium with their host

melts at any temperature (see, for example, Fig. 6 of Coogan 2014), and the very existence of a melt inclusion is evidence of rapid crystallization of its host crystal, plausibly caused by undercooling. Melt inclusions have sometimes been regarded as magic bullets to understand basalt petrogenesis, whereas the reality is that a better understanding of basalt petrogenesis is needed to understand melt inclusions.

*Siqueiros OFB olivine-hosted melt inclusions*

Saal et al. (2002) studied olivine-hosted melt inclusions in OFB from the Siqueiros Fracture Zone, however they did not measure Ni and Cu, so their claim that some of these melt inclusions were sulfide-undersaturated needs scrutiny. To a first approximation this may be done if it is assumed that these melt inclusions had the typical Ni and Cu contents for Ocean Floor Basaltic glasses as a function of [MgO]. To implement this idea, the datasets of Jenner and O'Neill (2012) and Gale et al. (2013) were combined, to give, for glasses with [MgO] > 5 wt% (n = 1060):

$$\log_{10} [\text{Ni}] (\pm 0.115) = 0.692 + 0.169 [\text{MgO}] \quad (54)$$

$$\log_{10} [\text{Cu}] (\pm 0.103) = 1.620 + 0.037 [\text{MgO}] \quad (55)$$

as shown in Fig. 17. The scatter, which is far outside analytical uncertainty, reflects real geochemical variability, which needs to be taken into account for the SCSS calculation. This may be done using the sensitivities in Table 4. The relationship between $[S]_{obs}$ and calculated SCSS enabled by these estimates for Ni and Cu abundances for the Siqueiros inclusions is shown in Fig. 18 for both the uncorrected analyses, and with their correction for post-entrapment crystallization. With the exception of four inclusions (out of 107) that have lower $[S]_{obs}$ than calculated SCSS, the inclusions appear to be sulfide-saturated within likely uncertainty. It cannot at present be excluded that the low S in the four anomalous inclusions are due to high Ni and/or Cu or disequilibrium during trapping as inferred for other melt inclusions (Fig. 16).

**The sulfur fugacity ($fS_2$) of Ocean Floor Basalts**

Given T, P and $fO_2$, the sulfur fugacity ($fS_2$) of a basalt at ambient pressure may be calculated from Eqn. (35) if it is sulfide-saturated, but this requires knowing $a_{FeO}^{sil\ melt}$ and $a_{FeS}^{sulf}$. More generally, at ambient pressure, given T and $fO_2$, $fS_2$ may also be calculated from its model $C_{S^{2-}}$ and observed S content, sulfide-saturated or not (Eqn. 3). There is insufficient information to calculate $fS_2$ at higher pressures by this latter route, because the effect of pressure has been constrained experimentally only on SCSS, and not separately on the four entities that make up SCSS, including $C_{S^{2-}}$. Ambient-pressure values for $fS_2$ calculated from the $C_{S^{2-}}$ route are plotted against the relative oxygen fugacity ΔQFM in Fig. 19a for 35 OFB glasses whose $Fe^{3+}/\sum Fe$ has been determined by Berry et al. (2018) by XANES, and whose S contents were measured by Jenner and O'Neill (2012). The parameterization of O'Neill et al. (2018) was used to convert $Fe^{3+}/\sum Fe$ into ΔQFM. The slope of the correlation between $\log_{10} fS_2$ and ΔQFM is 0.82 ± 0.08, somewhat less than the naïve value of 1 implied by Eqn. (3), due to the effects of silicate melt composition and temperature. This correlation flows on to one of $fSO_2$ with ΔQFM, since $1/2S_2 + O_2 = SO_2$ (Fig. 19b). The large increase in $fSO_2$ (hence $pSO_2$) with ΔQFM raises the possibility that some of the rare S-degassed OFB glasses (Fig. 9) may have been unusually oxidized (high $Fe^{3+}/Fe^{2+}$). A high oxidation state has been postulated elsewhere to lead to S degassing during submarine eruptions (Nilsson and Peach 1993; Jenner et al. 2010). Perversely, degassing of $S^{2-}$ as $SO_2$ would then reduce $Fe^{3+}/Fe^{2+}$ (Moussallam et al. 2016). The one glass with low S due to presumed degassing for which $Fe^{3+}/\sum Fe$ was measured, VG6822, shows no evidence of this hypothetical behavior (Fig. 10).

**Conclusions**

The "capacity" approach to understanding the thermodynamics of anion species in silicate melts leads to a thermodynamically based model for the "Sulfide Content at Sulfide Saturation" (SCSS) of basic to intermediate magmas. The model has a precision for calculating SCSS of better than 10%, if the composition of the sulfide can be adequately constrained. Application of this model to undegassed basaltic glasses from deep submarine eruptions show that nearly all have S contents

consistent with being saturated in a Fe-Ni-Cu-S-O sulfide matte on eruption. The agreement between analysed S and SCSS indicates that such magmas contained no more than a few percent of S as $S^{6+}$, which is supported by the results of XANES spectroscopy on their quenched glasses (e.g., Métrich et al. 2009). However, several uncertainties remain. There is a need to better constrain the effects of pressure relevant to the range over which many common basalts are generated and evolve (i.e., 0 to 1.5 Gpa). More experimental information is needed on the effects of $H_2O$, especially confirmation that H-S species (e.g., $HS^-$, $H_2S$) are negligible, as assumed here. Nothing is known about the effects of $CO_2$ or other volatile species. A fascinating problem in physical chemistry yet to be addressed is the kinetics of the electron-exchange interaction between $Fe^{3+}/Fe^{2+}$ and $S^{6+}/S^{2-}$ in silicate melts, which determines to what extent the equilibrium speciation in the silicate melt is preserved when cooled to glass.

**ACKNOWLEDGEMENTS**

Many thanks to John Mavrogenes, my long-term collaborator on matters sulfurous. Thanks also to another long-term colleague Andrew Berry for teaching me so much about spectroscopy and for the $H_2O$ determinations by FTIR in Table 3. Callum Reekie very kindly worked the Excel spreadsheet into an aesthetically pleasing format, and thanks to him and Fran Jenner for their comments and their encouragement. This paper was completed while I was enjoying a visit to the Institut für Mineralogie at the Westfälische Wilhelms-Universität Münster through the generosity of the Alexander-von-Humboldt Stiftung. I also thank two anonymous reviewers, and Roberto Moretti and Daniel Neuville for their editorial handling.

**REFERENCES**

Allertz, C., Selleby, M., & Sichen, D. (2016). The effect of oxygen potential on the sulfide capacity for slags containing multivalent species. Metallurgical and Materials Transactions B, 47, 3039-3045.

Ariskin, A. A., Danyushevsky, L. V., Bychkov, K. A., McNeill, A. W., Barmina, G. S., & Nikolaev, G. S. (2013). Modeling solubility of Fe-Ni sulfides in basaltic magmas: The effect of nickel. Economic Geology, 108, 1983-2003.

Baker, D. R., Barnes, S. J., Simon, G., & Bernier, F. (2001). Fluid transport of sulfur and metals between sulfide melt and basaltic melt. The Canadian Mineralogist, 39, 537-546.

Baker, D. R. (2008). The fidelity of melt inclusions as records of melt composition. Contributions to Mineralogy and Petrology, 156, 377-395.

Ballhaus, C., Fonseca, R. O., Münker, C., Rohrbach, A., Nagel, T., Speelmanns, I. M., Helmy, H. M., Zirner, A., Vogel, H. K. & Heuser, A. (2017). The great sulfur depletion of Earth's mantle is not a signature of mantle–core equilibration. Contributions to Mineralogy and Petrology, 172, 68.

Barin, I., Sauert, F., Schultze-Rhonhof, E. & Sheng, W. S. (1989). Thermochemical data of pure substances, part I and part II. Weinheim, Germany: VCH Verlagsgesellschaft, pp. 1-1739.

Bell, A. S., Simon, A., & Guillong, M. (2009). Experimental constraints on Pt, Pd and Au partitioning and fractionation in silicate melt–sulfide–oxide–aqueous fluid systems at 800 C, 150 Mpa and variable sulfur fugacity. Geochimica et Cosmochimica Acta, 73, 5778-5792.

Berry, A. J., Shelley, J. M. G., Foran, G. J., O'Neill, H. S. C., & Scott, D. R. (2003). A furnace design for XANES spectroscopy of silicate melts under controlled oxygen fugacities and temperatures to 1773 K. Journal of synchrotron radiation, 10, 332-336.

Berry, A. J., Stewart, G. A., O'Neill, H. S. C., Mallmann, G., & Mosselmans, J. F. W. (2018). A re-assessment of the oxidation state of iron in MORB glasses. Earth and Planetary Science Letters, 483, 114-123.

Borisov, A., Lahaye, Y., & Palme, H. (2004). The effect of $TiO_2$ on Pd, Ni, and Fe solubilities in silicate melts. American Mineralogist, 89, 564-571.

Borisov, A., Lahaye, Y., & Palme, H. (2006). The effect of sodium on the solubilities of metals in silicate melts. American Mineralogist, 91, 762-771.

1446 Borisov, A. A. (2007). Experimental study of the influence of $SiO_2$ on the solubility of cobalt
1447 and iron in silicate melts. Petrology, 15, 523-529.
1448 Botcharnikov, R. E., Linnen, R. L., Wilke, M., Holtz, F., Jugo, P. J., & Berndt, J. (2011) High
1449 gold concentrations in sulphide-bearing magma under oxidizing conditions. Nature Geoscience, 4,
1450 112-115.
1451 Buchanan, D. L., Nolan, J., Wilkinson, N. & de Villiers, J. P. R. (1983). An experimental
1452 investigation of 57ulphur solubility as a function of temperature in synthetic silicate melts.
1453 Geological Society of South Africa Special Publication 7, 383-391.
1454 Chan, A. H., & Fruehan, R. J. (1986). The sulfur partition ratio and the sulfide capacity of
1455 $Na_2O$-$SiO_2$ slags at 1200° C. Metallurgical Transactions B, 17(3), 491-496.
1456 Chan, A. H., & Fruehan, R. J. (1988). The sulfur partition ratio and the sulfide capacity of
1457 $Na_2O$-$SiO_2$ Slags at 1400° C. Metallurgical Transactions B, 19(2), 334-336.
1458 Chase Jr, M. W. (1998). NIST-JANAF thermochemical tables. National Institute of Standards
1459 and Technology.
1460 Clémente, B., Scaillet, B., & Pichavant, M. (2004). The solubility of 57ulphur in hydrous
1461 rhyolitic melts. Journal of Petrology, 45(11), 2171-2196.
1462 Coogan, L. A. (2014) The lower oceanic crust. In: Holland, HD, Turekian, KK (Eds.) Treatise
1463 on Geochemistry. Second Edition, Elsevier, Oxford. Vol. 4. The crust (ed. Rudnick, R. L.) pp. 497-
1464 541.
1465 Cottrell, E., & Kelley, K. A. (2011). The oxidation state of Fe in MORB glasses and the oxygen
1466 fugacity of the upper mantle. Earth and Planetary Science Letters, 305, 270-282.
1467 Czamanske, G. K., & Moore, J. G. (1977). Composition and phase chemistry of sulfide globules
1468 in basalt from the Mid-Atlantic Ridge rift valley near 37 N lat. Geological Society of America
1469 Bulletin, 88, 587-599.
1470 Danckwerth, P. A., Hess, P. C. & Rutherford, M. J. (1979). The solubility of sulfur in high-$TiO_2$
1471 mare basalts. Proceedings of the 10$^{th}$ Lunar Planetary Science Conference, pp. 517-530.

Davis, A. S., D. A. Clague, B. L. Cousens, R. Keaten, and J. B. Paduan. (2008) Geochemistry of basalt from the North Gorda segment of the Gorda Ridge: Evolution toward ultraslow spreading ridge lavas due to decreasing magma supply." Geochemistry, Geophysics, Geosystems 9, no. 4.

De Hoog, J. C. M., Mason, P. R. D. & Van Bergen, M. J. (2001). Sulfur and chalcophile elements in subduction zones: Constraints from a laser ablation ICP-MS study of melt inclusions from Galunggung Volcano, Indonesia. Geochimica et Cosmochimica Acta 65, 3147-3164.

De Hoog, J. C. M., Hattori, K. H., & Hoblitt, R. P. (2004). Oxidized sulfur-rich mafic magma at Mount Pinatubo, Philippines. Contributions to Mineralogy and Petrology, 146(6), 750-761.

Ding, S., Dasgupta, R., & Tsuno, K. (2014). Sulfur concentration of martian basalts at sulfide saturation at high pressures and temperatures–implications for deep sulfur cycle on Mars. Geochimica et Cosmochimica Acta, 131, 227-246.

Dixon, J. E., Clague, D. A. & Stolper, E. M. (1991). Degassing history of water, sulfur, and carbon in submarine lavas from Kilauea Volcano, Hawaii. Journal of Geology 99, 371-394.

Dixon, J. E., & Stolper, E. M. (1995). An experimental study of water and carbon dioxide solubilities in mid-ocean ridge basaltic liquids. Part II: applications to degassing. Journal of Petrology, 36(6), 1633-1646.

Doyle, C. D. (1988). Prediction of the activity of FeO in multicomponent magma from known values in [$SiO_2$-$KalO_2$-$CaAl_2Si_2O_8$] – FeO liquids. Geochimica et Cosmochimica Acta 52, 1827-1834.

Doyle, C. D. (1989). The effect of substitution of $TiO_2$ for $SiO_2$ on $a_{FeO}$ in magma. Geochimica et Cosmochimica Acta 53, 2631-2638.

Doyle, C. D. & Naldrett, A. J. (1986). Ideal mixing of divalent cations in mafic magma and its effect on the solution of ferrous oxide. Geochimica et Cosmochimica Acta 5 435-443.

D'Souza, R. J., & Canil, D. (2018). Effect of alkalinity on sulfur concentration at sulfide saturation in hydrous basaltic andesite to shoshonite melts at 1270 C and 1 Gpa. American Mineralogist: Journal of Earth and Planetary Materials, 103, 1030-1043.

1498 Evans, K. A., O'Neill, H. S. C., & Mavrogenes, J. A. (2008). Sulphur solubility and sulphide
1499 immiscibility in silicate melts as a function of the concentration of manganese, nickel, tungsten and
1500 copper at 1 atm and 1400 ºC. Chemical Geology, 255, 236-249.
1501 Evans, K. A., O'Neill, H. S. C., Mavrogenes, J. A., Keller, N. S., Jang, L. Y., & Lee, J. F.
1502 (2009). XANES evidence for 59ulphur speciation in Mn-, Ni-and W-bearing silicate melts.
1503 Geochimica et Cosmochimica Acta, 73, 6847-6867.
1504 Fincham, C. J. B. & Richardson, F. D. (1954). The behaviour of 59ulphur in silicate and
1505 aluminate melts. Proceedings of the Royal Society of London, Ser. A 223, 40-62.
1506 Flood, H., Forland, T. & Gzotheim, K. (1954). Ueber den Zusammenhang zwischen
1507 Konzentration und Aktivitäten in geschmolzenen Salzmischungen. Zeitschrift für Anorganische
1508 Allgemeine Chemie 276, 290-315.
1509 Fonseca, R. O., Campbell, I. H., O'Neill, H. StC., & Fitzgerald, J. D. (2008). Oxygen solubility
1510 and speciation in sulphide-rich mattes. Geochimica et Cosmochimica Acta, 72, 2619-2635.
1511 Fortin, M. A., Riddle, J., Desjardins-Langlais, Y., & Baker, D. R. (2015). The effect of water on
1512 the sulfur concentration at sulfide saturation (SCSS) in natural melts. Geochimica et Cosmochimica
1513 Acta, 160, 100-116.
1514 Fougeroux, T. (2014) Influence du 59ulphur géodynamique sur l'état d'oxydoréduction du fer
1515 dans les magmas. Thèse de doctorat. Nantes.
1516 Frost, D. J., & Wood, B. J. (1997). Experimental measurements of the fugacity of $CO_2$ and
1517 graphite/diamond stability from 35 to 77 kbar at 925 to 1650 C. Geochimica et Cosmochimica Acta,
1518 61(8), 1565-1574.
1519 Gaetani, G. A., & Grove, T. L. (1997). Partitioning of moderately siderophile elements among
1520 olivine, silicate melt, and sulfide melt: constraints on core formation in the Earth and Mars.
1521 Geochimica et Cosmochimica Acta, 61, 1829-1846.
1522 Gale, A., Dalton, C. A., Langmuir, C. H., Su, Y., & Schilling, J. G. (2013). The mean
1523 composition of ocean ridge basalts. Geochemistry, Geophysics, Geosystems, 14, 489-518.

1524 Grant, N. J., & Chipman, J. (1946). Sulphur equilibria between liquid iron and slags. Trans.
1525 AIME, 167, 134-154.
1526 Gurenko, A. A., Belousov, A. B., Trumbull, R. B., & Sobolev, A. V. (2005). Explosive basaltic
1527 volcanism of the Chikurachki Volcano (Kurile arc, Russia): Insights on pre-eruptive magmatic
1528 conditions and volatile budget revealed from phenocryst-hosted melt inclusions and groundmass
1529 glasses. Journal of Volcanology and Geothermal Research, 147, 203-232.
1530 Haughton, D. R., Roeder, P. L. & Skinner, B. J. (1974). Solubility of sulfur in mafic magmas.
1531 Economic Geology 69, 451-467.
1532 Hauri, E., Wang, J., Dixon, J. E., King, P. L., Mandeville, C., & Newman, S. (2002). SIMS
1533 analysis of volatiles in silicate glasses: 1. Calibration, matrix effects and comparisons with FTIR.
1534 Chemical Geology, 183, 99-114.
1535 Hillert, M. (1998) Phase equilibria, phase diagrams and phase transformations. Subtitled “Their
1536 thermodynamic basis”. Cambridge University Press.
1537 Hillert, M. (2001). The compound energy formalism. Journal of Alloys and Compounds, 320(2),
1538 161-176.
1539 Holmquist, S. (1966). Oxygen ion activity and the solubility of sulfur trioxide in sodium silicate
1540 melts. Journal of the American Ceramic Society, 49(9), 467-473.
1541 Holzheid, A., Palme, H., & Chakraborty, S. (1997). The activities of NiO, CoO and FeO in
1542 silicate melts. Chemical Geology, 139(1-4), 21-38.
1543 Holzheid, A., & Grove, T. L. (2002). Sulfur saturation limits in silicate melts and their
1544 implications for core formation scenarios for terrestrial planets. American Mineralogist, 87(2-3),
1545 227-237.
1546 Jarosewich, E., Nelen, J. A. & Norberg, J. A. (1979). Electron microprobe reference samples for
1547 mineral analyses. Smithsonian Contributions to Earth Sciences 20, 68-72.
1548 Jégo, S., & Dasgupta, R. (2014). The fate of sulfur during fluid-present melting of subducting
1549 basaltic crust at variable oxygen fugacity. Journal of Petrology, 55, 1019-1050.

1550 Jenner, F. E. & O'Neill, H. StC. (2012). Analysis of 60 Elements in 616 Ocean Floor Basaltic
1551 Glasses. *Geochemistry geophysics geosystems* **13**, DOI: 10.1029/2011GC004009.
1552 Jenner, F. E., O'Neill, H. St.C., Arculus, R. J. & Mavrogenes, J. A. (2010). The Magnetite
1553 Crisis in the Evolution of Arc-related Magmas and the Initial Concentration of Au, Ag, and Cu.
1554 *Journal of Petrology* **51**, 2445-2464.
1555 Jugo, P. J., Wilke, M., & Botcharnikov, R. E. (2010). Sulfur K-edge XANES analysis of natural
1556 and synthetic basaltic glasses: Implications for S speciation and S content as function of oxygen
1557 fugacity. Geochimica et Cosmochimica Acta, 74, 5926-5938.
1558 Kamenetsky V. S., Everard J. L., Crawford A. J., Varne R., Eggins S. M. and Lanyon R. (2000)
1559 Enriched end-member of primitive MORB melts: petrology and geochemistry of glasses from
1560 Macquarie Island (SW Pacific). J. Petrol. 41, 411–430.
1561 Kamenetsky, V. S. & Eggins, S. M. (2012). Systematics of metals, metalloids, and volatiles in
1562 MORB melts: Effects of partial melting, crystal fractionation and degassing (a case study of
1563 Macquarie Island glasses). Chemical Geology 302-303, 76-86.
1564 Kamenetsky, V. S., Gurenko, A. A., & Kerr, A. C. (2010). Composition and temperature of
1565 komatiite melts from Gorgona Island, Colombia, constrained from olivine-hosted melt inclusions.
1566 Geology, 38(11), 1003-1006.
1567 Kang, Y. B., & Pelton, A. D. (2009). Thermodynamic model and database for sulfides dissolved
1568 in molten oxide slags. Metallurgical and Materials Transactions B, 40(6), 979-994.
1569 Katsura, T. & Nagashima, S. (1974). Solubility of sulfur in some magmas at 1 atmosphere.
1570 Geochimica et Cosmochimica Acta 38, 517-531.
1571 Kendrick, M. A., Jackson, M. G., Kent, A. J., Hauri, E. H., Wallace, P. J., & Woodhead, J.
1572 (2014). Contrasting behaviours of $CO_2$, S, $H_2O$ and halogens (F, Cl, Br, and I) in enriched-mantle
1573 melts from Pitcairn and Society seamounts. Chemical Geology, 370, 69-81.

Kiseeva, E. S., & Wood, B. J. (2013). A simple model for chalcophile element partitioning between sulphide and silicate liquids with geochemical applications. Earth and Planetary Science Letters, 383, 68-81.

Kiseeva, E. S., & Wood, B. J. (2015). The effects of composition and temperature on chalcophile and lithophile element partitioning into magmatic sulphides. Earth and Planetary Science Letters, 424, 280-294.

Kress, V. (1997). Thermochemistry of sulfide liquids. I. the system O-S Fe at 1 bar. Contributions to Mineralogy and Petrology 127, 176-186.

Kress, V., Greene, L.E., Ortiz, M.D., and Mioduszewski, L (2008) Thermochemistry of sulfide liquids IV: density measurements and the thermodynamics of O–S–Fe–Ni–Cu liquids at low to moderate pressures. Contributions to Mineralogy and Petrology 156, 785-797.

Lange RA, Carmichael ISE (1990) Thermodynamic properties of silicate liquids with an emphasis on density, thermal expansion and compressibility. In: J Nicholls, JK Russell (eds) Modern Methods of Igneous Petrology: Understanding Magmatic Processes. (Reviews in Mineralogy 24) Mineral Soc Am, Washington, D.C., pp 25-64.

Laurenz, V., Fonseca, R. O., Ballhaus, C., Jochum, K. P., Heuser, A., & Sylvester, P. J. (2013). The solubility of palladium and ruthenium in picritic melts: 2. The effect of sulfur. Geochimica et Cosmochimica Acta, 108, 172-183.

Le Voyer, M., Cottrell, E., Kelley, K. A., Brounce, M. & Hauri, E. H. (2015). The effect of primary versus secondary processes on the volatile content of MORB glasses: An example from the equatorial Mid-Atlantic Ridge (5°N–3°S). Journal of Geophysical Research: Solid Earth 120, 125-144.

Le Voyer, M., Kelley, K. A., Cottrell, E., & Hauri, E. H. (2017). Heterogeneity in mantle carbon content from CO 2-undersaturated basalts. Nature Communications, 8, 14062.

1598 Li, J., Agee, C. B. (2001) The effect of pressure, temperature, oxygen fugacity and composition
1599 on partitioning of nickel and cobalt between liquid Fe–Ni–S alloy and liquid silicate: implications
1600 for the Earth's core formation. Geochimica Cosmochimica Acta 65,1821–1832.
1601 Li, C. & Naldrett, A. J. (1993). Sulfide capacity of magma: a quantitative model and its
1602 application to the formation of sulfide ores at Sudbury, Ontario. Economic Geology 88, 1253-1260.
1603 Liu, X., O'Neill, H. St.C., & Berry, A. J. (2005). The effects of small amounts of $H_2O$, $CO_2$ and
1604 $Na_2O$ on the partial melting of spinel lherzolite in the system CaO–MgO–$Al_2O_3$–
1605 $SiO_2$±$H_2O$±$CO_2$±$Na_2O$ at 1.1 Gpa. Journal of Petrology, 47, 409-434.
1606 Liu, Y., Samaha, N. T., & Baker, D. R. (2007). Sulfur concentration at sulfide saturation (SCSS)
1607 in magmatic silicate melts. Geochimica et Cosmochimica Acta, 71, 1783-1799.
1608 Luhr, J. F. (1990). Experimental phase relations of water-and sulfur-saturated arc magmas and
1609 the 1982 eruptions of El Chichón volcano. Journal of Petrology, 31, 1071-1114.
1610 Luhr, J. F. (2008). Primary igneous anhydrite: Progress since its recognition in the 1982 El
1611 Chichón trachyandesite. Journal of Volcanology and Geothermal Research, 175(4), 394-407.
1612 Martin, M. (2001) Life and achievements of Carl Wagner, 100$^{th}$ birthday. Solid State Ionics.
1613 152-153: 15–17.
1614 Mathez, E. A. (1976). Sulfur solubility and magmatic sulfides in submarine basalt glass. Journal
1615 of Geophysical Research 81, 4269-4276.
1616 Matjuschkin, V., Blundy, J. D., & Brooker, R. A. (2016). The effect of pressure on 63ulphur
1617 speciation in mid-to deep-crustal arc magmas and implications for the formation of porphyry copper
1618 deposits. Contributions to Mineralogy and Petrology, 171, 66.
1619 Mavrogenes, J. A. & O'Neill, H. S. C. (1999). The relative effects of pressure, temperature and
1620 oxygen fugacity on the solubility of sulfide in mafic magmas. Geochim. Cosmochim. Acta 63,
1621 1173-1180.

Métrich, N., Joron, J.-L. and Berthier B. (1998) Occurrence of boron-rich potassic melts in the Vulsini Volcanic District, Italy: Evidence from melt inclusions. Geochim. Cosmochim. Acta, 62, 507-514.

Métrich, N., Berry, A. J., O'Neill, H. St.C., & Susini, J. (2009). The oxidation state of sulfur in synthetic and natural glasses determined by X-ray absorption spectroscopy. Geochimica et Cosmochimica Acta, 73, 2382-2399.

Michael, P. (1995). Regionally distinctive sources of depleted MORB: Evidence from trace elements and $H_2O$. Earth and Planetary Science Letters, 131, 301-320.

Moussallam, Y., Edmonds, M., Scaillet, B., Peters, N., Gennaro, E., Sides, I., & Oppenheimer, C. (2016). The impact of degassing on the oxidation state of basaltic magmas: a case study of Kīlauea volcano. Earth and Planetary Science Letters, 450, 317-325.

Mungall, J. E., & Brenan, J. M. (2014). Partitioning of platinum-group elements and Au between sulfide liquid and basalt and the origins of mantle-crust fractionation of the chalcophile elements. Geochimica et Cosmochimica Acta, 125, 265-289.

Mysen, B. O. (1983). The structure of silicate melts. Annual Review of Earth and Planetary Sciences, 11, 75-97.

Mysen, B. O., and Richet, P. (2005). Silicate glasses and melts: properties and structure (Vol. 10). Elsevier.

Naldrett, A. J., & Richardson, S. W. (1967). Effect of water on the melting of pyrrhotite-magnetite assemblages. Carnegie Institute of Washington, Year Book, 66, 429-431.

Nash, W. M., Smythe, D. J., & Wood, B. J. (2019). Compositional and temperature effects on sulfur speciation and solubility in silicate melts. Earth and Planetary Science Letters, 507, 187-198.

Nilsson, K., & Peach, C. L. (1993). Sulfur speciation, oxidation state, and sulfur concentration in backarc magmas. Geochimica et Cosmochimica Acta, 57, 3807-3813.

O'Neill, H. St.C., & Berry, A. J. (2006). Activity coefficients at low dilution of CrO, NiO and CoO in melts in the system $CaO–MgO–Al_2O_3–SiO_2$ at 1400 C: using the thermodynamic behaviour

1648 of transition metal oxides in silicate melts to probe their structure. Chemical Geology, 231(1-2), 77-
1649 89.
1650 O'Neill, H. St.C., Berry, A. J. and Mallmann G. (2018). The oxidation state of iron in Mid-
1651 Ocean Ridge basaltic (MORB) glasses: implications for their petrogenesis and oxygen fugacities.
1652 Earth and Planetary Science Letters, 504, 152-162.
1653 O'Neill, H. St.C. and Eggins, S. M. (2002). The effect of melt composition on trace element
1654 partitioning: an experimental investigation of the activity coefficients of FeO, NiO, CoO, MoO2
1655 and $MoO_3$ in silicate melts. Chemical Geology 186, 151-181.
1656 O'Neill, H. St.C., & Mavrogenes, J. A. (2002). The sulfide capacity and the sulfur content at
1657 sulfide saturation of silicate melts at 1400 C and 1 bar. Journal of Petrology, 43, 1049-1087.
1658 O'Neill, H. St.C., & Mavrogenes, J. A. (2019). The sulfate capacity of silicate melts at
1659 atmospheric pressure. Goldschmidt Abstracts, 2019.
1660 O'Neill, H. S. C., & Pownceby, M. I. (1993). Thermodynamic data from redox reactions at high
1661 temperatures. I. An experimental and theoretical assessment of the electrochemical method using
1662 stabilized zirconia electrolytes, with revised values for the Fe-"FeO", Co-CoO, Ni-NiO and Cu-
1663 $Cu_2O$ oxygen buffers, and new data for the W-$WO_2$ buffer. Contributions to Mineralogy and
1664 Petrology, 114, 296-314.
1665 Patten, C., Barnes, S. J., & Mathez, E. A. (2012). Textural variations in MORB sulfide droplets
1666 due to differences in crystallization history. The Canadian Mineralogist, 50(3), 675-692.
1667 Patten, C., Barnes, S. J., Mathez, E. A., & Jenner, F. E. (2013). Partition coefficients of
1668 chalcophile elements between sulfide and silicate melts and the early crystallization history of
1669 sulfide liquid: LA-ICP-MS analysis of MORB sulfide droplets. Chemical Geology, 358, 170-188.
1670 Peach, C. L., & Mathez, E. A. (1993). Sulfide melt-silicate melt distribution coefficients for
1671 nickel and iron and implications for the distribution of other chalcophile elements. Geochimica et
1672 Cosmochimica Acta, 57(13), 3013-3021.

1673 Peach, C. L., Mathez, E. A., Keays, R. R., & Reeves, S. J. (1994). Experimentally determined
1674 sulfide melt-silicate melt partition coefficients for iridium and palladium. Chemical Geology, 117,
1675 361-377.
1676 Pelton, A. D., Eriksson, G. & Romero-Serrano, A. (1993). Calculation of sulfide capacities of
1677 multicomponent slags. Metallurgical Transactions B 24B, 817-825.
1678 Poulson, S. R. & Ohmoto, H. (1990). An evaluation of the solubility of sulfide sulfur in silicate
1679 melts from experimental data and natural samples. Chemical Geology 85, 57-75.
1680 Putirka, K. D. (2008). Thermometers and Barometers for Volcanic Systems. Reviews in
1681 Mineralogy and Geochemistry 69, 61-120.
1682 Reddy, R. G., & Blander, M. (1987). Modeling of sulfide capacities of silicate melts.
1683 Metallurgical Transactions B, 18B, 591-596.
1684 Righter, K., Pando, K., & Danielson, L. R. (2009). Experimental evidence for sulfur-rich
1685 martian magmas: Implications for volcanism and surficial sulfur sources. Earth and Planetary
1686 Science Letters, 288, 235-243.
1687 Ripley, E. M., Brophy, J. G., & Li, C. (2002). Copper solubility in a basaltic melt and sulfide
1688 liquid/silicate melt partition coefficients of Cu and Fe. Geochimica et Cosmochimica Acta, 66(15),
1689 2791-2800.
1690 Roberge, J., White, R. V., & Wallace, P. J. (2004). Volatiles in submarine basaltic glasses from
1691 the Ontong Java Plateau (ODP Leg 192): implications for magmatic processes and source region
1692 compositions. Geological Society, London, Special Publications, 229, 239-257.
1693 Robie, R.A., Hemingway, B.S. (1995) Thermodynamic properties of minerals and related
1694 substances at 298.15 K and 1 bar ($10^5$ Pascals) pressure and at higher temperatures. US Geological
1695 Survey Bulletin 2131, 1-461.
1696 Roeder, P. L. (1974). Activity of iron and olivine solubility in basaltic liquids. Earth and
1697 Planetary Science Letters 23, 397-410.

1698 Sattari, P., Brenan, J. M., Horn, I., & McDonough, W. F. (2002). Experimental constraints on
1699 the sulfide-and chromite-silicate melt partitioning behavior of rhenium and platinum-group
1700 elements. Economic Geology, 97, 385-398.
1701 Schrama, F. N. H., Beunder E. M.,, Van den Berg, B., Yang, Y.-X. and Boom, R. (2017)
1702 Sulphur removal in ironmaking and oxygen steelmaking, Ironmaking & Steelmaking, 44:5, 333-
1703 343.
1704 Schmalzried, H. (1995) Chemical Kinetics of Solids, VCH, Weinheim
1705 Self, S., Blake, S., Sharma, K., Widdowson, M., & Sephton, S. (2008). Sulfur and chlorine in
1706 Late Cretaceous Deccan magmas and eruptive gas release. Science, 319(5870), 1654-1657.
1707 Shima, H. & Naldrett, A. J. (1975). Solubility of sulfur in ultramafic melt and the relevance of
1708 the system Fe-S-O. Economic Geology 70, 960-967.
1709 Shimizu, K., Saal, A. E., Myers, C. E., Nagle, A. N., Hauri, E. H., Forsyth, D. W., Kamenetsky,
1710 V.S., & Niu, Y. (2016). Two-component mantle melting-mixing model for the generation of mid-
1711 ocean ridge basalts: implications for the volatile content of the Pacific upper mantle. Geochimica et
1712 Cosmochimica Acta, 176, 44-80.
1713 Stolper, E., Sherman, S., Garcia, M., Baker, M., & Seaman, C. (2004). Glass in the submarine
1714 section of the HSDP2 drill core, Hilo, Hawaii. Geochemistry, Geophysics, Geosystems, 5(7)
1715 Q07G15.
1716 Smythe, D. J., Wood, B. J., & Kiseeva, E. S. (2017). The S content of silicate melts at sulfide
1717 saturation: new experiments and a model incorporating the effects of sulfide composition. American
1718 Mineralogist, 102, 795-803.
1719 Thordarson, T., Self, S., Óskarsson, N. & Hulsebosch, T. (1996). Sulfur, chlorine, and fluorine
1720 degassing and atmospheric loading by the 1783-1784 AD Laki (Skaftár Fires) eruption in Iceland.
1721 Bulletin of Volcanology 58, 205-225.
1722 Thornber, C. R., Sherrod, D. R., Siems, D. F., Heliker, C. C., Meeker, G. P., Oscarson, R. L.,
1723 Kauahikaua, J. P., 2002, Whole-rock and glass major-element geochemistry of Kilauea Volcano,

1724 Hawaii, near-vent eruptive products: September 1994 through September 2001: U.S. Geological
1725 Survey Open-File Report 2002-17, https://pubs.usgs.gov/of/2002/0017/.
1726 Tuff, J., & O'Neill, H. S. C. (2010). The effect of sulfur on the partitioning of Ni and other first-
1727 row transition elements between olivine and silicate melt. Geochimica et Cosmochimica Acta, 74,
1728 6180-6205.
1729 Vidal, C. M., Métrich, N., Komorowski, J. C., Pratomo, I., Michel, A., Kartadinata, N., Robert,
1730 V. & Lavigne, F. (2016). The 1257 Samalas eruption (Lombok, Indonesia): the single greatest
1731 stratospheric gas release of the Common Era. Scientific Reports, 6, 34868.
1732 Wallace, P. & Carmichael, I. S. E. (1992). Sulfur in basaltic magmas. Geochimica et
1733 Cosmochimica Acta 56, 1683-1874.
1734 Waldner, P., & Pelton, A. D. (2005). Thermodynamic modeling of the Fe-S system. Journal of
1735 phase equilibria and diffusion, 26(1), 23-38.
1736 Wilke, M., Jugo, P. J., Klimm, K., Susini, J., Botcharnikov, R., Kohn, S. C., & Janousch, M.
1737 (2008). The origin of $S^{4+}$ detected in silicate glasses by XANES. American Mineralogist, 93, 235-
1738 240.
1739 Wilke, M., Klimm, K., & Kohn, S. C. (2011). Spectroscopic studies on sulfur speciation in
1740 synthetic and natural glasses. Reviews in Mineralogy and Geochemistry, 73, 41-78.
1741 Wood, B. J. & Nicholls, J. (1978). The thermodynamic properties of reciprocal solid solutions.
1742 Contributions to Mineralogy and Petrology 66, 389-400.
1743 Wood, B. J., & Wade, J. (2013). Activities and volatilities of trace components in silicate melts:
1744 a novel use of metal–silicate partitioning data. *Contributions to Mineralogy and Petrology*, *166*(3),
1745 911-921.
1746

Table 1. Experimental studies used in parameterizing the sulfide content at sulfide saturation (SCSS) in silicate melts.

| Reference | T range (ºC) | P range (Gpa) | No. data used | Chalcophile elements |
|---|---|---|---|---|
| *Anhydrous* | | | | |
| Haughton et al. (1974) | 1200 | $10^{-4}$ | $C_{S^{2-}}$ only | - |
| Danckwerth et al. (1979) | 1200 -1260 | $10^{-4}$ | 14 | - |
| Peach and Mathez (1993) | 1450 | 0.8 | 10 | Ni |
| Peach et al. (1994) | 1450 | 0.8 | 24 | - |
| Gaetani and Grove (1997) | 1350 | $10^{-4}$ | 22 | Ni & Cu |
| Mavrogenes and O'Neill (1999) | 1400-1800 | 0.5 – 5.5 | 16 | - |
| Baker et al. (2001) | 1225-1450 | 1.0 | 6 | - |
| O'Neill and Mavrogenes (2002) | 1400 | $10^{-4}$ | 34 | - |
| Holzheid and Grove (2002) | 1350 – 1600 | 0.9 – 2.7 | 4 | Ni |
| Ripley et al. (2002) | 1245 | $10^{-4}$ | 22 | Cu |
| Sattari et al. (2002) | 1330 | 1.0 | 5 | |
| Jugo et al. (2005) | 1355 | 1.6 | 7 | - |
| Liu et al. (2007) | 1150 – 1450 | 0.5 – 1.0 | 41 | - |
| Brenan (2008) | 1200 – 1300 | $10^{-4}$, 0.9 – 1.6 | 21 | Ni & Cu |
| Righter et al. (2009) | 1200 – 1500 | $10^{-4}$, 0.8 | 16 | - |
| Tuff and O'Neill (2010) | 1370 | $10^{-4}$ | 15 | minor Ni |
| Kiseeva and Wood (2013) | 1400 | 1.5 | 14 | Ni & Cu |
| Ding et al. (2014) | 1500 – 1700 | 1 – 4 | 25 | - |
| Kiseeva and Wood (2015) | 1300 – 1700 | 1.5 | 29 | Ni & Cu |
| Wood and Kiseeva (2015) | 1400 - 1460 | 1 – 1.5 | 9 | minor Ni |
| Wykes et al. (2015) | 1400 | 1.5 | 12 | - |
| Fortin et al. (2015) | 1250 | 1.0 | 3 | - |
| Smythe et al. (2017) | 1400 - 1800 | 1.5 – 5.5 | 36 | Ni & Cu |
| O'Neill and Mavrogenes (in prep.) | 1300 | $10^{-4}$ | 22 | - |
| *Hydrous* | | | | |
| Moune et al. (2009) | 1045 | 0.2 – 0.3 | 16 | - |
| Fortin et al. (2015) | 1250 | 1.0 | 10 | - |
| D'Souza and Canil (2018) | 1270 | 1.0 | 13 | - |
| This study (Table 3) | 1400 | 1.5 | 6 | - |

Table 2. Sulfur analyses in natural OFB glass VG2 (USNM 111240/52) by electron microprobe, unless identified otherwise (italics). Also listed are analyses of JDFD2 (USNM 117354/46), which has often been presumed to be the same sample. The identification of JDFD2 as a different glass (VG7432) is based on the information in Cottrell and Kelley (2011).

| S (ppm) | s(S) (ppm) | No. analyses | Reference |
|---|---|---|---|
| 1340 | 80 | 19 | Dixon et al. (1991) |
| 1420 | 40 | 6 | Wallace and Carmichael (1991)[a] |
| *1320* | *50* | *2* | *Wallace and Carmichael (1991)* [a,b] |
| 1400 | 40 | ? | Nilsson and Peach (1993) [a] |
| 1348 | 62 | 135 | Thordarson et al. (1996)[c] |
| 1365 | 29 | 139 | Thordarson et al. (1996)[c] |
| 1450 | 30 | ? | Métrich et al. (1999) |
| 1416 | 36 | 10 | De Hoog et al. (2001) |
| 1403 | 31 | ? | O'Neill and Mavrogenes (2002) |
| 1305 | 35 | 203 | Thornber et al. (2002) |
| 1310 | 130 | 57 | Stolper et al. (2004) |
| 1380 | 60 | ? | De Hoog et al. (2004) |
| 1549 | 166 | ? | Roberge et al. (2004) |
| 1490 | 60 | 38 | Gurenko et al. (2005) |
| 1414 | 30 | 38 | Liu et al. (2007) |
| 1405 | 39 | ? | Baker (2008) |
| 1362 | 160 | 48 | Davis et al. (2008) |
| 1410 | 60 | 23 | Self et al. (2008) |
| 1300 | 44 | ? | Bell et al. (2009) |
| 1400 | 115 | 37 | Kamenetsky et al. (2010) |
| 1415 | 68 | 247[d] | Jenner and O'Neill (2012) |
| 1440 | 30 | ? | Laurenz et al. (2013) |
| 1610 | 30 | ? | Jégo and Dasgupta (2014) |
| 1422 | 11 | 17 x 5 | Fougeroux (2014)[a] |
| 1392 | 61 | 21 | Wykes et al. (2015) |
| 1402 | 28 | 4 | Fortin et al. (2015) |
| 1435 | 40 | 43 | Vidal et al. (2016) |
| *1486* | *27* | *77* | *LeVoyer et al. (2017)*[e] |
| 1521 | 41 | 18 | D'Souza and Canil (2018) |

[a] glass identified as JDFD2 rather than VG2; [b] wet chemistry; [c] Two different EMPA routines; [d] in 19 sessions, spanning two years; [e] SIMS

Table 3. SCSS experiments in Re capsules at 1400ºC, 1.5 GPa using the starting composition and experimental methods described in Wykes et al. (2015).

| run number | G60* | G61 | G70 | G76* | G93 | G94* |
|---|---|---|---|---|---|---|
| added $H_2O$ | 1.4 | 1.8 | 4 | 0.2 | 0.2 | 5 |
| $Na_2O$ | 2.64 | 2.61 | 2.46 | 2.59 | 2.48 | 2.41 |
| MgO | 9.5 | 9.5 | 9.4 | 9.7 | 9.3 | 9.4 |
| $Al_2O_3$ | 19.6 | 19.5 | 19.3 | 19.5 | 19.1 | 19.2 |
| $SiO_2$ | 50.4 | 50.5 | 49.8 | 50.2 | 49.1 | 50.1 |
| CaO | 10.7 | 10.7 | 10.1 | 10.5 | 10.3 | 10.2 |
| $TiO_2$ | 1.27 | 1.28 | 1.21 | 1.19 | 1.23 | 1.14 |
| FeO(t) | 5.2 | 5.3 | 7.3 | 5.6 | 8.2 | 7.3 |
| $H_2O$ | 0.44 | 0.43 | 0.21 | 0.60 | 0.17 | 0.15 |
| S | 1176 | 1193 | 1332 | 1434 | 1268 | 1256 |
| s(S) | 82 | 90 | 69 | 79 | 169 | 24 |

* Sulfur K-edge XANES spectra for these samples were obtained by Métrich et al. (2009)

1766 Table 4. SCSS model sensitivities (anhydrous model)
1767

| Variable (X) | Unit ($n_X$) | $\partial[S]_{SCSS}/\partial n_X$ (ppm $n_X^{-1}$) |
|---|---|---|
| $Na_2O$ | 1 wt% | 7 |
| MgO | 1 wt% | 60 |
| $Al_2O_3$ | 1 wt% | -37 |
| $SiO_2$ | 1 wt% | -19 |
| CaO | 1 wt% | 45 |
| $TiO_2$ | 1 wt% | 31 |
| MnO | 0.1 wt% | 17.9 |
| $FeO_t$ | 1 wt% | 106 |
| Ni | 1 ppm | -1.1 |
| Cu | 1 ppm | -1.9 |
| $Fe^{3+}/\sum Fe$ | 0.01 | -12 |
| T | 1 K | 2.25 |
| P | 0.01 GPa | 1.5 |

1768
1769

**FIGURE CAPTIONS**

Figure 1. Comparison between values of $A_M^{S^{2-}}$ from O'Neill and Mavrogenes (2002) and Evans et al. (2008) with thermodynamic data for the difference in the free energies of the orthosilicate and sulfide solid phases, $(\frac{1}{2}\mu^o_{M_{\frac{4}{z}}SiO_4} - \mu^o_{M_{\frac{2}{x}}S})/1400R$. The correlation suggests how approximate values of $A_{Ni}^{S^{2-}}$ and $A_{Cu}^{S^{2-}}$, which are difficult to measure experimentally (Evans et al. 2008), may be estimated.

Figure 2. The relationship between $S^{6+}/\sum S$ and $Fe^{3+}/\sum Fe$, estimated by combining the results of Jugo et al. (2010) on hydrated basalt at 1050ºC and 0.2 GPa, with those of Berry et al. (2018) on MORB glasses (dashed curve), compared to the model of Nash et al. (2019) calculated at 1190ºC (solid curve). The ± 2s range of measured $Fe^{3+}/\sum Fe$ in MORB glasses from Berry et al. (2018), taken here to correspond to 95% of the population by assuming a normal distribution of $Fe^{3+}/\sum Fe$, is indicated by the shaded region. The model of Nash et al. (2019) predicts only a few percent $S^{6+}/\sum S$ even in the more oxidized MORB glasses.

Figure 3. a) Observed values of the sulfide capacity, $C_{S^{2-}}$, at 1400ºC of silicate melts at with NBO/T from 0.05 to 2, compared to the parameterization of this work (Eqn. 33). The experimental data are from O'Neill and Mavrogenes (2002) and Tuff and O'Neill (2010). Only the data with ln $C_{S^{2-}}$ > -4 are plotted, as the few data at lower $C_{S^{2-}}$ have NBO/T ~ 0, and furthermore are imprecise due to low S. b) Calculated values of $C_{S^{2-}}$ from Eqn. (34) versus the measured values of Haughton et al. (1974) at 1200ºC.

Figure 4. Comparison between measured values of the activity coefficient of FeO in silicate melts ($\gamma_{FeO}^{sil\ melt}$) with the parameterization of Equation (46).
a) Data of Doyle and Naldrett (1986), and Doyle (1987, 1988), all at 1327ºC. b) Data of Roeder (1974), O'Neill and Eggins (2002), Borisov et al. (2004, 2006), and Borisov (2007), temperatures

between 1150 and 1500ºC. All experiments equilibrated silicate melt with Fe metal at imposed oxygen fugacity. The grey areas on either side of the 1:1 lines indicates ± 10% relative error.

Figure 5. The oxygen contents as the component FeO in sulfide mattes coexisting with silicate melt. Data from Brenan (2008), Kiseeva and Wood (2013, 2015), Wood and Kiseeva (2015) and Smythe et al. (2017). The dashed line is the least-squares best fit, $[FeO]_{sulf} = 1.20\ (\pm 0.04)\ [FeO]_{sil\ melt}$, with $R^2 = 0.81$. The solid line is $[FeO]_{sulf} = [FeO]_{sil\ melt}$, which was used in the SCSS modeling for simplicity.

Figure 6. The effect of pressure on the SCSS, comparing Eqn. (43) of this study, calculated starting from $[S]_{SCSS}$ = 1400 ppm at ambient pressure, with the equations for SCSS from Mavrogenes and O'Neill (1999), Holzheid and Grove (2002) and Smythe et al. (2017), all at 1400ºC. The different calculated values of $[S]_{SCSS}$ at P = 0 are due in part to the different compositions studied. The effect of pressure found by Wendlandt (1982) is similar to that of Mavrogenes and O'Neill (1999) and Holzheid and Grove (2002), and is not shown for clarity. The effect of pressure from Smythe et al. (2017) is smaller than those from Mavrogenes and O'Neill (1997) or Holzheid and Grove (2002), but is similar to the hypothetical parameterization postulated in this study at > 1 GPa. This comparison shows the desirability of integrating experiments at high pressure with those at 1 bar, to constrain the effect of pressure more precisely in the range 1 bar to 1.5 GPa.

Figure 7. SCSS for a binary compositional join between FeO-free "matrix" and FeO. Experimental data from Wykes et al. (2015) and this study (Table 3) compared to the SCSS model. The model gives a good fit to the data at < 1 wt% FeO, which were not used as input, and also to the data at high FeO, which have not been well fitted by previous models, see Fig. 9 of Wykes et al. (2015).

Figure 8. The effect of $H_2O$ on SCSS. Data from Moune et al. (2009) at 1045ºC, ~ 0.3 GPa, in equilibrium with pyrrhotite; Fortin et al. (2015), 1250ºC, 1 GPa; D'Souza and Canil (2018), 1270ºC, 1 GPa; and this work, Table 3, 1400ºC, 1.5 GPa. a) The difference ln $[S]_{obs}$ - ln $[S]_{SCSS}$(dil), which is equivalent to ln $C_{S^{2-}}^{H}$, see text for further explanation. b) $[S]_{SCSS}$ calculated from the model vs. $[S]_{obs}$. The shaded area around the 1:1 line indicates ± 10%.

Figure 9. Sulfur saturation in Ocean Floor Basaltic (OFB) glasses from Jenner and O'Neill (2012). a) Calculated SCSS versus S contents analysed by electron microprobe. Of the 329 glasses, only 11 (3%) were identified as probably having lost S. (Two samples with very low S plot off the diagram). b) This S loss is correlated with decreasing S/Se. The vector for this loss is calculated assuming 1000 ppm S and 0.33 ppm Se, with Se contents of the melt assumed to be conserved (Jenner et al. 2010).

Figure 10. The difference between $[S]_{obs}$ and the calculated SCSS from the model for 35 OFB glasses from Jenner and O'Neill (2012) compared against their $Fe^{3+}/\sum Fe$ determined from XANES by Berry et al. (2018). There is almost no correlation ($R^2$ =0.16). One glass, VG6822, not used in the regression, has low S due to loss by volatility, but retains typical $Fe^{3+}/\sum Fe$.

Figure 11. Calculated atomic Ni/Fe (a) and Cu/Fe (b) in sulfide liquid in equilibrium with the OFB glasses analysed by Jenner and O'Neill (2012), compared to observed Ni/Fe and Cu/Fe in sulfide globules from basalts analysed by electron microprobe, by Czamanske and Moore (1977) and Patten et al. (2012). Also plotted are calculated Ni/Fe and Cu/Fe for the same OFB glasses from the model of Smythe et al. (2017).

Figure 12. Comparison with the SCSS model of Smythe et al. (2017). a) Calculated $[S]_{SCSS}$ for the OFB glasses of Jenner and O'Neill (2012) from the model of Smythe et al. (2017) vs. $[S]_{obs}$,

1847 compared to the model of this work. b) The difference between the models is a function of the FeO
1848 content of the glasses.
1849
1850 Figure 13. a) Reproducibility of S analyses in basaltic glasses: a comparison of SIMS vs. EMPA.
1851 SIMS analyses of Macquarie Island glasses from Shimizu et al. (2016) are compared against EMPA
1852 analyses of the same glasses from Kamenetsky et al. (2000), and SIMS and EMPA analyses of
1853 some Ocean Island Basalt glasses from Kendrick et al. (2014). b) Comparison of model $[S]_{SCSS}$
1854 calculated from the analyses of Shimizu et al. (2016) with those calculated for the same glasses
1855 from the analyses of Kamenetsky et al. (2000) and Kamenetsky and Eggins (2012).
1856
1857 Figure 14. Comparison of model $[S]_{SCSS}$ with $[S]_{obs}$ for Macquarie Island basaltic glasses, using the
1858 analyses of Shimizu et al. (2016) and those of Kamenetsky et al. (2000) and Kamenetsky and
1859 Eggins (2012). The latter scatter around the 1:1 line, the former are displaced to higher model
1860 $[S]_{SCSS}$, which, if accurate could be interpreted as indicating sulfide-undersaturation. The shaded
1861 area surrounding the 1:1 line indicates ± 10% uncertainty
1862
1863 Figure 15. Comparison between model $[S]_{SCSS}$ and $[S]_{obs}$ for two sets of glasses from Shimizu et al.
1864 (2016) analysed by SIMS. Most glasses are displaced to high $[S]_{obs}$ by 9% (dashed line) from the
1865 1:1 line, which could be a systematic analytical artifact. However, a few glasses have even higher
1866 $[S]_{obs}$, suggesting excess S as $SO_4^{2-}$. These glasses could be checked for $Fe^{3+}/\sum Fe$ and $S^{6+}/\sum S$ by
1867 XANES.
1868
1869 Figure 16. Olivine-hosted melt inclusions from Le Voyer et al. (2017). a) model $[S]_{SCSS}$ compared
1870 to $[S]_{obs}$, both uncorrected (i.e., as analysed), and with silicate melt compositions corrected for post-
1871 entrapment crystallization. The agreement for the uncorrected compositions is mostly within ± 10%
1872 (shaded area). B) shows that the larger the correction for post-entrapment crystallization, the worse

1873 the discrepancy between $[S]_{obs}$ and calculated $[S]_{SCSS}$. However, there is also a significant
1874 correlation ($R^2 = 0.43$) between $[S]_{obs}$ and calculated $[S]_{SCSS}$ for the uncorrected data, indicating that
1875 the perceived need for correction may be a sign of disequilibrium between olivine and melt at the
1876 time of entrapment.
1877
1878 Figure 17. Ni and Cu abundances in Ocean Floor Basaltic (OFB) glasses versus MgO. Data from
1879 Jenner and O'Neill (2012) and Gale et al. (2013).
1880
1881 Figure 18. Calculated $[S]_{SCSS}$ vs. $[S]_{obs}$ for olivine-hosted melt inclusions from the Siqueiros
1882 Fracture Zone (Saal et al. 2002), with Ni and Cu contents estimated using the correlations with
1883 MgO shown in Fig. 17. Both the uncorrected melt compositions and those corrected for post-
1884 entrapment crystallization plot around the 1:1 line, indicating that most inclusions are likely sulfide-
1885 saturated. Only four inclusions have significantly lower [S] than expected for saturation.
1886
1887 Figure 19. a) $\log_{10} fS_2$ and b) $\log_{10} fSO_2$ calculated for 35 sulfide-saturated OFB glasses. S analyses
1888 from Jenner and O'Neill (2012), $Fe^{3+}/\sum Fe$ from Berry et al. (2018), calculated $\Delta$QFM from O'Neill
1889 et al. (2018).
1890

Figure 1

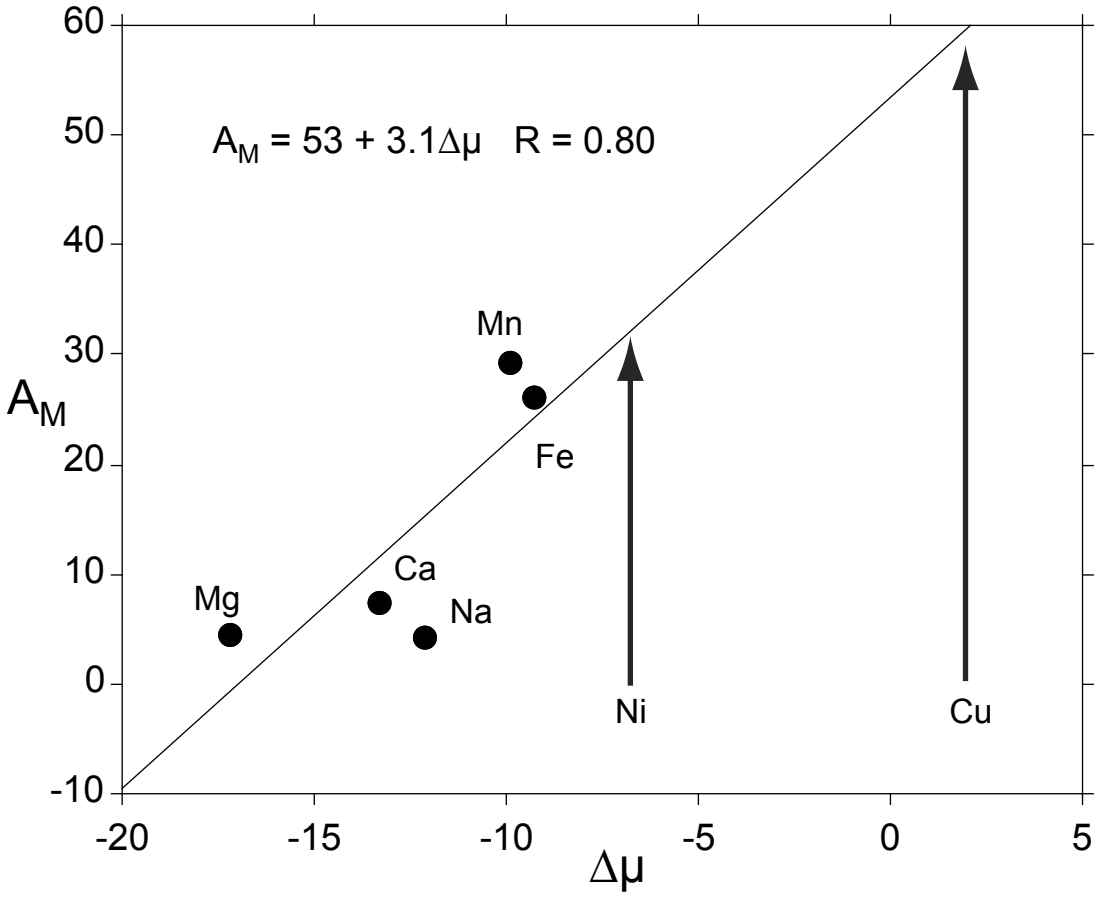
$A_M = 53 + 3.1\Delta\mu$ R = 0.80
$A_M$
$\Delta\mu$
60
50
40
30
20
10
0
-10
-20
-15
-10
-5
0
5
Mn
Fe
Ca
Na
Mg
Ni
Cu

Figure 2

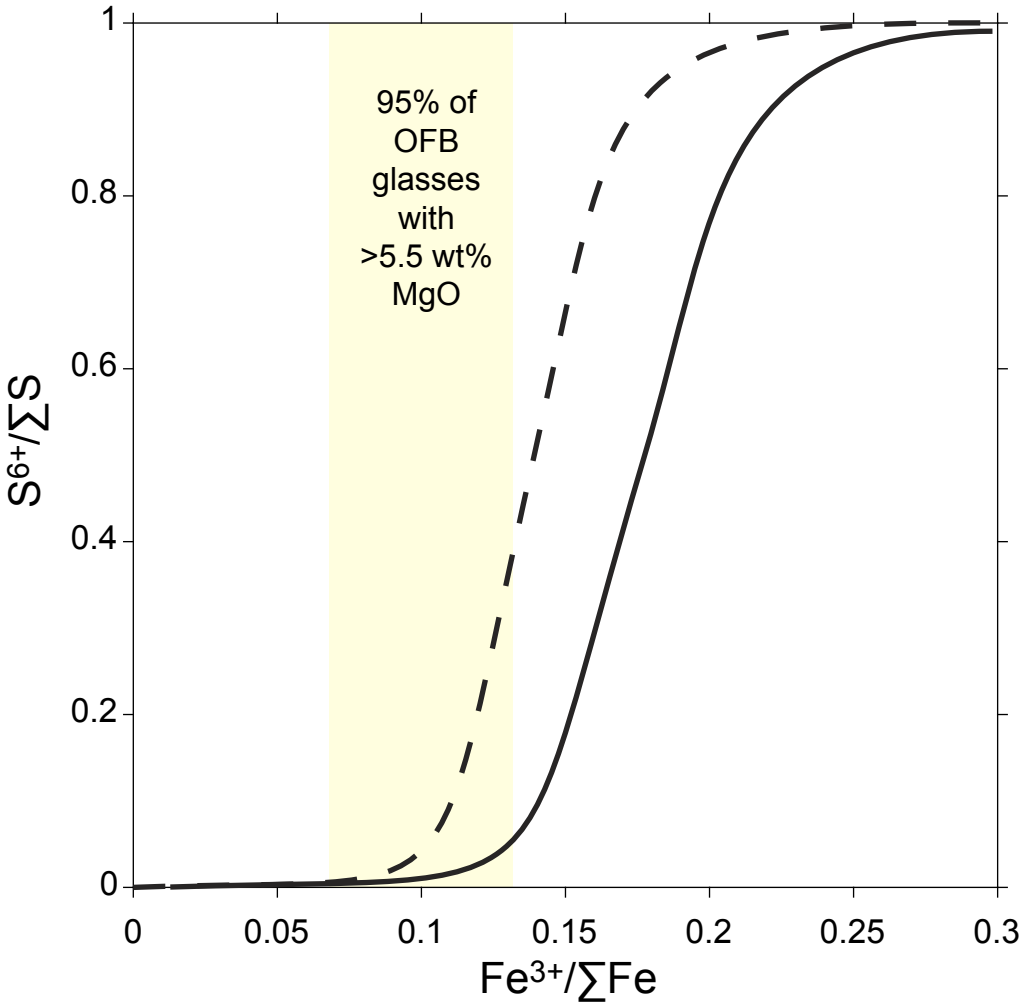
95% of
OFB
glasses
with
>5.5 wt%
MgO
1
0.8
0.6
0.4
0.2
0
0
0.05
0.1
0.15
0.2
0.25
0.3
S6+/∑S
Fe3+/∑Fe

Figure 3

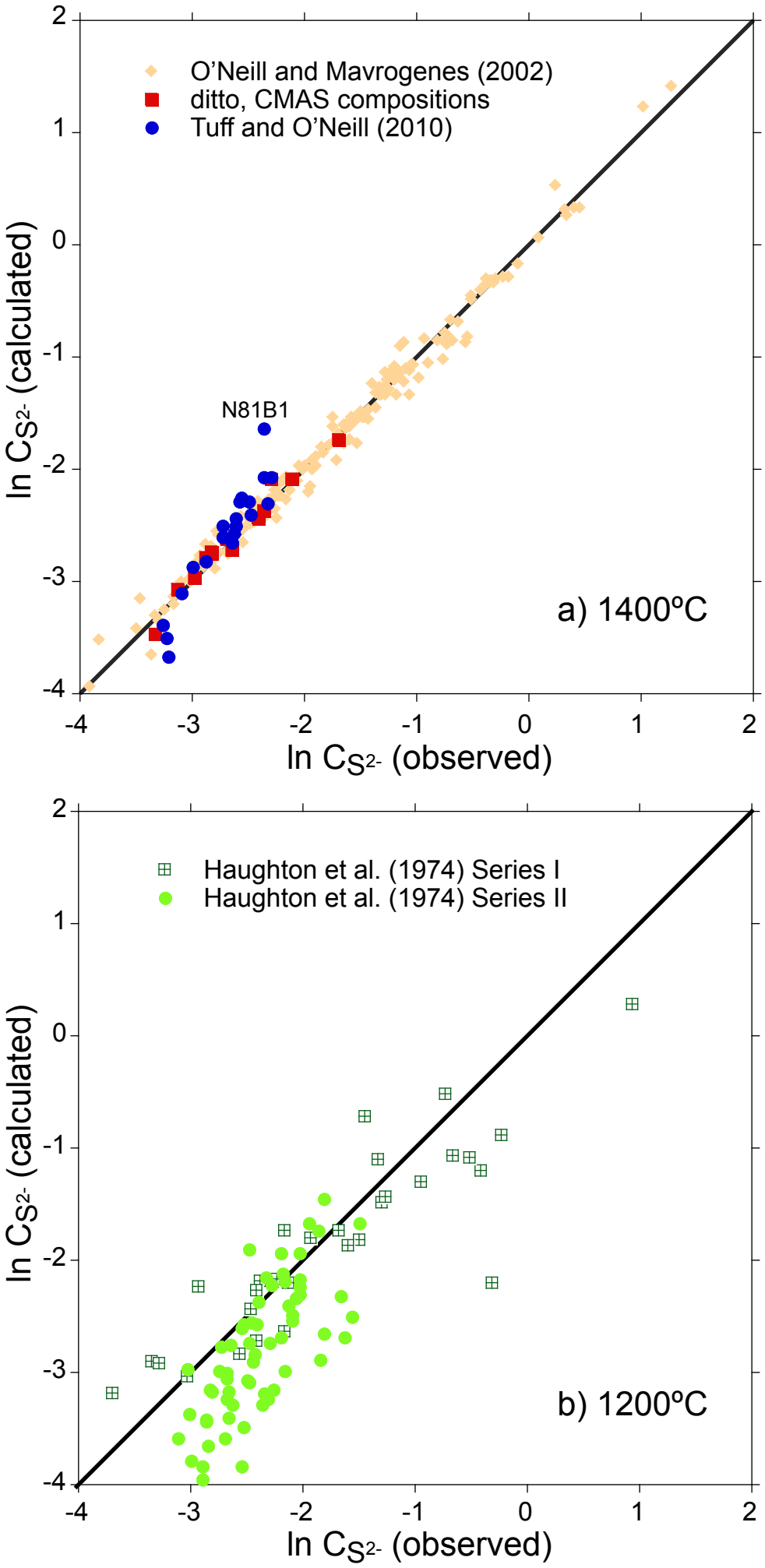
O'Neill and Mavrogenes (2002)
ditto, CMAS compositions
Tuff and O'Neill (2010)
N81B1
a) 1400ºC
ln $C_{S^{2-}}$ (calculated)
ln $C_{S^{2-}}$ (observed)
Haughton et al. (1974) Series I
Haughton et al. (1974) Series II
b) 1200ºC
ln $C_{S^{2-}}$ (calculated)
ln $C_{S^{2-}}$ (observed)

Figure 4

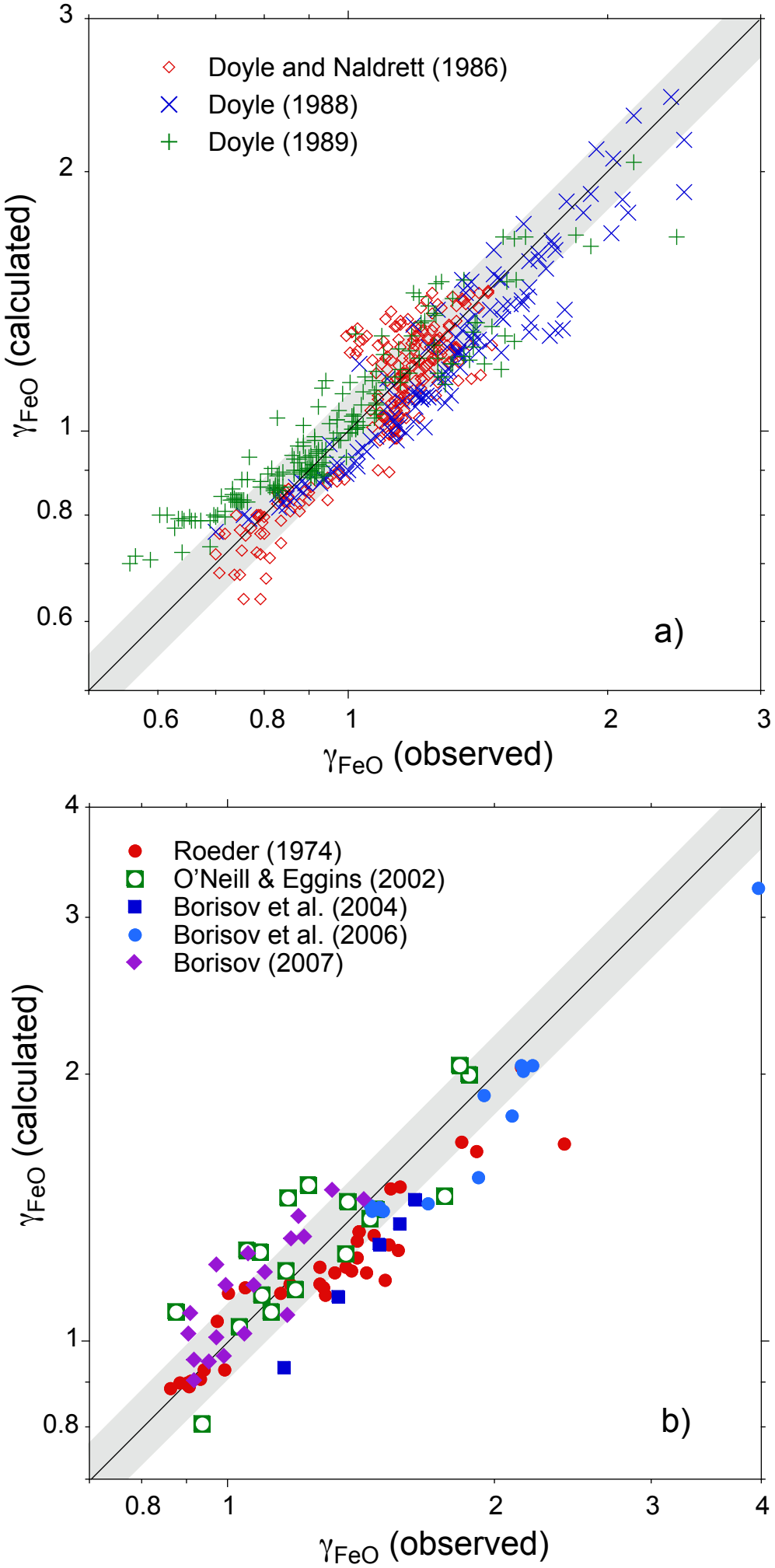
Doyle and Naldrett (1986)
Doyle (1988)
Doyle (1989)
a)
γFeO (calculated)
γFeO (observed)
Roeder (1974)
O'Neill & Eggins (2002)
Borisov et al. (2004)
Borisov et al. (2006)
Borisov (2007)
b)
γFeO (calculated)
γFeO (observed)

Figure 5

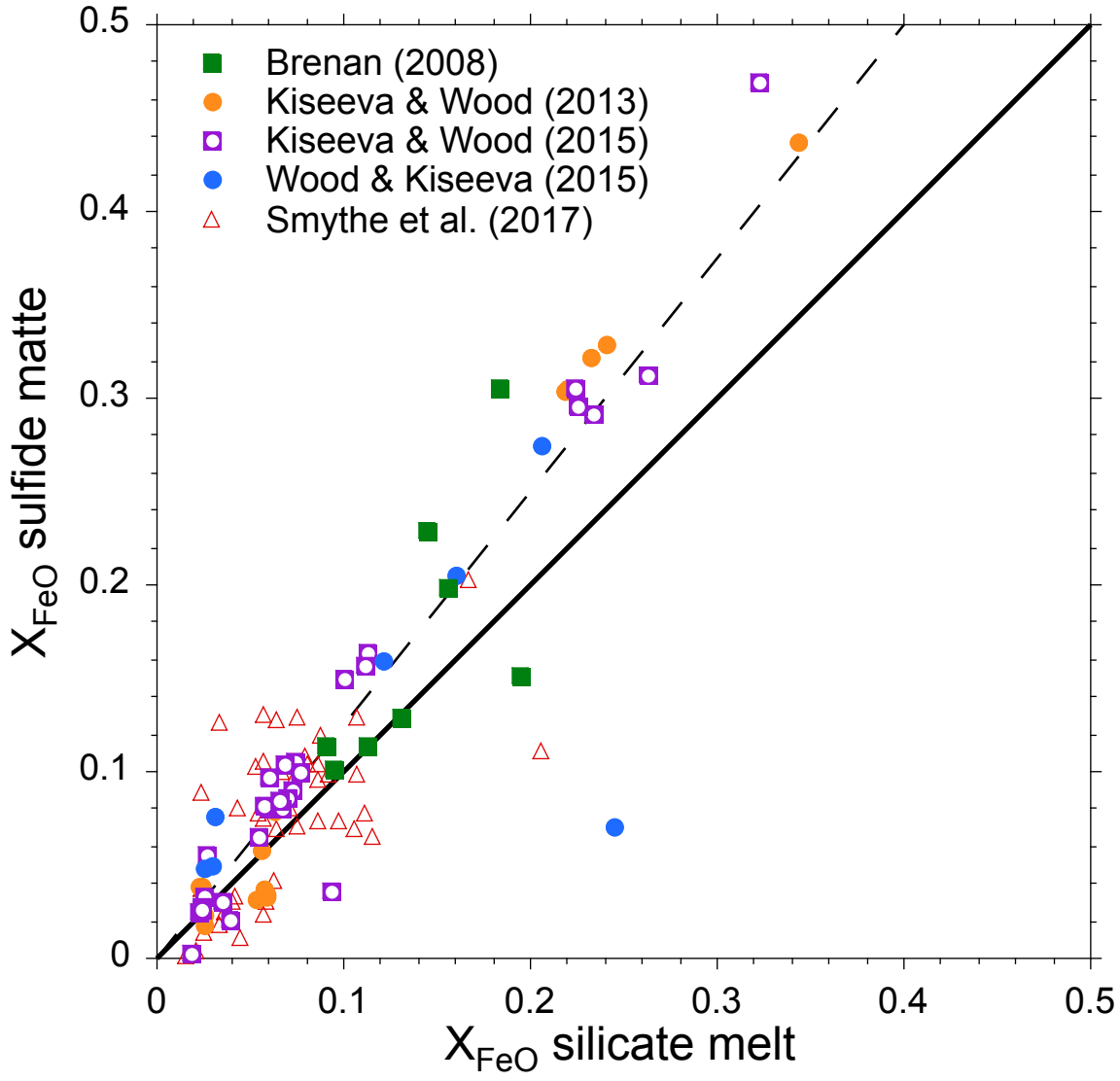
Brenan (2008)
Kiseeva & Wood (2013)
Kiseeva & Wood (2015)
Wood & Kiseeva (2015)
Smythe et al. (2017)
$X_{FeO}$ sulfide matte
$X_{FeO}$ silicate melt
0
0.1
0.2
0.3
0.4
0.5

Figure 6

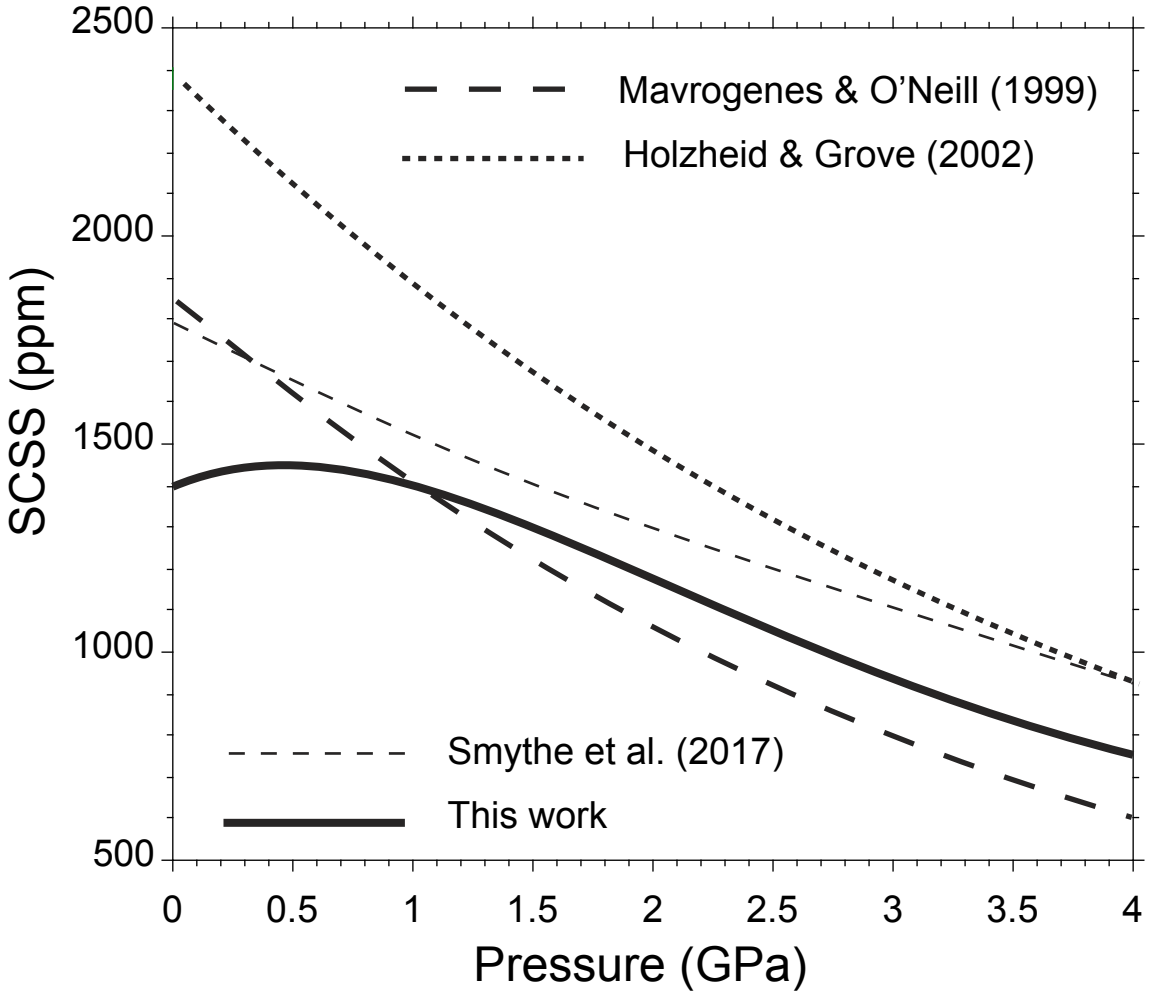
2500
2000
1500
1000
500
SCSS (ppm)
0
0.5
1
1.5
2
2.5
3
3.5
4
Pressure (GPa)
Mavrogenes & O'Neill (1999)
Holzheid & Grove (2002)
Smythe et al. (2017)
This work

Figure 7

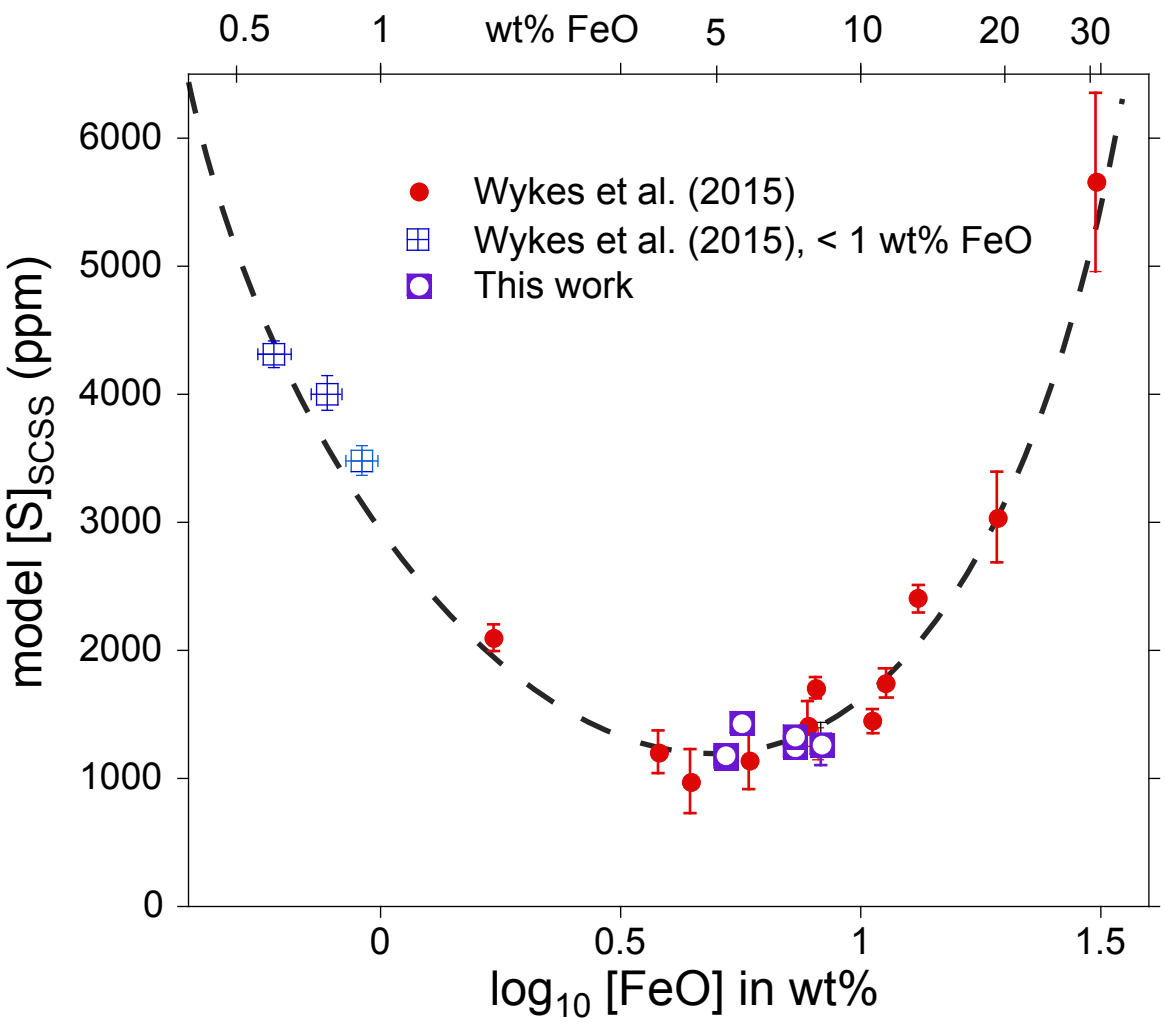
0.5
1
wt% FeO
5
10
20
30
6000
5000
4000
3000
2000
1000
0
model [S]SCSS (ppm)
Wykes et al. (2015)
Wykes et al. (2015), < 1 wt% FeO
This work
0
0.5
1
1.5
log10 [FeO] in wt%

Figure 8

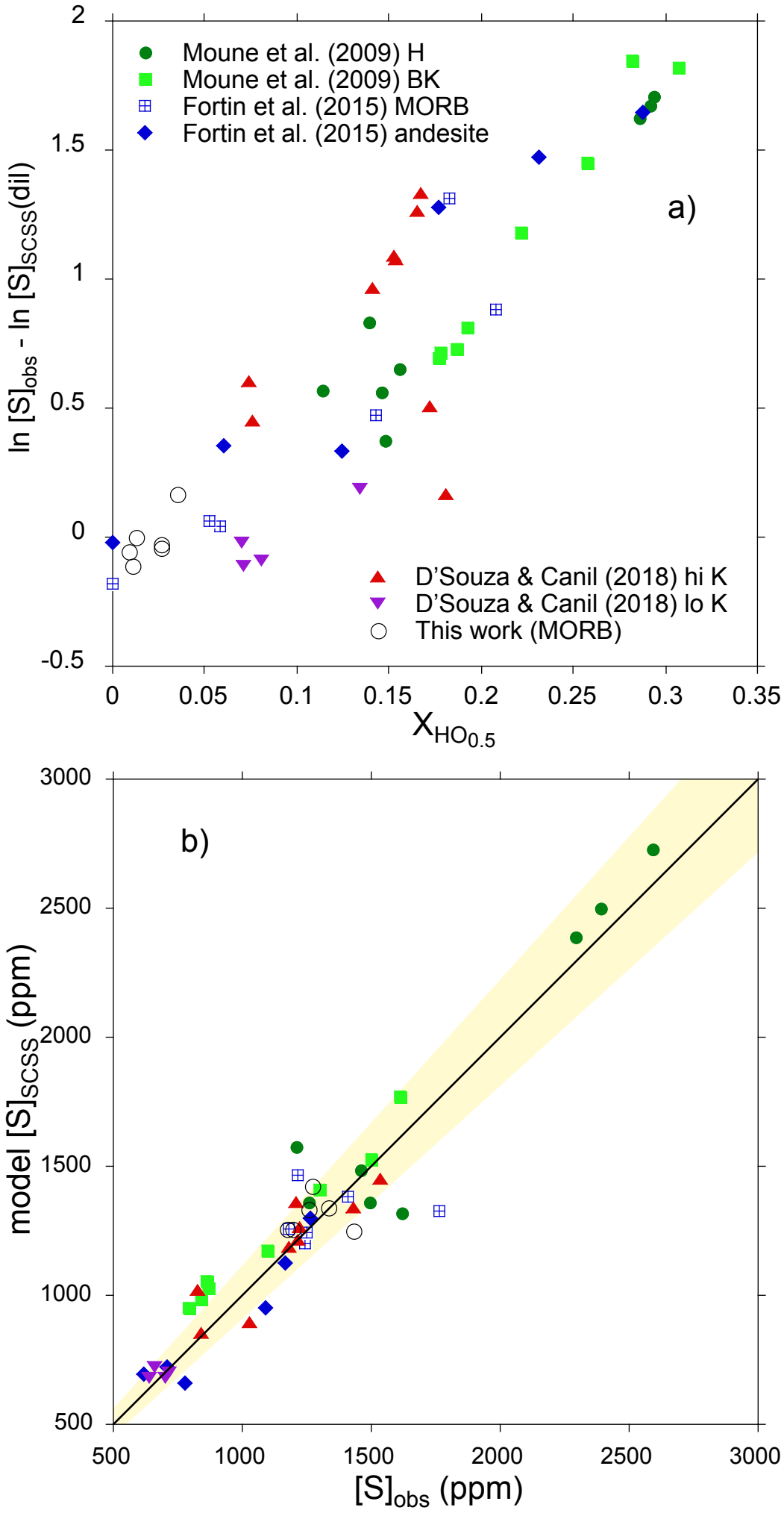
Moune et al. (2009) H
Moune et al. (2009) BK
Fortin et al. (2015) MORB
Fortin et al. (2015) andesite
D'Souza & Canil (2018) hi K
D'Souza & Canil (2018) lo K
This work (MORB)
a)
b)
ln [S]obs - ln [S]SCSS(dil)
XHO0.5
model [S]SCSS (ppm)
[S]obs (ppm)

Figure 9

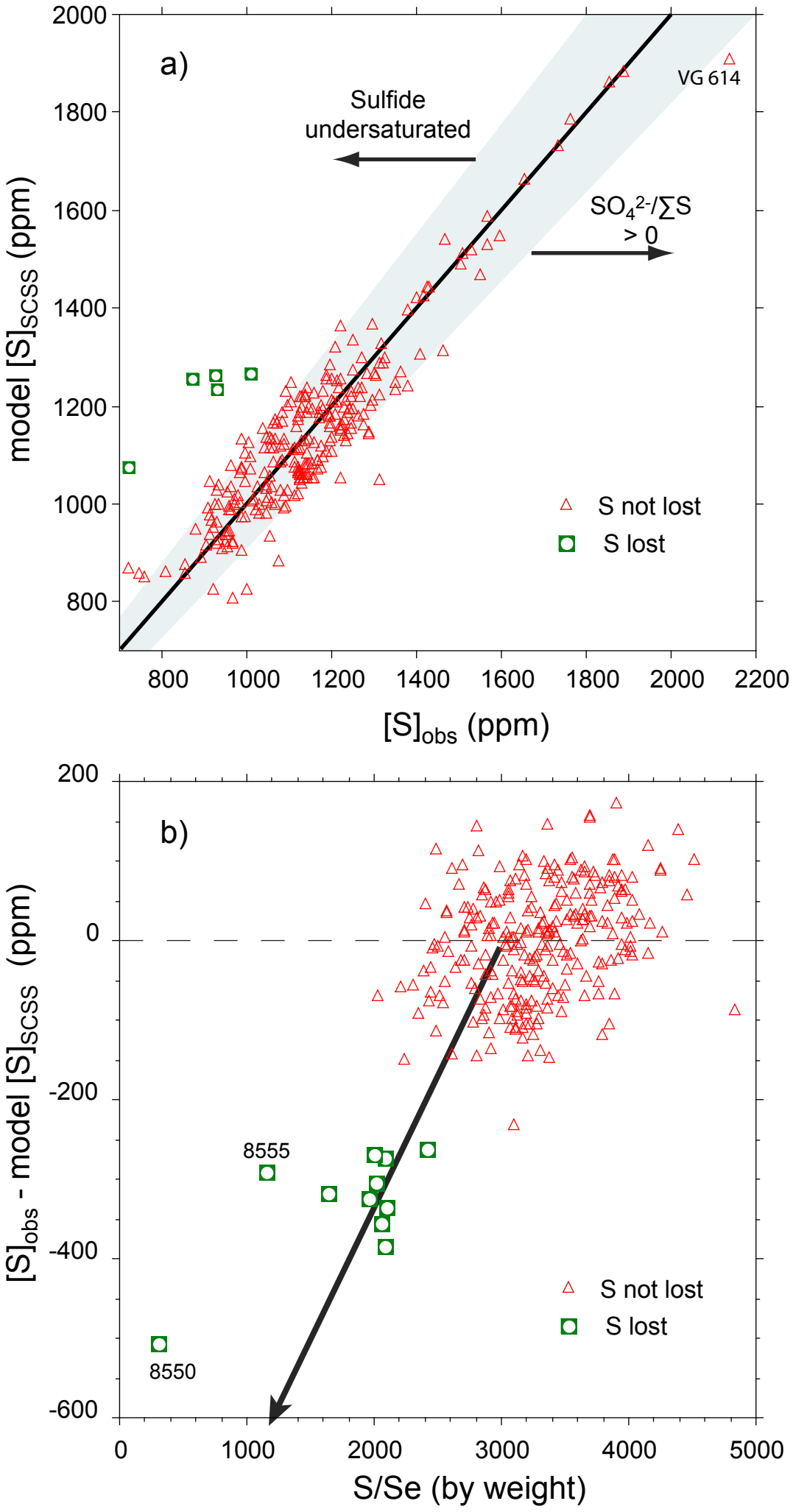
a)
VG 614
Sulfide
undersaturated
$SO_4^{2-}/\sum S$
> 0
S not lost
S lost
model $[S]_{SCSS}$ (ppm)
$[S]_{obs}$ (ppm)
2000
1800
1600
1400
1200
1000
800
800
1000
1200
1400
1600
1800
2000
2200
b)
8555
8550
S not lost
S lost
$[S]_{obs}$ - model $[S]_{SCSS}$ (ppm)
S/Se (by weight)
200
0
-200
-400
-600
0
1000
2000
3000
4000
5000

Figure 10

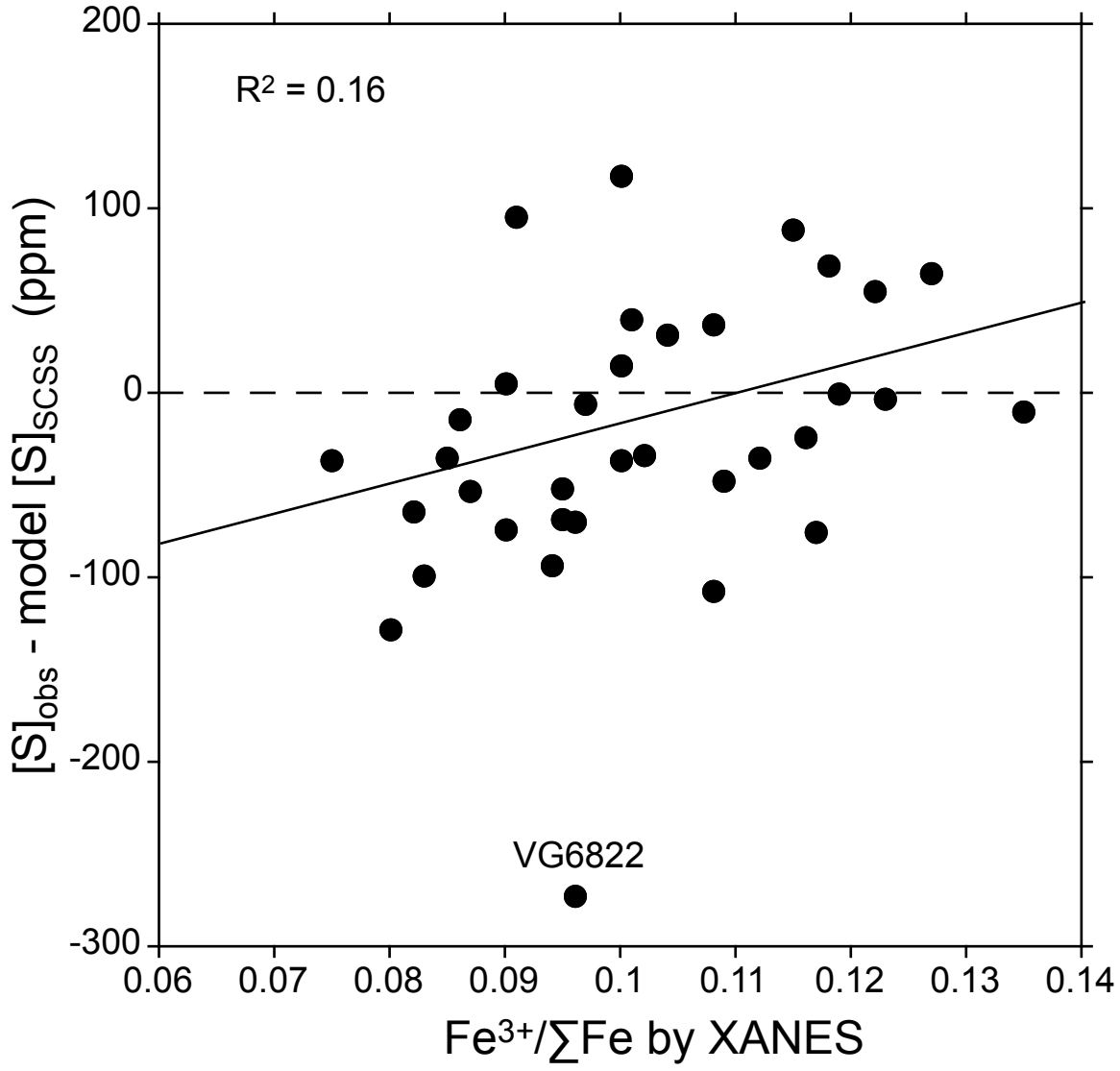
200
100
0
-100
-200
-300
R2 = 0.16
VG6822
[S]obs - model [S]SCSS (ppm)
0.06
0.07
0.08
0.09
0.1
0.11
0.12
0.13
0.14
Fe3+/∑Fe by XANES

Figure 11

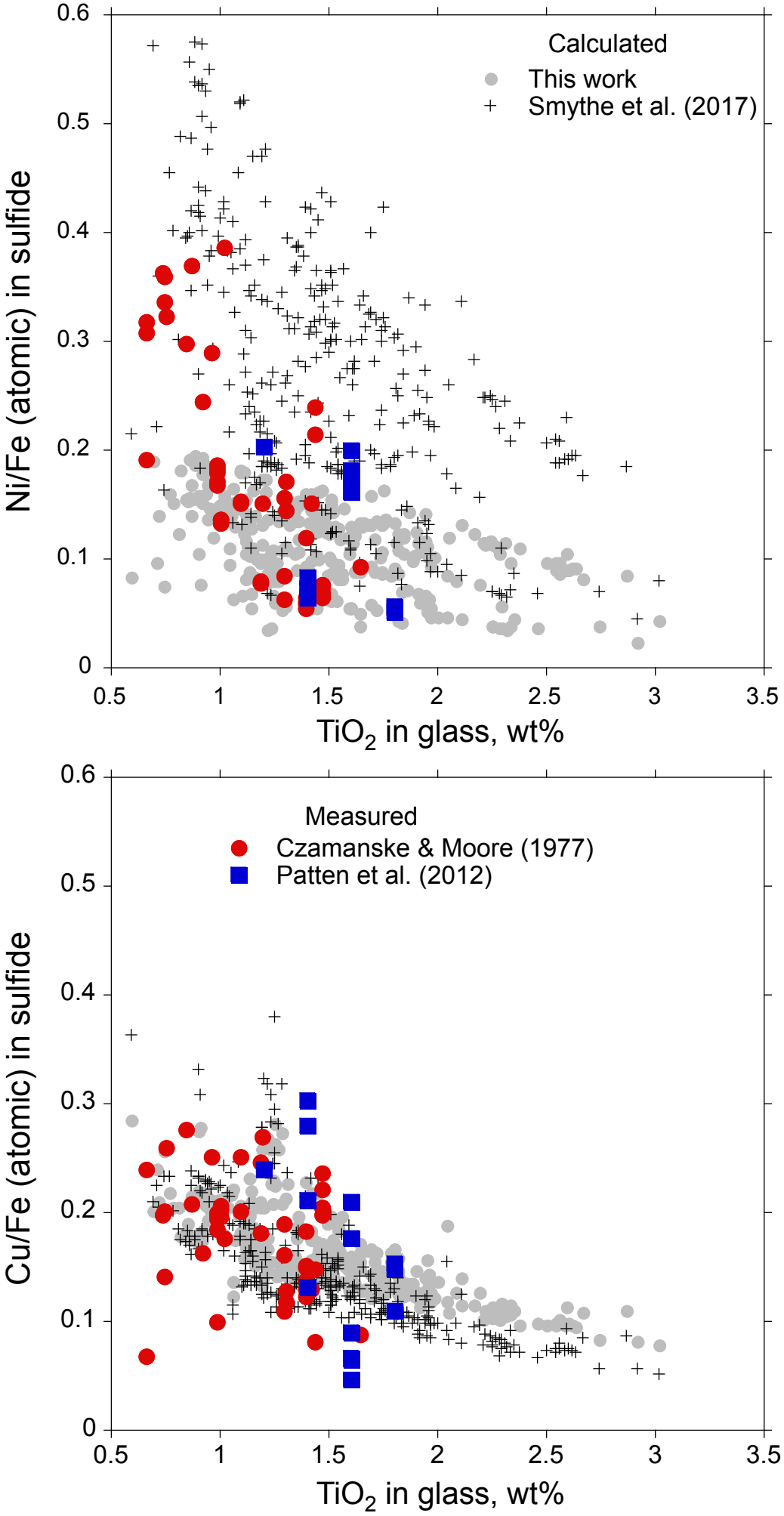
Calculated
This work
Smythe et al. (2017)
Ni/Fe (atomic) in sulfide
TiO2 in glass, wt%
Measured
Czamanske & Moore (1977)
Patten et al. (2012)
Cu/Fe (atomic) in sulfide
TiO2 in glass, wt%

Figure 12

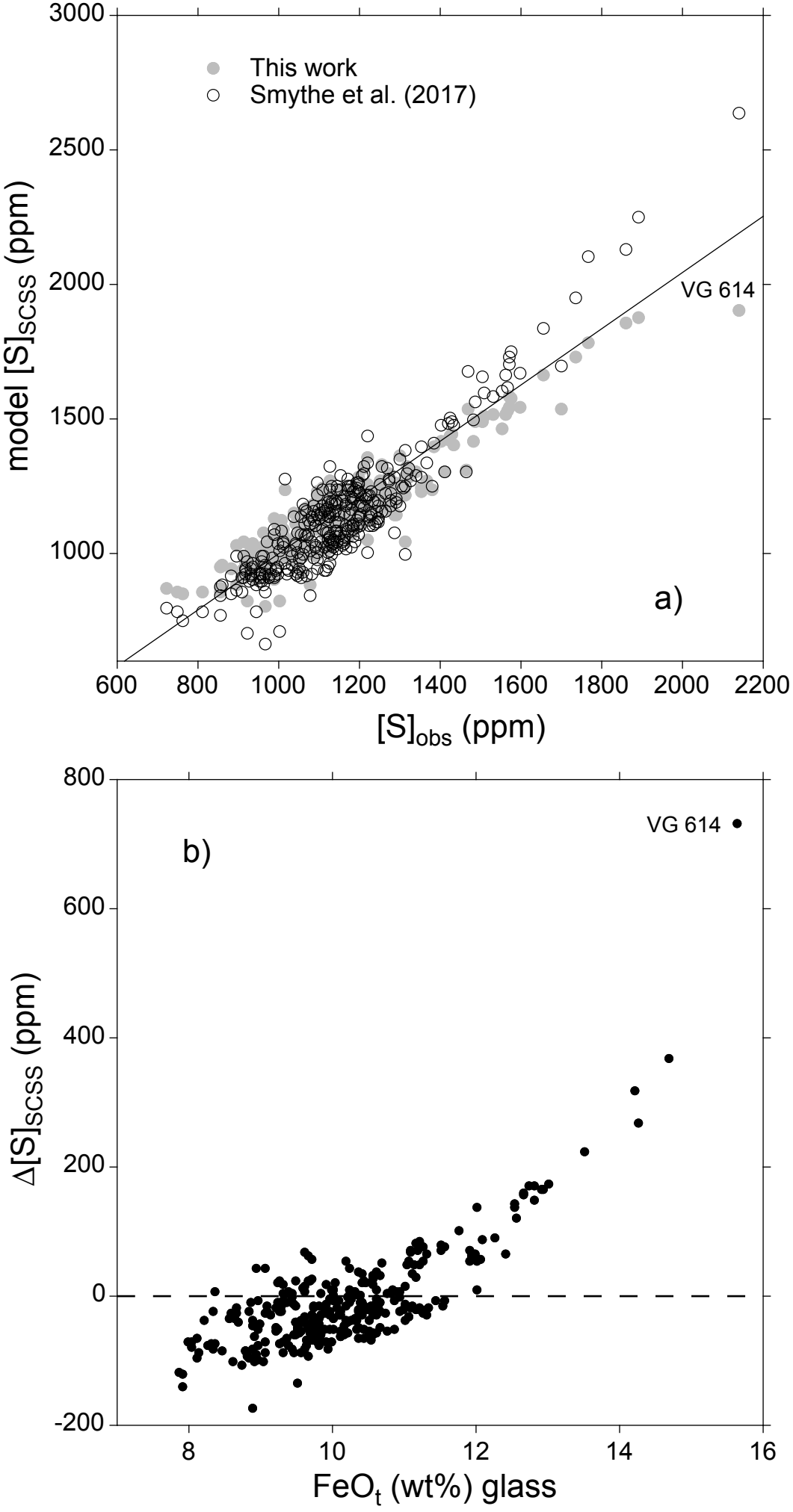
This work
Smythe et al. (2017)
VG 614
a)
model [S]SCSS (ppm)
[S]obs (ppm)
3000
2500
2000
1500
1000
600
800
1000
1200
1400
1600
1800
2000
2200
b)
VG 614
Δ[S]SCSS (ppm)
FeOt (wt%) glass
800
600
400
200
0
-200
8
10
12
14
16

Figure 13

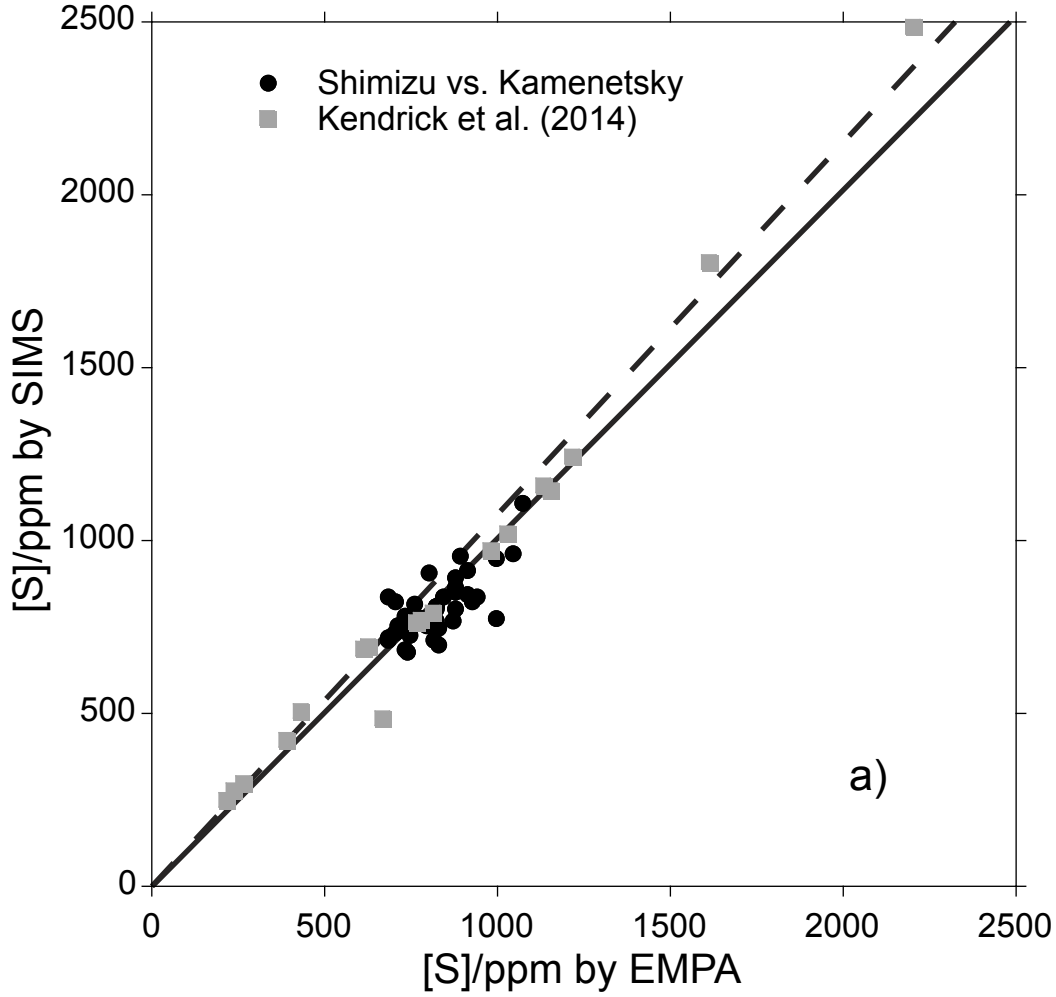
Shimizu vs. Kamenetsky
Kendrick et al. (2014)
[S]/ppm by SIMS
[S]/ppm by EMPA
a)
0
500
1000
1500
2000
2500

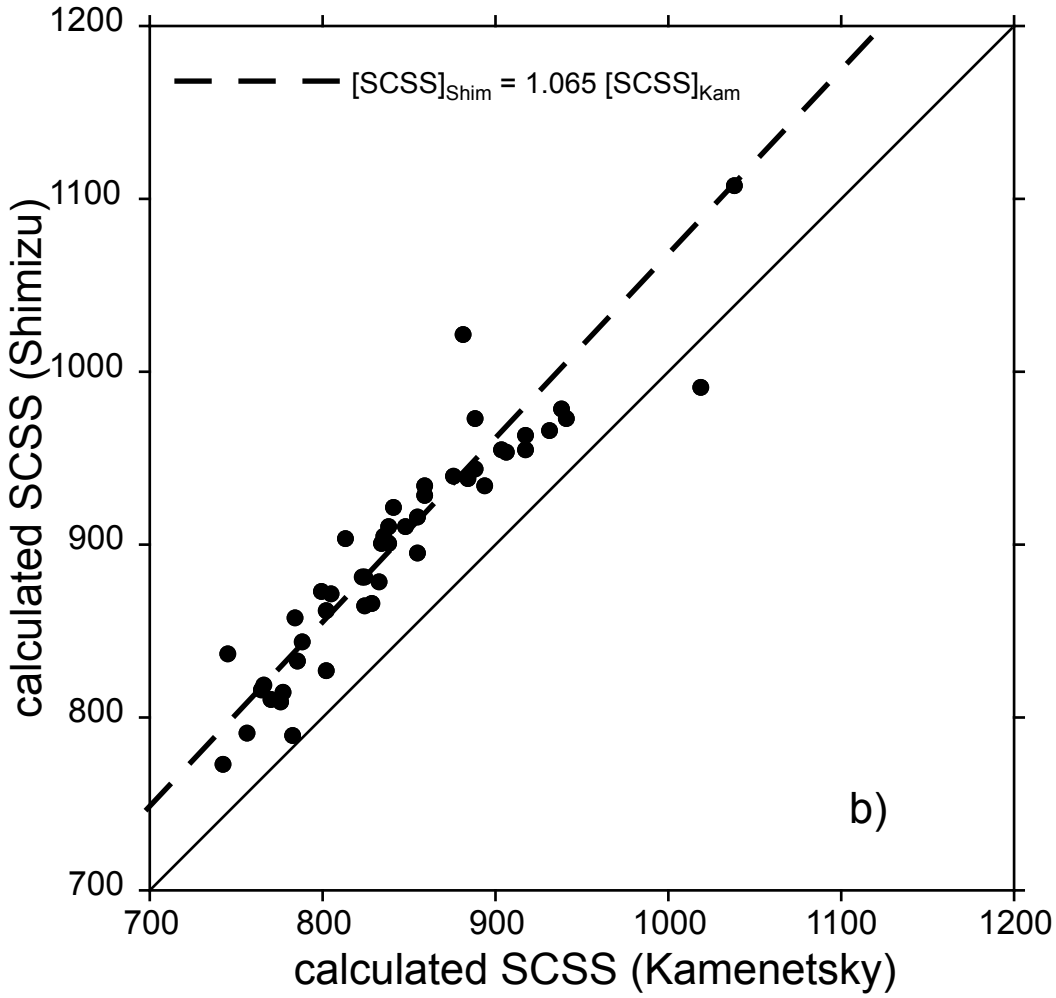
[SCSS]Shim = 1.065 [SCSS]Kam
calculated SCSS (Shimizu)
calculated SCSS (Kamenetsky)
b)
700
800
900
1000
1100
1200

Figure 14

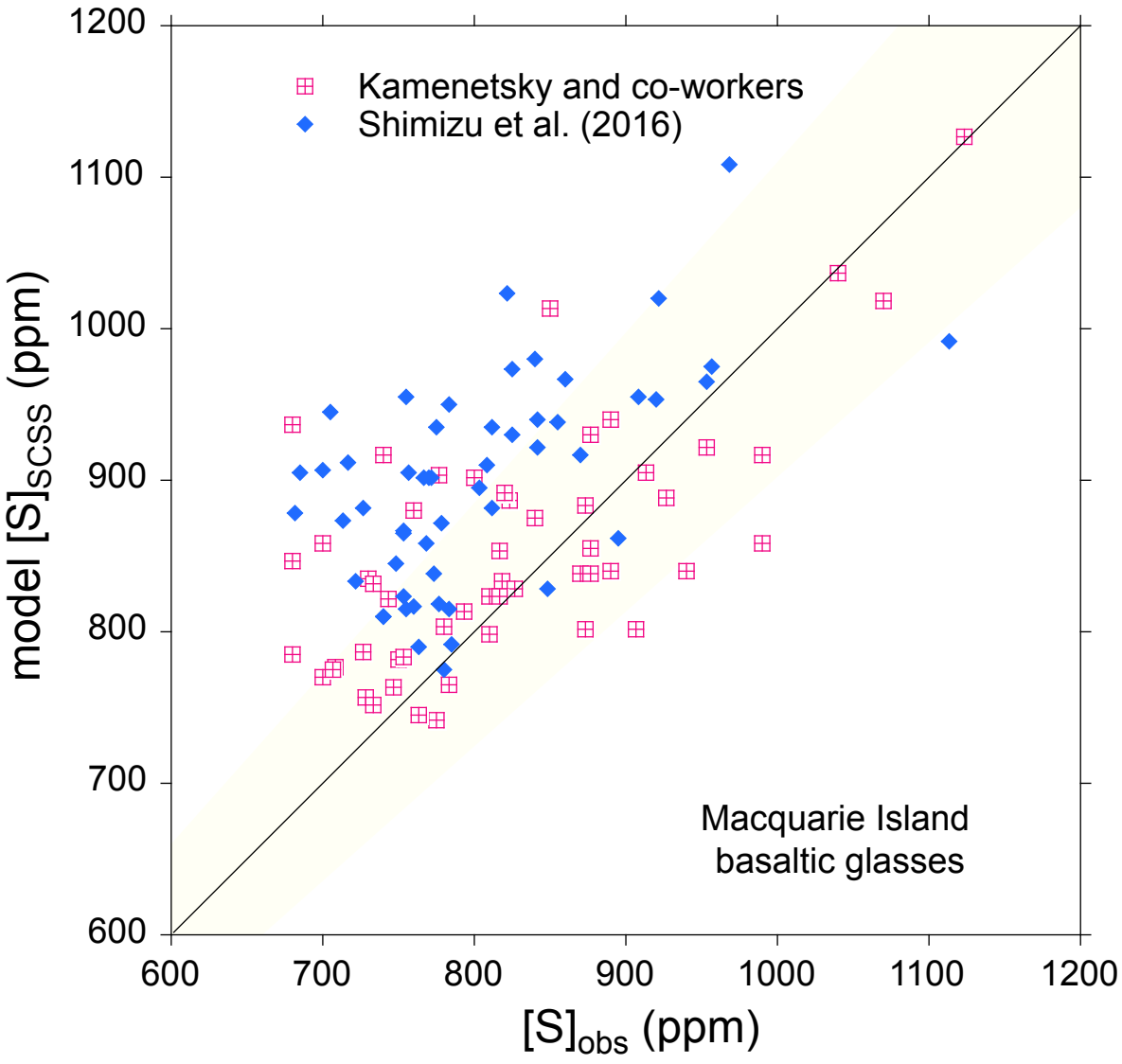
Kamenetsky and co-workers
Shimizu et al. (2016)
Macquarie Island
basaltic glasses
model [S]SCSS (ppm)
[S]obs (ppm)
600
700
800
900
1000
1100
1200

Figure 15

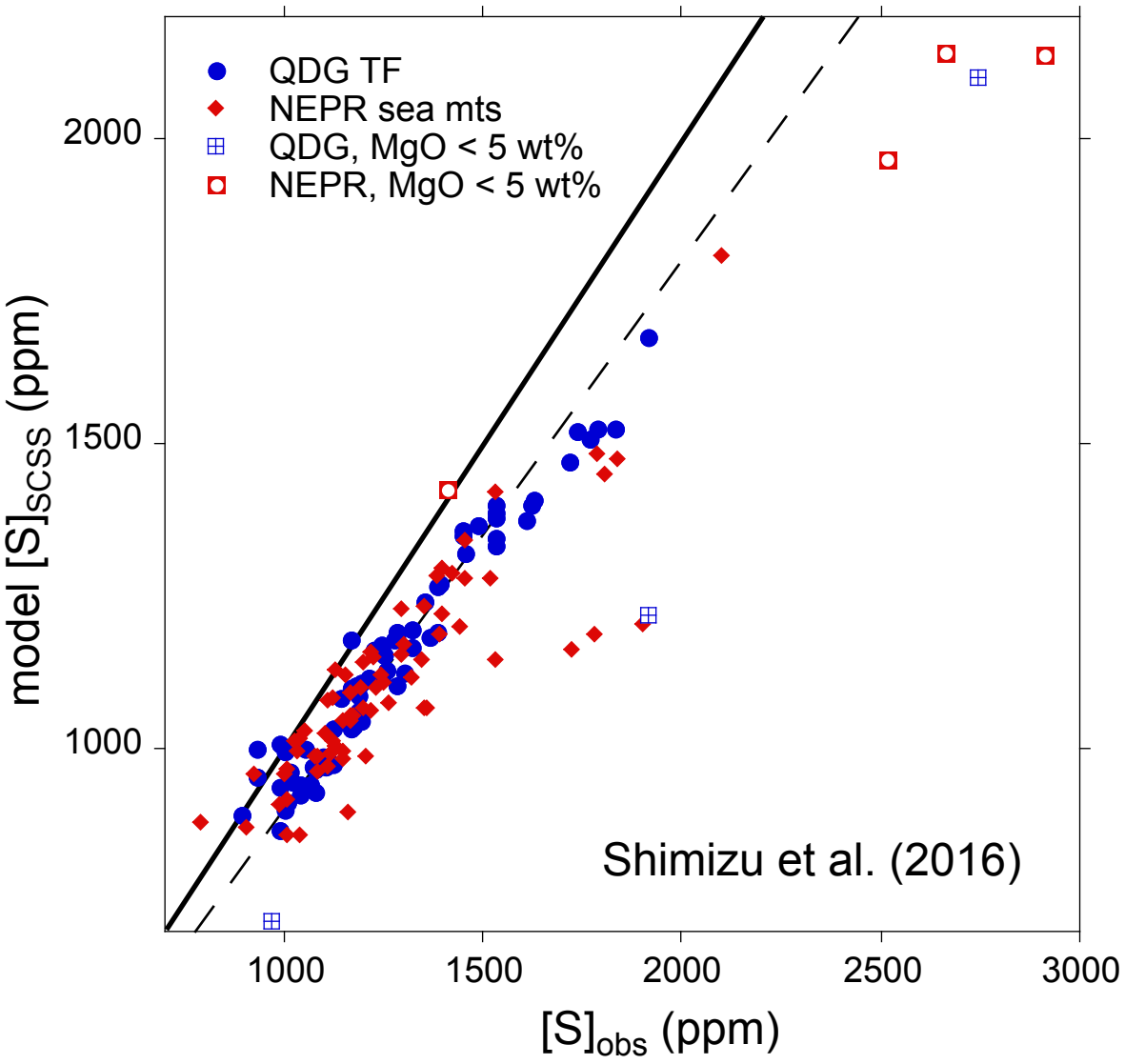
QDG TF
NEPR sea mts
QDG, MgO < 5 wt%
NEPR, MgO < 5 wt%
Shimizu et al. (2016)
model [S]SCSS (ppm)
[S]obs (ppm)
1000
1500
2000
2500
3000

Figure 16

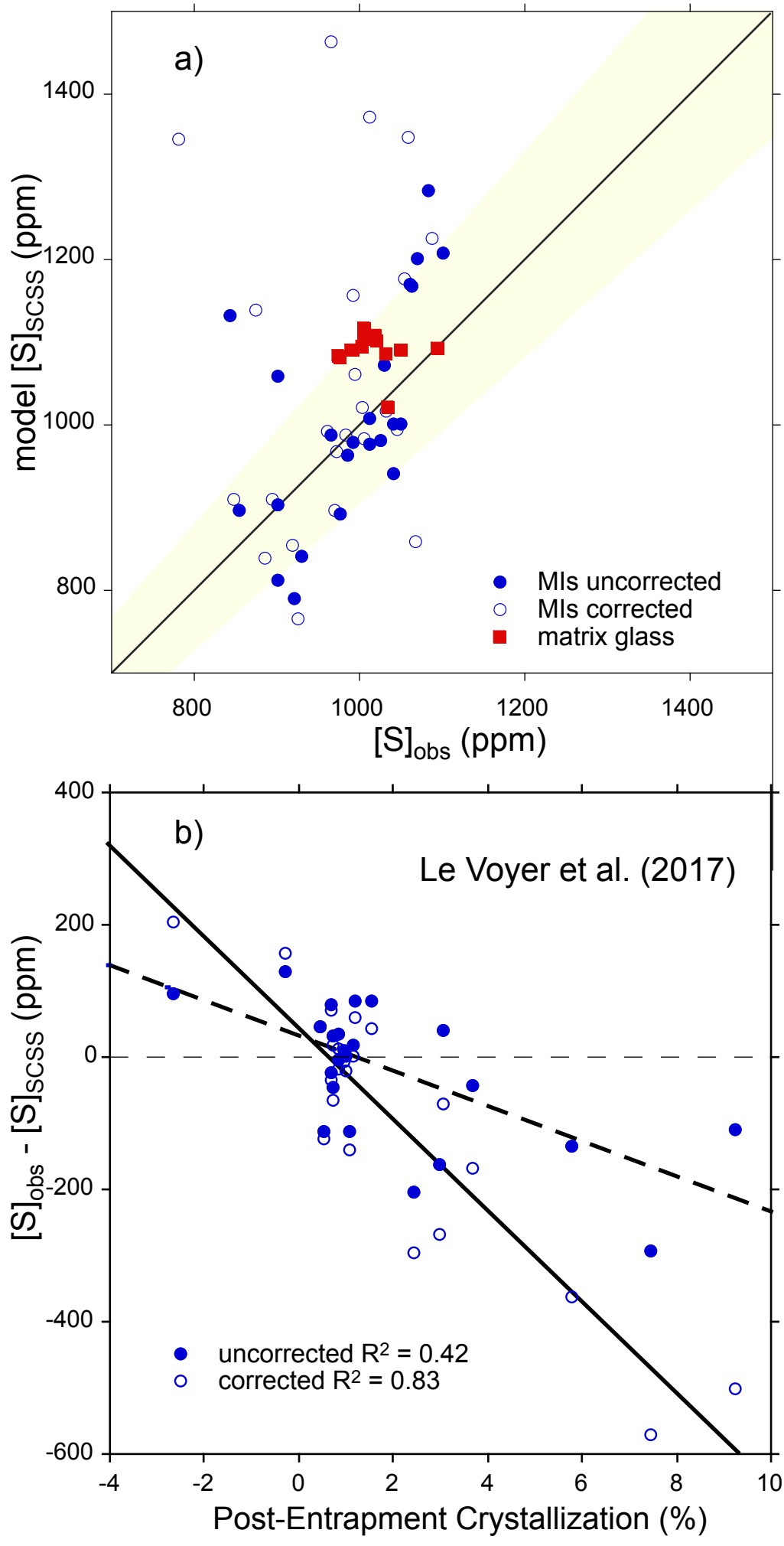
a)
model [S]scss (ppm)
[S]obs (ppm)
MIs uncorrected
MIs corrected
matrix glass
b)
Le Voyer et al. (2017)
[S]obs - [S]scss (ppm)
uncorrected R2 = 0.42
corrected R2 = 0.83
Post-Entrapment Crystallization (%)

Figure 17

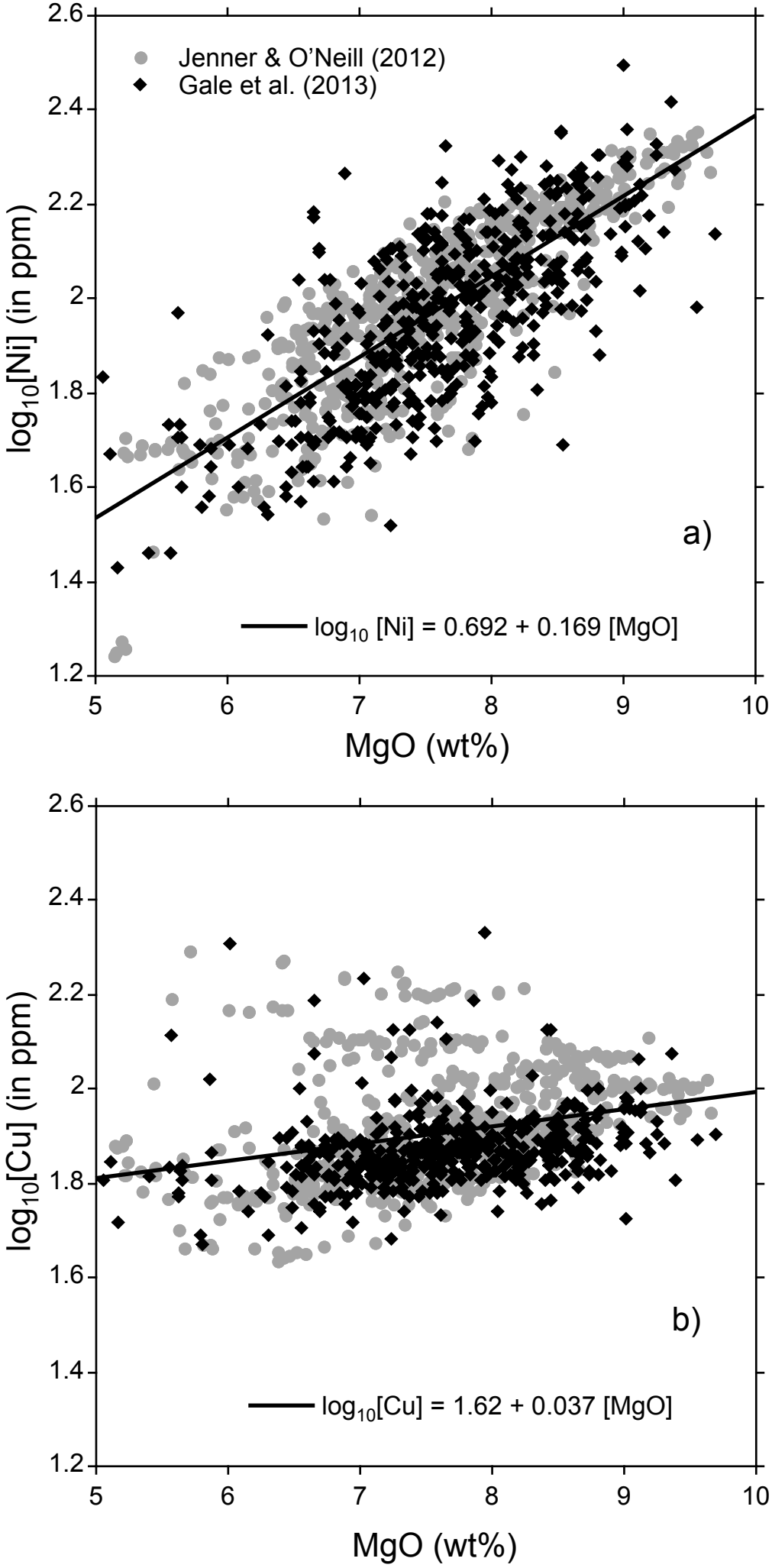
Jenner & O'Neill (2012)
Gale et al. (2013)
log10[Ni] (in ppm)
MgO (wt%)
a)
log10 [Ni] = 0.692 + 0.169 [MgO]
log10[Cu] (in ppm)
MgO (wt%)
b)
log10[Cu] = 1.62 + 0.037 [MgO]

Figure 18

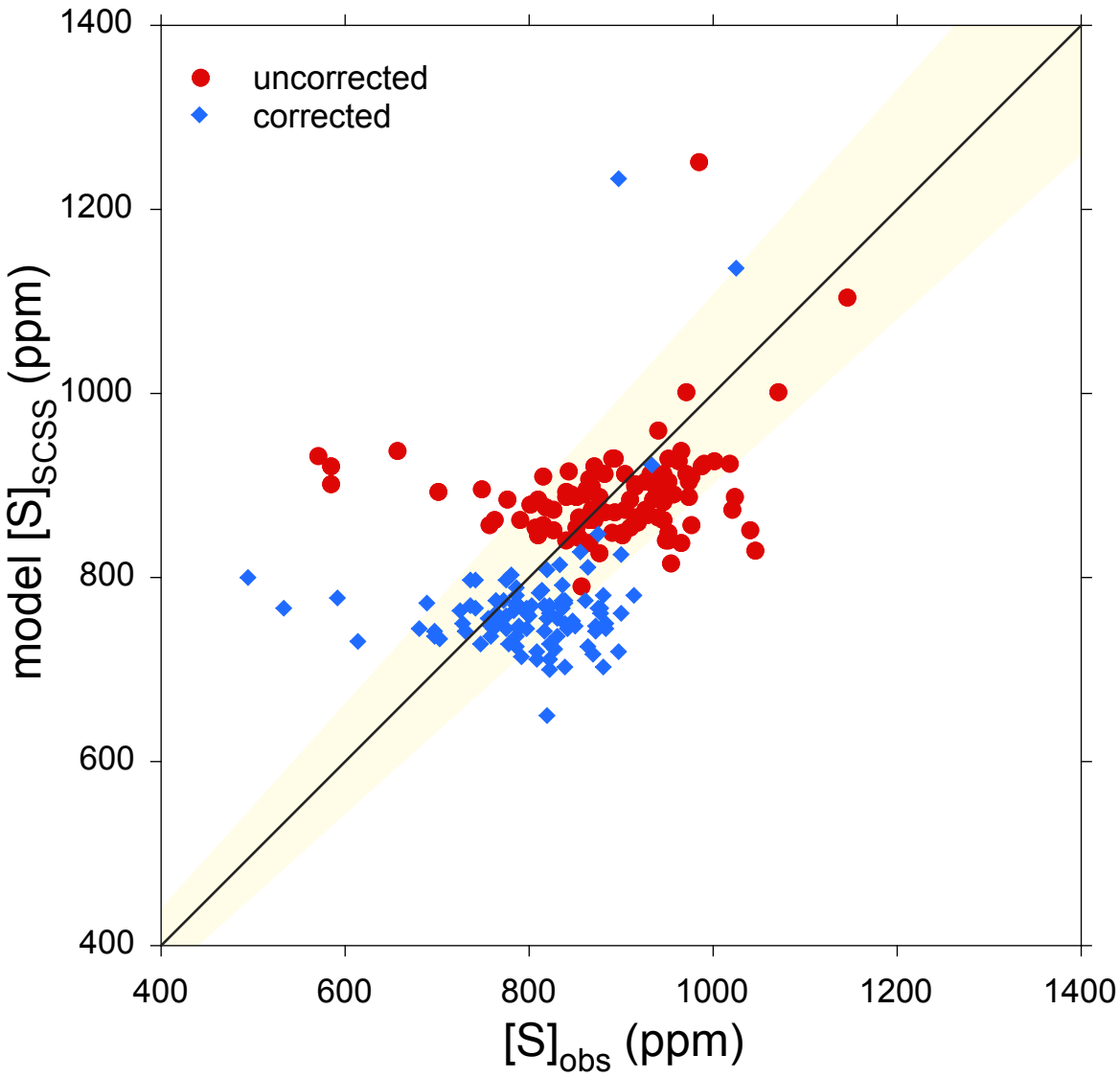
uncorrected
corrected
1400
1200
1000
800
600
400
400
600
800
1000
1200
1400
model [S]SCSS (ppm)
[S]obs (ppm)

Figure 19

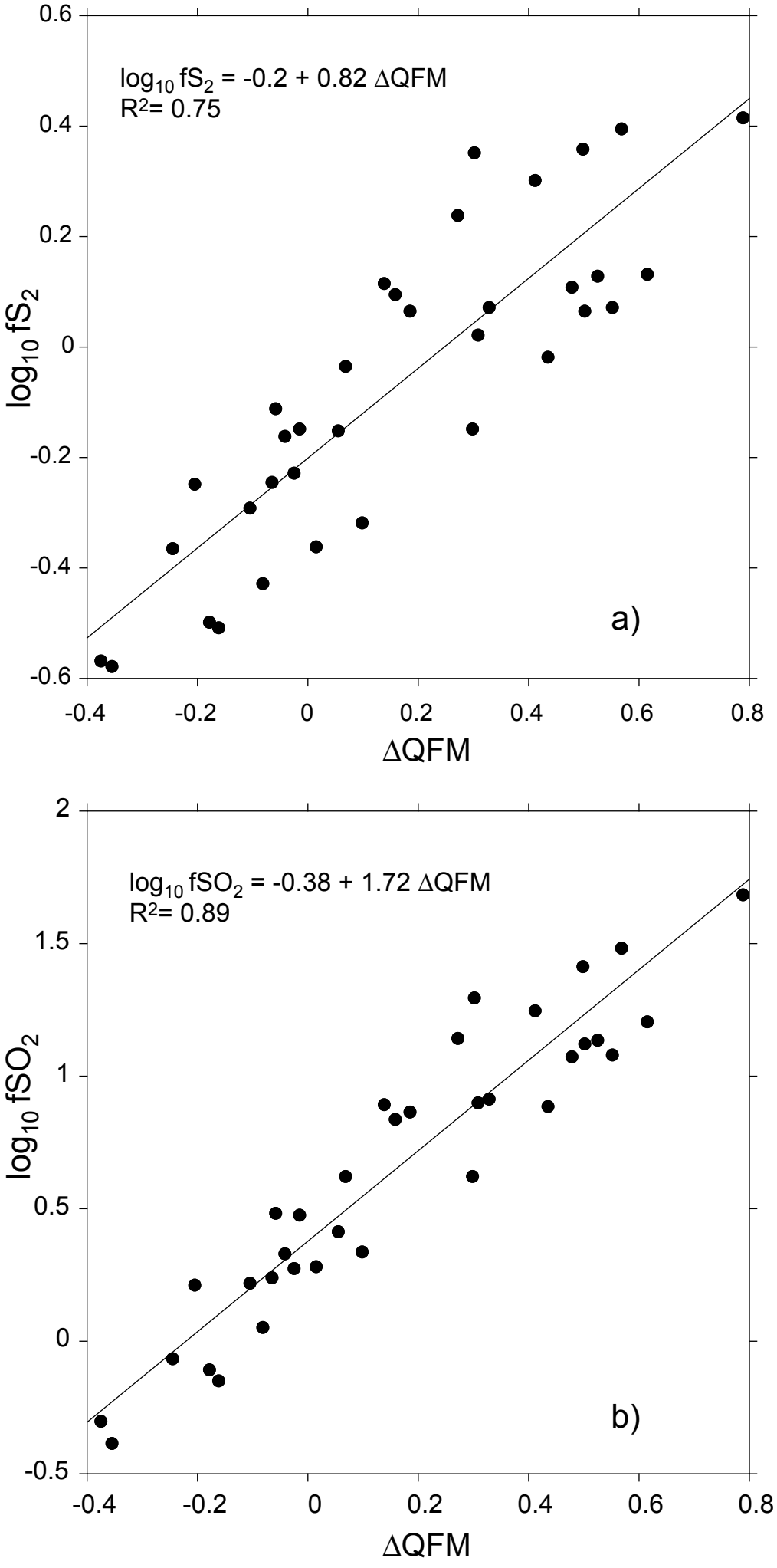
log10 fS2 = -0.2 + 0.82 ΔQFM
R2= 0.75
log10 fS2
ΔQFM
a)
log10 fSO2 = -0.38 + 1.72 ΔQFM
R2= 0.89
log10 fSO2
ΔQFM
b)